Journal of Molecular Structure 1318 (2024) 139323

Contents lists available at ScienceDirect

Journal of Molecular Structure

journal homepage: www.elsevier.com/locate/molstr

Microwave-assisted click synthesis, characterisation, and *In silico* studies of novel 2*H*-chromene-1,2,3-triazolyl glycoconjugates as potent anticancer and antibacterial agents

Bhabani Shankar Panda [a], Mohammed Ansar Ahemad [a], Suhasini Mohapatra [a], Eeshara Naik [b], Sabita Nayak [a,*], Seetaram Mohapatra [a], Pradeep Kumar Naik [b], Debdutta Bhattacharya [c], Chita Ranjan Sahoo [c], Malaya K. Sahoo [d]

[a] *Organic Synthesis Laboratory, Department of Chemistry, Ravenshaw University, Cuttack 753003, Odisha, India*
[b] *Centre of Excellence in Natural Products and Therapeutic, Department of Biotechnology and Bioinformatics, Sambalpur University, Jyoti vihar, Burla, Sambalpur 768019, Odisha, India*
[c] *ICMR-Regional Medical Research Centre, Department of Health Research, Ministry of Health & Family Welfare, Govt. of India, Bhubaneswar 751023, Odisha, India*
[d] *School of Chemical Science (SCS), National Institute of Science Education and Research (NISER) an OCC of Homi Bhabha National Institute (HBNI), Khurda 752050, Odisha, India*

ARTICLE INFO

Keywords:
2*H*-chromene
1,2,3-triazole
Click synthesis
Microwave irradiation
ADMET
Anticancer
Antibacterial agents

ABSTRACT

A series of novel 2*H*-chromene-1,2,3-triazolyl glycoconjugates **10a-w** were synthesized, well characterized and evaluated for their *in vitro* antimicrobial and anticancer activities. Among the tested compounds, **10a, 10b, 10u, 10v**, and **10w** exhibited the most excellent potency against both gram-positive (*S. aureus*) and gram-negative (*E. coli*) bacterial strains relative to the standard drug, Gentamicin. The anticancer results showed that in MCF-7 cell line all the tested compounds exhibited better activity as compared to other two cancer cell lines (MDA-MB-231 and A549). Compounds **10t, 10u, 10v**, and **10w** showed significant cytotoxicity against MCF-7 cell line. The molecular docking studies suggested that all the four potent compounds exhibited a greater affinity for the selected receptors. Experimentally and computationally observed structure-activity relationships indicates, -OCH_3 group at R^2 position in benzopyran ring with tosyl-protected sugar containing compound **10b** and benzyl-protected sugar containing compound **10t** enhanced the antibacterial and anticancer activity respectively. Frontier molecular orbital analysis of compounds using the global reactivity parameters indicated that benzyl-protected sugar and acetyl-protected sugar containing compounds are stable and exhibits low reactivity. Moreover, molecular electrostatic potential analysis plots clearly showed that the compounds have strong electrophonic reaction potential. Moreover, the assessment of ADMET predictions revealed favourable pharmacokinetic properties of the investigated compounds. Collectively, it was observed that compounds **10u, 10v**, and **10w** could be considered as promising dual anticancer antibiotic inhibitors.

1. Introduction

Cancer remains one of the most common life-threatening diseases characterized by the uncontrolled proliferation and dissemination of abnormal cells. Presently, it stands as a primary cause of mortality after accidents and injuries [1]. According to World Health Organization (WHO), the mortality rates associated with cancer will double in the coming years [2]. The significant morbidity and mortality rates of cancer are linked to the growing prevalence of risk factors like infections, environmental influences (radiation, chemicals, foreign substances), exposure to carcinogens, smoking, dietary habits, genetic factors, and increased ageing [3]. Indeed, chemotherapy is the primary method used to treat cancer, although it has limitations such as a lack of selectivity, unwanted side effects, and multidrug resistance (MDR) [4]. Though chemotherapy is widely used in cancer treatment, it often leads to severe side effects owing to its cytotoxic and mutagenic impact on healthy cells [5]. Therefore, it is essential to develop alternative pharmaceutical leading candidates with reduced or negligible adverse effects

* Corresponding author.
E-mail address: sabitanayak18@gmail.com (S. Nayak).

https://doi.org/10.1016/j.molstruc.2024.139323
Received 24 April 2024; Received in revised form 7 July 2024; Accepted 14 July 2024
Available online 17 July 2024

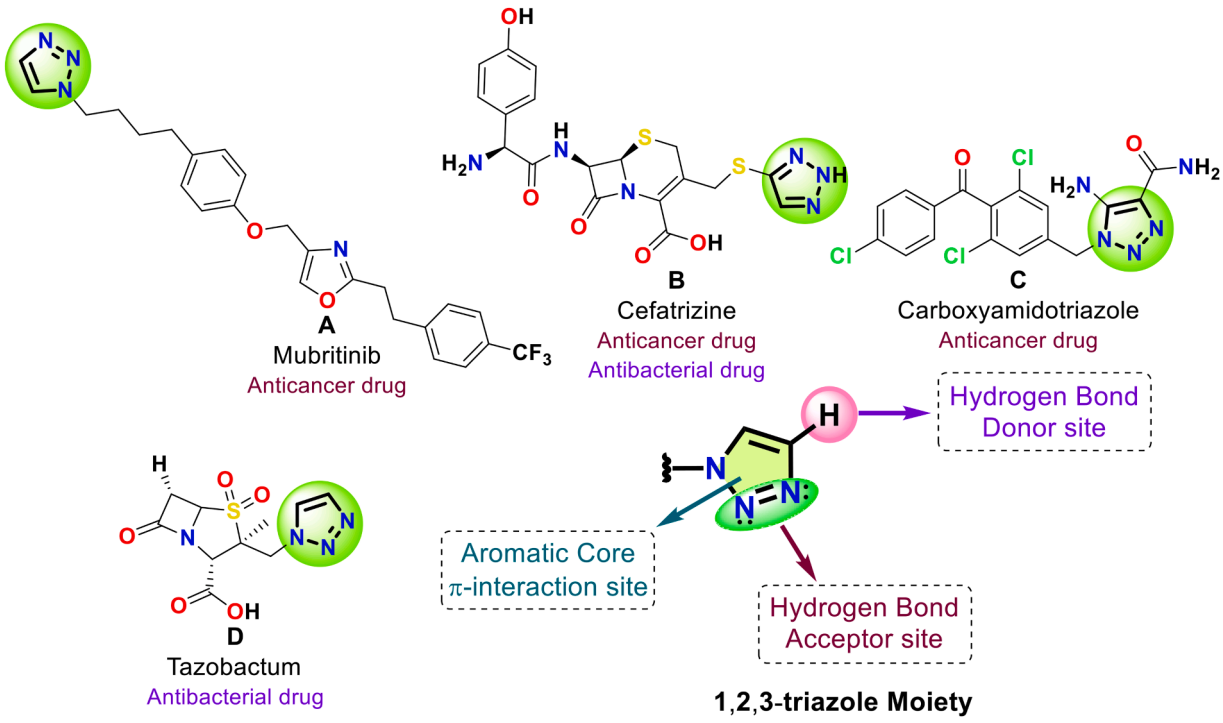

Fig. 1. Some FDA-approved drugs having 1,2,3-triazole ring (**A-D**) and various secondary interaction sites of 1,2,3-triazole moiety.

on the human body. Cancer patients undergoing chemotherapy treatments are more susceptible to microbial infections because of weakened immune systems [6]. Therefore, using a single therapy that acts as an anticancer and antimicrobial agent could be cost-effective and lower the frequency of drug administration, side effects, and antimicrobial resistance.

Over the past few decades, the frequency of microbial infections has been increasing consistently across several environments due to the quick evolution and development of resistance to antimicrobial treatments [7,8]. Bacterial infections pose a significant challenge to public health, primarily because of the rise and dissemination of pathogens resistant to existing antibiotics [9]. Most of the antimicrobials are focused on a small group of well corroborated targets thereby inhibiting the growth of microorganisms. Consequently, there is a persistent need drug discovery and development for the target-based synthesis of novel antimicrobial agents.

Nitrogen containing heterocycles have played a crucial role in drug discovery. Among various nitrogen functional heterocyclics, Polynitrogen-based five-membered heterocyclic frameworks (particularly 1,2,3-triazole) play a tremendous role in the field of medicinal chemistry due to their excellent stability as well as reliability. 1,2,3-triazole was found as a pharmacophore in many FDA-approved anticancer drugs such as Mubritinib **A** [10], Cefatrizine **B** [11], Carboxyamidotriazole (CAI) **C** [12] and antibacterial drugs such as Tazobactam **D** [13], Cefatrizine **B** [11]. Additionally, the 1,2,3-triazole has arisen as a commanding synthetic unit to deploy MDR. This scaffold displays less toxicity and can be fused with other heterocycles besides being found naturally. It functions as a drug-like molecule with several efficient interactions with biological targets because it has two strong hydrogen bond accepting sites through two nitrogen atoms, a weak hydrogen bond donor site (C−H) that helps the triazole moiety to anchor with several biological targets, and a π-assemblage interaction site through an aromatic ring (Fig. 1) [14]. In this scenario, 1,2,3-triazole has been recognized as a versatile scaffold exhibiting numerous biological activities such as anti-HIV [15], anti-tubercular [16], anti-malarial, anti-inflammatory [17], anti-fungal [18,19], anticancer [21-25] and antibacterial activity [20,26-28]. Various research groups have given significant effort in the development of potent anticancer and antibacterial activity of 1,2,3-triazole derivatives (**E-I**) [21-23,26,27], as shown in Fig. 2.

Consequently, the 2*H*-chromene is an imperative class of benzo-fused oxa-heterocycle and a significant structural framework of many bioactive natural products [29-32]. Furthermore, chromene nucleus exhibits a promising scaffold in the advancement of potent anti-cancer agents such as Lonchocarpin, Acronycine, Seselin, and Xanthylein [33-35] and anti-bacterial agents [36,37-39]. Several studies have additionally emphasized the efficacy of 2*H*-chromene derivatives (**J-M**) [35,37,38,40] in combating cancer and bacterial infections, as depicted in Fig. 2.

On the other hand, the well-known versatile glucoside scaffolds have proved worthy as a reliable paternal motif, owing to their several notable attributes including biocompatibility, low toxicity, and also enhanced hydrophilicity [41,42]. These molecules are the most abundant in nature and play crucial roles in cellular metabolism, signal transduction, and physiology of nearly all living species [43,44]. Integrating the glycosylic structure into a molecule reduces its toxicity and enhances hydrophilicity. Therefore, Click chemistry-inspired glycoconjugated triazoles are focused for developing potential bioactive moieties.

The "Click Chemistry Approach" for the synthesis of 1,2,3-triazole by copper(I)-catalyzed 1,3-dipolar cycloaddition reaction of an alkyne and azide [14,41,45], has become a well-liked and the most exploited reaction in the field of medicinal chemistry because of the cost-effectiveness, efficacious, ease of purification, mild reaction conditions, high versatility and productivity [46]. In the search for new bioactive molecules, our research group has been constantly developing new chromene-based hybrid molecules over the past few years [34-36,38,39,47,48]. In recent years, there has been a substantial growth in the production of triazole-fused chromene derivatives, aimed to discover compounds with pharmaceutical applications using a more efficient and direct approach [49,50]. In this regard, the present study planned to fuse three moieties (2*H*-chromene, triazole, and glycosyl) in a single molecular entity to construct more potent hybrid molecules. Thus, we have synthesised 23 numbers of new 2*H*-chromene-1,2,3-triazolyl glycoconjugates and evaluated their anti-cancer, anti-bacterial, DFT,

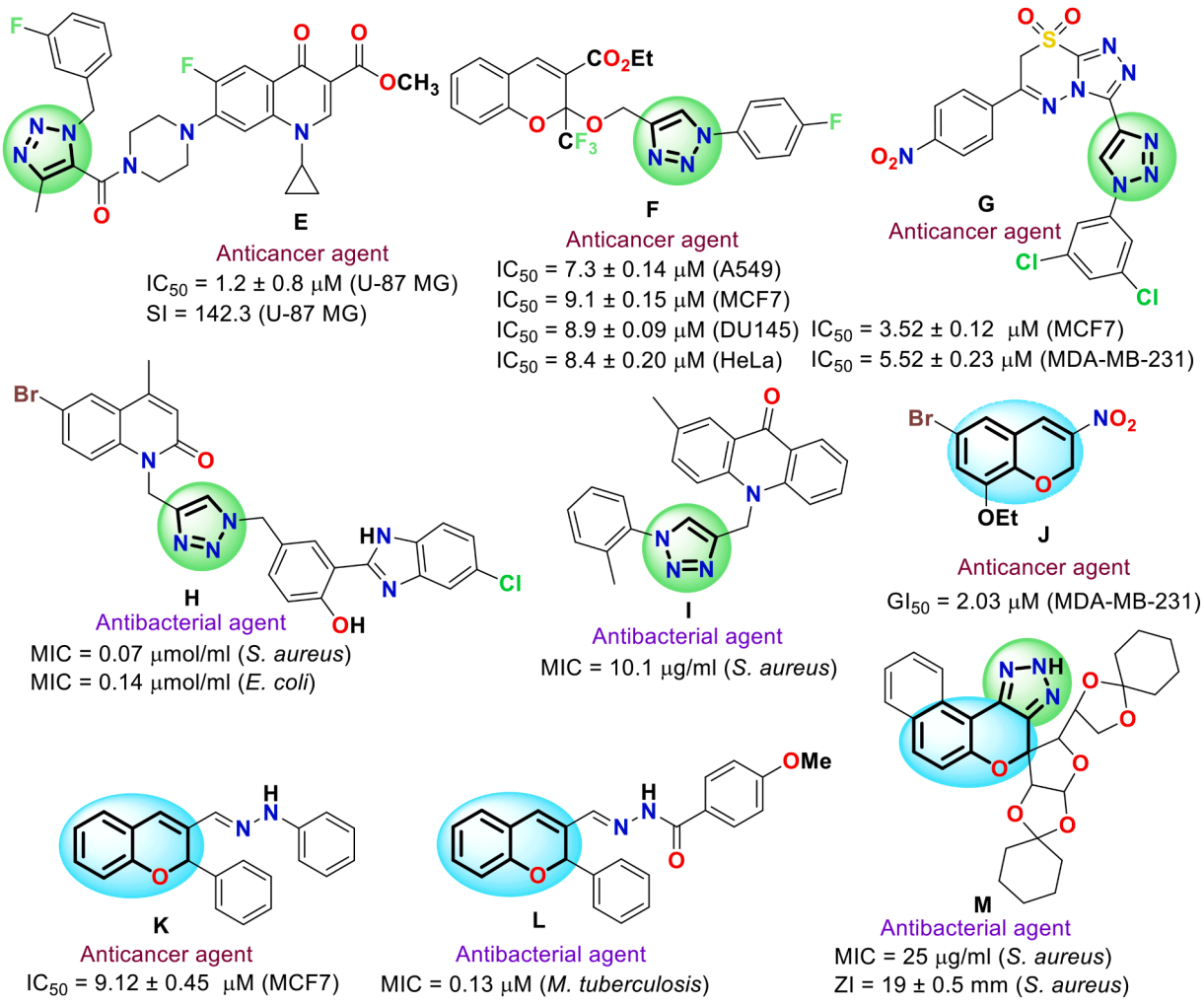

Fig. 2. Some potent 1,2,3-triazole derivatives (**E-I**) and 2*H*-chromene derivatives (**J-M**) having anticancer and antibacterial activities.

molecular docking and ADMET studies.

2. Materials and methods

2.1. Reagents, materials and instrumentation

The chemicals and solvents were purchased from Sigma-Aldrich, Merck, Finar and used without further purification. The TLC plates (Merck, silica gel 60 F254) (20 × 20 cm) were used to monitor the progress of reactions and visualized by UV chamber (Short-UV light at 254 nm). A JEOL 400 MHz NMR spectrometer at NMR Lab, Central Instrument Facility, Ravenshaw University, Cuttack, was used to record the nuclear magnetic resonance (^{1}H & ^{13}C NMR) spectra. Chemical shifts (δ) are reported in parts per million (ppm). ^{1}H and ^{13}C NMR signals were referenced to tetramethyl silane (TMS, δ = 0.00 ppm) and the solvent shifts of $CDCl_3$ (^{1}H: δ = 7.26 ppm, ^{13}C: δ = 77.0 ppm) and DMSO-d6 (^{1}H: δ = 2.49 ppm, ^{13}C: δ = 39.5 ppm). Coupling constants (*J*) are reported in Hertz (Hz). The abbreviations used in reporting ^{1}H NMR data were denoted as follows: s, singlet; dd, double doublet; d, doublet; t, triplet; m, multiplet. The coupling constant values (*J*) were recorded in hertz (Hz). The melting points were measured with an electrothermal (Stuart SPM10) apparatus. High-resolution mass spectra were determined at the Department of Chemical Sciences, IISER-Berhampur using Mass spectrometer (Model: Xevo G2-XS QTof). The Microplate reader (Model: iMark^{TM}) and Inverted microscope (Model: Nikon ECLIPSE T$_S$2R) were used for cytotoxicity study and morphological observation respectively.

2.2. Synthesis

2.2.1. Procedure for synthesis of 2H-chromene-3-carbaldehyde oximes (6a-o)

The 2*H*-chromene-3-carbaldehydes were successfully synthesized by the reaction of salicylaldehydes **1a-k** and acrolein **2**/ cinnamaldehyde **3** in the presence of K_2CO_3/pyrrolidine [51,52]. Then, in an oven-dried round bottom flask 2*H*-chromene-3-carbaldehydes (1 equiv.), sodium acetate (3.2 equiv.), and 5 ml of ethanol were taken and staired continuously for 5 minutes. After that hydroxyl amine hydrochloride (3 equiv.) were added to the above reaction mixture and again stirred for 3 hours at room temperature. After the reaction was completed, the reaction mixture was poured into cold water [53], and the precipitate was filtered out to obtain the desired compounds **6a-o** (79-99%). All the compounds were characterised by ^{1}H and ^{13}C NMR spectral analysis technique.

2.2.1.1. 2H-chromene-3-carbaldehyde oxime (6a). Light Brown Solid (98%), Melting Point: 161-162°C; ^{1}H NMR (400 MHz, $CDCl_3$) δ_H (ppm): 7.83 (s, 1H, HC=N), 7.19-7.14 (m, 1H, Ar-H), 7.05 (dd, J_{12} = 1.2, J_{13} = 7.2 Hz, 1H, Ar-H), 6.92-6.88 (m, 1H, Ar-H), 6.83 (d, *J* = 7.6 Hz, 1H, Ar-H), 6.62 (s, 1H, Ar-H), 5.03 (s, 2H, Ar-O-CH_2); ^{13}C NMR (100 MHz, $CDCl_3$) δ_C (ppm): 154.4 (Ar-C), 148.9 (HC=N), 130.4 (Ar-C), 128.4 (Ar-C), 127.5 (Ar-C), 126.39 (Ar-C), 121.6 (Ar-C), 121.5 (Ar-C), 115.9 (Ar-C), 64.2 (Ar-O-CH_2).

*2.2.1.2. 8-methoxy-2H-chromene-3-carbaldehyde oxime (**6b**).* Yellow Solid (99%), Melting Point: 177-178°C; 1H NMR (400 MHz, $CDCl_3$) δ_H (ppm): 7.83 (s, 1H, HC=N), 6.88-6.81 (m, 2H, Ar-H), 6.71 (dd, $J_{12} = 2.4$ Hz, $J_{13} = 6.8$ Hz, 1H, Ar-H), 6.61 (s, 1H, Ar-H), 5.10 (s, 2H, Ar-O-CH_2), 3.88 (s, 3H, OCH_3); ^{13}C NMR (100 MHz, $CDCl_3$) δ_C (ppm): 148.9 (Ar-C), 147.7 (HC=N), 128.2 (Ar-C), 126.6 (Ar-C), 122.2 (Ar-C), 121.2 (Ar-C), 119.7 (Ar-C), 113.0 (Ar-C), 64.5 (Ar-O-CH_2), 56.1 (OCH_3).

*2.2.1.3. 8-ethoxy-2H-chromene-3-carbaldehyde oxime (**6c**).* Greenish Yellow Solid (94%), Melting Point: 172-173°C; ^1H NMR (400 MHz, $CDCl_3$) δ_H (ppm): 7.83-7.81 (m, 2H, HC=N, OH), 6.86-6.80 (m, 2H, Ar-H), 6.72-6.67 (m, 1H, Ar-H), 6.60 (s, 1H, Ar-H), 5.10 (s, 2H, Ar-O-CH_2), 4.10 (q, $J = 7.2$ Hz, 2H, OCH_2), 1.45 (t, $J = 6.8$ Hz, 3H, CH_3); ^{13}C NMR (100 MHz, $CDCl_3$) δ_C (ppm): 148.8 (Ar-C), 146.9 (HC=N), 143.6 (Ar-C), 128.2 (Ar-C), 126.5 (Ar-C), 122.3 (Ar-C), 121.2 (Ar-C), 119.7 (Ar-C), 114.5 (Ar-C), 64.5 (Ar-O-CH_2), 64.5 (OCH_2), 14.8 (CH_3).

*2.2.1.4. 6-nitro-2H-chromene-3-carbaldehyde oxime (**6d**).* Redish Yellow Solid (97%), Melting Point: 182-183°C; ^1H NMR (400 MHz, $CDCl_3$) δ_H (ppm): 8.06 (dd, $J_{12} = 2.8$ Hz, $J_{13} = 8.8$ Hz, 1H, Ar-H), 7.96 (d, $J = 2.4$ Hz, 1H, Ar-H), 7.85 (s, 1H, HC=N), 7.65 (s, 1H, OH), 6.88 (d, $J = 8.4$ Hz, 1H, Ar-H), 6.63 (s, 1H, Ar-H), 5.18 (s, 2H, Ar-O-CH_2); ^{13}C NMR (100 MHz, $CDCl_3$) δ_C (ppm): 148.1 (HC=N), 130.9 (Ar-C), 128.8 (Ar-C), 128.1 (Ar-C), 126.1 (Ar-C), 125.7 (Ar-C), 122.9 (Ar-C), 121.1 (Ar-C), 116.3 (Ar-C), 65.3 (Ar-O-CH_2).

*2.2.1.5. 3H-benzo[f]chromene-2-carbaldehyde oxime (**6e**).* Yellow Solid (89%), Melting Point: 179-180°C; ^1H NMR (400 MHz, DMSO-d_6) δ_H (ppm): 11.34 (s, 1H, OH), 8.08 (d, $J = 8.4$ Hz, 1H, Ar-H), 8.00 (s, 1H, HC=N), 7.84 (d, $J = 7.6$ Hz, 1H, Ar-H), 7.78 (d, $J = 8.8$ Hz, 1H), Ar-H, 7.58 (s, 1H, Ar-H), 7.56-7.52 (m, 1H, Ar-H), 7.41-7.37 (m, 1H, Ar-H), 7.11 (d, $J = 8.8$ Hz, 1H, Ar-H), 5.06 (s, 2H, Ar-O-CH_2); ^{13}C NMR (100 MHz, DMSO-d_6) δ_C (ppm): 152.2 (Ar-C), 147.5 (HC=N), 130.2 (Ar-C), 129.6 (Ar-C), 129.0 (Ar-C), 128.5 (Ar-C), 127.1 (Ar-C), 126.2 (Ar-C), 124.1 (Ar-C), 122.4 (Ar-C), 121.5 (Ar-C), 117.3 (Ar-C), 114.7 (Ar-C), 63.8 (Ar-O-CH_2).

*2.2.1.6. 6-chloro-2H-chromene-3-carbaldehyde oxime (**6f**).* Pale Yellow Solid (82%), Melting Point: 175-176°C; ^1H NMR (400 MHz, DMSO-d_6) δ_H (ppm): 11.47 (s, 1H, OH), 7.86 (s, 1H, HC=N), 7.23-7.15 (m, 2H, Ar-H), 6.82 (d, $J = 8.8$ Hz, 1H, Ar-H), 6.75 (s, 1H, Ar-H), 4.97 (s, 2H, Ar-O-CH_2); ^{13}C NMR (100 MHz, DMSO-d_6) δ_C (ppm): 152.4 (Ar-C), 146.9 (HC=N), 129.2 (Ar-C), 128.8 (Ar-C), 16.6 (Ar-C), 125.1 (Ar-C), 124.7 (Ar-C), 123.4 (Ar-C), 117.2 (Ar-C), 64.1 (Ar-O-CH_2).

*2.2.1.7. 6-bromo-2H-chromene-3-carbaldehyde oxime (**6g**).* Cream Yellow Solid (79%), Melting Point: 183-184°C; ^1H NMR (400 MHz, DMSO-d_6) δ_H (ppm): 11.47 (s, 1H, OH), 7.85 (s, 1H, HC=N), 7.33 (d, $J = 2.8$ Hz, 1H, Ar-H), 7.27 (dd, $J_{12} = 2.4$ Hz, $J_{13} = 8.4$ Hz, 1H, Ar-H), 6.77-6.74 (m, 2H, Ar-H), 4.97 (s, 2H, Ar-O-CH_2); ^{13}C NMR (100 MHz, DMSO-d_6) δ_C (ppm): 152.9 (Ar-C), 146.9 (HC=N), 132.1 (Ar-C), 129.4 (Ar-C), 128.7 (Ar-C), 124.6 (Ar-C), 124.0 (Ar-C), 117.7 (Ar-C), 112.8 (Ar-C), 64.1 (Ar-O-CH_2).

*2.2.1.8. 6-bromo-8-chloro-2H-chromene-3-carbaldehyde oxime (**6h**).* Light Yellow Solid (87%), Melting Point: 176-177°C; ^1H NMR (400 MHz, DMSO-d_6) δ_H (ppm): 11.59 (s, 1H, OH), 7.89 (s, 1H, HC=N), 7.52 (d, $J = 2.4$ Hz, 1H, Ar-H), 7.28 (d, $J = 2$ Hz, 1H, Ar-H), 6.77 (s, 1H, Ar-H), 5.11 (s, 2H, Ar-O-CH_2); ^{13}C NMR (100 MHz, DMSO-d_6) δ_C (ppm): 149.3 (Ar-C), 146.5 (HC=N), 131.5 (Ar-C), 129.5 (Ar-C), 126.1 (Ar-C), 125.5 (Ar-C), 124.3 (Ar-C), 124.1 (Ar-C), 109.5 (Ar-C), 65.1 (Ar-O-CH_2).

*2.2.1.9. 6,8-dichloro-2H-chromene-3-carbaldehyde oxime (**6i**).* Greenish Yellow Solid (83%), Melting Point: 172-173°C; ^1H NMR (400 MHz, DMSO-d_6) δ_H (ppm): 11.59 (s, 1H, OH), 7.89 (s, 1H, HC=N), 7.41 (d, $J = 2.8$ Hz, 1H, Ar-H), 7.25 (d, $J = 2.4$ Hz, 1H, Ar-H), 6.78 (s, 1H, Ar-H), 5.11 (s, 2H, Ar-O-CH_2); ^{13}C NMR (100 MHz, DMSO-d_6) δ_C (ppm): 148.2 (Ar-C), 146.6 (HC=N), 129.5 (Ar-C), 128.8 (Ar-C), 125.6 (Ar-C), 125.1 (Ar-C), 124.4 (Ar-C), 123.9 (Ar-C), 120.4 (Ar-C), 64.9 (Ar-O-CH_2).

*2.2.1.10. 6,8-dibromo-2H-chromene-3-carbaldehyde oxime (**6j**).* Yellow Solid (89%), Melting Point: 179-180°C; ^1H NMR (400 MHz, DMSO-d_6) δ_H (ppm): 11.59 (s, 1H, OH), 7.88 (s, 1H, HC=N), 7.62 (d, $J = 2.0$ Hz, 1H, Ar-H), 7.39 (d, $J = 2.4$ Hz, 1H, Ar-H), 6.77 (s, 1H, Ar-H), 5.11 (s, 2H, Ar-O-CH_2); ^{13}C NMR (100 MHz, DMSO-d_6) δ_C (ppm): 149.7 (Ar-C), 146.5 (HC=N), 134.1 (Ar-C), 129.4 (Ar-C), 128.9 (Ar-C), 124.9 (Ar-C), 123.9 (Ar-C), 112.9 (Ar-C), 109.9 (Ar-C), 65.1 (Ar-O-CH_2).

*2.2.1.11. 6-bromo-8-methoxy-2H-chromene-3-carbaldehyde oxime (**6k**).* Brownish Yellow Solid (91%), Melting Point: 183-184 °C; ^1H NMR (400 MHz, DMSO-d_6) δ_H (ppm): 11.46 (s, 1H, OH), 7.49 (s, 1H, HC=N), 7.05 (d, $J = 1.6$ Hz, 1H, Ar-H), 6.97 (d, $J = 2.4$ Hz, 1H, Ar-H), 6.73 (s, 1H, Ar-H), 4.94 (s, 2H, Ar-O-CH_2), 3.76 (s, 3H, OCH_3); ^{13}C NMR (100 MHz, DMSO-d_6) δ_C (ppm): 148.4 (Ar-C), 146.8 (HC=N), 141.93 (Ar-C), 128.7 (Ar-C), 124.8 (Ar-C), 123.9 (Ar-C), 121.4 (Ar-C), 115.8 (Ar-C), 112.4 (Ar-C), 63.9 (Ar-O-CH_2), 56.1 (OCH_3).

*2.2.1.12. 2-phenyl-2H-chromene-3-carbaldehyde oxime (**6l**).* Light Brown Solid (84%), Melting Point: 156-157°C; ^1H NMR (400 MHz, DMSO-d_6) δ_H (ppm): 11.27 (s, 1H, OH), 7.96 (s, 1H, HC=N), 7.34-7.25 (m, 5H, Ar-H), 7.21 (dd, $J_{12} = 2$Hz, $J_{13} = 7.6$ Hz, 1H, Ar-H), 7.13-7.09 (m, 1H, Ar-H), 7.07 (s, 1H, Ar-H), 6.90-6.86 (m, 1H, Ar-H), 6.73(d, $J = 8$ Hz, 1H, Ar-H), 6.24 (s, 1H, Ar-O-CH); ^{13}C NMR (100 MHz, DMSO-d_6) δ_C (ppm): 152.3 (Ar-C), 147.5 (HC=N), 138.5 (Ar-C), 130.3 (Ar-C), 128.9 (Ar-C), 128.4 (Ar-C), 127.4 (Ar-C), 127.3 (Ar-C), 126.7 (Ar-C), 121.8 (Ar-C), 121.6 (Ar-C), 116.3 (Ar-C), 74.3 (Ar-O-CH).

*2.2.1.13. 8-ethoxy-2-phenyl-2H-chromene-3-carbaldehyde oxime (**6m**).* Brownish Yellow Solid (90%), Melting Point: 163-164°C; ^1H NMR (400 MHz, DMSO-d_6) δ_H (ppm): 11.30 (s, 1H, OH), 7.97 (s, 1H, HC=N), 7.36-7.33 (m, 2H, Ar-H), 7.30-7.24 (m, 3H, Ar-H), 7.02 (s, 1H, Ar-H), 6.86-6.74 (m, 3H, Ar-H), 6.28 (s, 1H, Ar-O-CH), 3.94-3.87 (m, 2H, OCH_2), 1.21 (t, $J = 6.8$ Hz, 3H, CH_3); ^{13}C NMR (100 MHz, DMSO-d_6) δ_C (ppm): 147.7 (Ar-C), 147.1 (HC=N), 141.5 (Ar-C), 138.6 (Ar-C), 129.1 (Ar-C), 128.3 (Ar-C), 127.1 (Ar-C), 126.8 (Ar-C), 122.6 (Ar-C), 121.3 (Ar-C), 119.5 (Ar-C), 115.4 (Ar-C), 73.9 (Ar-O-CH), 64.2 (OCH_2), 14.7 (CH_3) .

*2.2.1.14. 6-bromo-2-phenyl-2H-chromene-3-carbaldehyde oxime (**6n**).* White Solid (81%), Melting Point: 156-157°C; ^1H NMR (400 MHz, DMSO-d_6) δ_H (ppm): 11.41 (s, 1H, OH), 7.94 (s, 1H, HC=N), 7.44 (s, $J = 2.8$ Hz, 1H, Ar-H), 7.32-7.28 (m, 5H, Ar-H), 7.25 (dd, $J_{12} = 2.4$ Hz, $J_{13} = 8.4$ Hz, 1H, Ar-H), 7.06 (s, 1H, Ar-H), 6.70 (d, $J = 8.8$ Hz, 1H, Ar-H), 6.27 (s, 1H, Ar-O-CH); ^{13}C NMR (100 MHz, DMSO-d_6) δ_C (ppm): 151.2 (Ar-C), 147.3 (HC=N), 137.9 (Ar-C), 132.5 (Ar-C), 130.1 (Ar-C), 129.4 (Ar-C), 128.7 (Ar-C), 128.5 (Ar-C), 127.4 (Ar-C), 125.4 (Ar-C), 124.0 (Ar-C), 118.5 (Ar-C), 112.8 (Ar-C), 74.6 (Ar-O-CH).

*2.2.1.15. 6,8-dichloro-2-phenyl-2H-chromene-3-carbaldehyde oxime (**6o**).* Light Yellow Solid (82%), Melting Point: 146-147°C; ^1H NMR (400 MHz, DMSO-d_6) δ_H (ppm): 11.54 (s, 1H, OH), 8.00 (s, 1H, HC=N), 7.38 (d, $J = 2.4$ Hz, 1H, Ar-H), 7.35-7.28 (m, 6H, Ar-H), 7.09 (s, 1H, Ar-H), 6.42 (s, 1H, Ar-O-CH); ^{13}C NMR (100 MHz, DMSO-d_6) δ_C (ppm): 147.1 (Ar-C), 146.6 (HC=N), 137.5 (Ar-C), 131.1 (Ar-C), 129.1 (Ar-C), 128.8 (Ar-C), 128.5 (Ar-C), 127.2 (Ar-C), 125.5 (Ar-C), 125.3 (Ar-C), 124.9 (Ar-C), 121.3 (Ar-C), 75.2 (Ar-O-CH).

2.2.2. Procedure for synthesis of 2H-chromene-3-carbaldehyde O-prop-2-yn-1-yl oximes (8a-o)

In an oven-dried two-necked round bottom flask fitted with an efficient reflux condenser, the synthesised Oxime (1 equiv.) was dissolved

in dry DMF (10 ml) followed by the addition of K_2CO_3 (1.5 equiv.). The reaction mixture was heated to 70-75 °C for 10 min and cooled to room temperature. Then Propargyl bromide (1.3 equiv.) was added dropwise to that reaction mixture. The reaction mixture was stirred at the same temperature in N_2 atmosphere and the reaction progress was monitored by TLC. After consumption of the starting materials (about 1.5 hours), the reaction mixture was diluted with water and extracted with EtOAc. The organic layers were separated, dried over anhydrous Na_2SO_4 and concentrated under reduced pressure [54]. The crude product was purified by general silica gel (100-200 mesh) column chromatography using ethyl acetate/hexane (1:9) to furnish the pure compounds **8a-o** in 72-98% yield. All the compounds were confirmed through ^1H and ^{13}C NMR spectral data.

*2.2.2.1. 2H-chromene-3-carbaldehyde O-prop-2-yn-1-yl oxime (**8a**).* Light Brown Solid (97%), Melting Point: 117-118°C; ^1H NMR (400 MHz, $CDCl_3$) δ_H (ppm): 7.81 (s, 1H, HC=N), 7.19-7.14 (m, 1H, Ar-H), 7.05 (dd, $J_{12} = 1.2$ Hz, $J_{13} = 7.2$ Hz, 1H, Ar-H), 6.91-6.87 (m, 1H, Ar-H), 6.83 (d, $J = 8$ Hz, 1H, Ar-H), 6.61 (s, 1H, Ar-H), 5.04 (s, 2H, Ar-O-CH_2), 4.70 (s, 2H, N-O-CH_2), 2.50 (t, $J = 2.8$ Hz, 1H, C≡CH); ^{13}C NMR (100 MHz, $CDCl_3$) δ_C (ppm): 154.7 (Ar-C), 148.6 (HC=N), 130.6 (Ar-C), 128.9 (Ar-C), 127.7 (Ar-C), 126.4 (Ar-C), 121.7 (Ar-C), 121.7 (Ar-C), 116.0 (Ar-C), 79.3 (C≡CH), 74.9 (C≡CH), 64.3 (Ar-O-CH_2), 62.0 (N-O-CH_2).

*2.2.2.2. 8-methoxy-2H-chromene-3-carbaldehyde O-prop-2-yn-1-yl oxime (**8b**).* Brownish white Solid (98%), Melting Point: 126-127°C; ^1H NMR (400 MHz, $CDCl_3$) δ_H (ppm): 7.81 (s, 1H, HC=N), 6.87-6.82 (m, 2H, Ar-H), 6.69 (dd, $J_{12} = 2.4$ Hz, $J_{13} = 6.8$ Hz, 1H, Ar-H), 6.60 (s, 1H, Ar-H), 5.10 (s, 2H, Ar-O-CH_2), 4.71 (s, 2H, N-O-CH_2), 3.88 (s, 3H, OCH_3), 2.50 (t, $J = 2.4$ Hz, 1H, C≡CH); ^{13}C NMR (100 MHz, $CDCl_3$) δ_C (ppm): 148.4 (Ar-C), 147.7 (HC=N), 143.4 (Ar-C), 128.8 (Ar-C), 126.4 (Ar-C), 122.2 (Ar-C), 121.2 (Ar-C), 119.8 (Ar-C), 113.2 (Ar-C), 79.1 (C≡CH), 74.8 (C≡CH), 64.5 (Ar-O-CH_2), 61.9 (N-O-CH_2), 56.1 (OCH_3).

*2.2.2.3. 8-ethoxy-2H-chromene-3-carbaldehyde O-prop-2-yn-1-yl oxime (**8c**).* Light Brown Solid (95%), Melting Point: 123-125°C; ^1H NMR (400 MHz, $CDCl_3$) δ_H (ppm): 7.80 (s, 1H, HC=N), 6.84-6.80 (m, 2H, Ar-H), 6.71-6.67 (m, 1H, Ar-H), 6.60 (s, 1H, Ar-H), 5.09 (s, 2H, Ar-O-CH_2), 4.71 (s, 2H, N-O-CH_2), 4.10 (q, $J = 6.8$ Hz, 2H, OCH_2), 2.50 (t, $J = 2.0$ Hz, 1H, C≡CH), 1.45 (t, $J = 6.8$ Hz, 3H, CH_3); ^{13}C NMR (100 MHz, $CDCl_3$) δ_C (ppm): 148.5 (Ar-C), 147.1 (HC=N), 143.9 (Ar-C), 131.0 (Ar-C), 129.0 (Ar-C), 128.9 (Ar-C), 126.4 (Ar-C), 122.5 (Ar-C), 121.2 (Ar-C), 119.95 (Ar-C), 114.9 (Ar-C), 79.2 (C≡CH), 74.9 (C≡CH), 64.5 (Ar-O-CH_2), 64.5 (OCH_2), 62.0 (N-O-CH_2), 14.9 (CH_3).

*2.2.2.4. 6-nitro-2H-chromene-3-carbaldehyde O-prop-2-yn-1-yl oxime (**8d**).* Yellow Solid (96%), Melting Point: 131-132°C; ^1H NMR (400 MHz, $CDCl_3$) δ_H (ppm): 8.06 (dd, $J_{12} = 2.8$ Hz, $J_{13} = 9.2$ Hz, 1H, Ar-H), 7.95 (d, $J = 2.8$ Hz, 1H, Ar-H), 7.83 (s, 1H, HC=N), 6.88 (d, $J = 9.2$ Hz, 1H, Ar-H), 6.63 (s, 1H, Ar-H), 5.20 (s, 2H, Ar-O-CH_2) 4.72 (s, 2H, N-O-CH_2), 2.52 (t, $J = 2.4$ Hz, 1H, C≡CH); ^{13}C NMR (100 MHz, $CDCl_3$) δ_C (ppm): 159.6 (Ar-C), 147.5 (HC=N), 128.8 (Ar-C), 127.8 (Ar-C), 126.3 (Ar-C), 123.0 (Ar-C), 121.0 (Ar-C), 116.3 (Ar-C), 78.9 (C≡CH), 75.0 (C≡CH), 65.3 (Ar-O-CH_2), 62.2 (N-O-CH_2).

*2.2.2.5. 3H-benzo[f]chromene-2-carbaldehyde O-prop-2-yn-1-yl oxime (**8e**).* Yellow Solid (81%), Melting Point: 128-129°C; ^1H NMR (400 MHz, $CDCl_3$) δ_H (ppm): 7.96-7.93 (m, 2H, Ar-H, HC=N), 7.76 (d, $J = 8.0$ Hz, 1H, Ar-H), 7.70 (d, $J = 8.8$ Hz, 1H, Ar-H), 7.54-7.50 (m, 1H, Ar-H), 7.40 (m, 1H, Ar-H), 7.30-7.26 (m, 1H, Ar-H), 7.09 (d, $J = 8.8$ Hz, 1H, Ar-H), 5.13 (s, 2H, Ar-O-CH_2), 4.74 (s, 2H, N-O-CH_2), 2.52 (t, $J = 2.4$ Hz, 1H, C≡CH); ^{13}C NMR (100 MHz, $CDCl_3$) δ_C (ppm): 153.5 (Ar-C), 148.8 (HC=N), 130.9 (Ar-C), 130.0 (Ar-C), 129.3 (Ar-C), 128.7 (Ar-C), 127.2 (Ar-C), 125.0 (Ar-C), 124.5 (Ar-C), 124.0 (Ar-C), 121.1 (Ar-C), 117.5 (Ar-C), 114.7 (Ar-C), 79.3 (C≡CH), 74.8 (C≡CH), 64.1 (Ar-O-CH_2), 61.9 (N-O-CH_2).

*2.2.2.6. 6-chloro-2H-chromene-3-carbaldehyde O-prop-2-yn-1-yl oxime (**8f**).* Light Yellow Solid (86%), Melting Point: 123-124°C; ^1H NMR (400 MHz, $CDCl_3$) δ_H (ppm): 7.80 (s, 1H, HC=N), 7.10 (dd, $J_{12} = 2.0$ Hz, $J_{13} = 8.4$ Hz, 1H, Ar-H), 7.02 (d, $J = 2.4$ Hz, 1H, Ar-H), 6.76 (d, $J = 8.8$ Hz, 1H, Ar-H), 6.53 (s, 1H, Ar-H), 5.03 (s, 2H, Ar-O-CH_2), 4.71 (s, 2H, N-O-CH_2), 2.50 (t, $J = 2.0$ Hz, 1H, C≡CH); ^{13}C NMR (100 MHz, $CDCl_3$) δ_C (ppm): 153.0 (Ar-C), 148.1 (HC=N), 129.8 (Ar-C), 127.5 (Ar-C), 126.9 (Ar-C), 126.2 (Ar-C), 122.8 (Ar-C), 117.2 (Ar-C), 79.1 (C≡CH), 74.9 (C≡CH), 64.3 (Ar-O-CH_2), 62.0 (N-O-CH_2).

*2.2.2.7. 6-bromo-2H-chromene-3-carbaldehyde O-prop-2-yn-1-yl oxime (**8g**).* White Solid (83%), Melting Point: 128-129°C; ^1H NMR (400 MHz, $CDCl_3$) δ_H (ppm): 7.79 (s, 1H, HC=N), 7.26-7.22 (m, 1H, Ar-H), 7.15 (d, $J = 2.8$ Hz, 1H, Ar-H), 6.71 (d, $J = 8.8$ Hz, 1H, Ar-H), 6.52 (s, 1H, Ar-H), 5.03 (s, 2H, Ar-O-CH_2), 4.71(s, 2H, N-O-CH_2), 2.49 (t, $J = 2.4$ Hz, 1H, C≡CH); ^{13}C NMR (100 MHz, $CDCl_3$) δ_C (ppm): 153.6 (Ar-C), 148.0 (HC=N), 132.9 (Ar-C), 129.8 (Ar-C), 127.5 (Ar-C), 127.3 (Ar-C), 123.4 (Ar-C), 117.7 (Ar-C), 113.4 (Ar-C), 79.1 (C≡CH), 74.9 (C≡CH), 64.4 (Ar-O-CH_2), 62.0 (N-O-CH_2).

*2.2.2.8. 6-bromo-8-chloro-2H-chromene-3-carbaldehyde O-prop-2-yn-1-yl oxime (**8h**).* Brownish White Solid (86%), Melting Point: 130-131°C; ^1H NMR (400 MHz, $CDCl_3$) δ_H (ppm): 7.81 (s, 1H, HC=N), 7.36 (d, $J = 2.0$ Hz, 1H, Ar-H), 6.98 (d, $J = 2.8$ Hz, 1H, Ar-H), 6.51 (s, 1H, Ar-H), 5.15 (s, 2H, Ar-O-CH_2), 4.72 (s, 2H, N-O-CH_2), 2.51 (t, $J = 2.4$ Hz, 1H, C≡CH); ^{13}C NMR (100 MHz, $CDCl_3$) δ_C (ppm): 149.9 (Ar-C), 147.5 (HC=N), 132.7 (Ar-C), 128.1 (Ar-C), 126.7 (Ar-C), 126.5 (Ar-C), 126.1 (Ar-C), 123.5 (Ar-C), 110.3 (Ar-C), 78.9 (C≡CH), 75.0 (C≡CH), 65.1 (Ar-O-CH_2), 63.2 (N-O-CH_2).

*2.2.2.9. 6,8-dichloro-2H-chromene-3-carbaldehyde O-prop-2-yn-1-yl oxime (**8i**).* White Solid (87%), Melting Point: 124-125°C; ^1H NMR (400 MHz, $CDCl_3$) δ_H (ppm): 7.81 (s, 1H, HC=N), 7.21 (d, $J = 2.4$ Hz, 1H, Ar-H), 6.94 (d, $J = 2.4$ Hz, 1H, Ar-H), 6.52 (s, 1H, Ar-H), 5.15 (s, 2H, Ar-O-CH_2), 4.72 (s, 2H, N-O-CH_2), 2.51 (t, $J = 2.0$ Hz, 1H, C≡CH); ^{13}C NMR (100 MHz, $CDCl_3$) δ_C (ppm): 148.9 (Ar-C), 147.6 (HC=N), 130.0 (Ar-C), 128.1 (Ar-C), 126.6 (Ar-C), 126.0 (Ar-C), 125.4 (Ar-C), 123.6 (Ar-C), 121.7 (Ar-C), 78.9 (C≡CH), 75.0 (C≡CH), 65.0 (Ar-O-CH_2), 62.2 (N-O-CH_2).

*2.2.2.10. 6,8-dibromo-2H-chromene-3-carbaldehyde O-prop-2-yn-1-yl oxime (**8j**).* Yellowish White Solid (91%), Melting Point: 133-134°C; ^1H NMR (400 MHz, $CDCl_3$) δ_H (ppm): 7.81 (s, 1H, HC=N), 7.50 (d, $J = 2.0$ Hz, 1H, Ar-H), 7.11 (d, $J = 2.0$ Hz, 1H, Ar-H), 6.50 (s, 1H, Ar-H), 5.16 (s, 2H, Ar-O-CH_2), 4.72 (s, 2H, N-O-CH_2), 2.50 (t, $J = 2.4$ Hz, 1H, C≡CH); ^{13}C NMR (100 MHz, $CDCl_3$) δ_C (ppm): 150.4 (Ar-C), 147.5 (HC=N), 135.4 (Ar-C), 128.9 (Ar-C), 128.0 (Ar-C), 126.5 (Ar-C), 124.1 (Ar-C), 113.3 (Ar-C), 110.7 (Ar-C), 78.9 (C≡CH), 75.0 (C≡CH), 65.1 (Ar-O-CH_2), 62.2 (N-O-CH_2).

*2.2.2.11. 6-bromo-8-methoxy-2H-chromene-3-carbaldehyde O-prop-2-yn-1-yl oxime (**8k**).* Yellow Solid (89%), Melting Point: 131-132°C; ^1H NMR (400 MHz, $CDCl_3$) δ_H (ppm): 7.80 (s, 1H, HC=N), 6.92 (d, $J = 2.4$ Hz, 1H, Ar-H), 683 (d, $J = 2.0$ Hz, 1H, Ar-H), 6.51 (s, 1H, Ar-H), 5.09 (s, 2H, Ar-O-CH_2), 4.71 (s, 2H, N-O-CH_2), 3.87 (s, 3H, OCH_3), 2.51 (t, $J = 2.0$ Hz, 1H, C≡CH); ^{13}C NMR (100 MHz, $CDCl_3$) δ_C (ppm): 148.5 (Ar-C), 148.0 (HC=N), 142.5 (Ar-C), 127.4 (Ar-C), 127.3 (Ar-C), 123.4 (Ar-C), 121.9 (Ar-C), 116.1 (Ar-C), 113.0 (Ar-C), 79.0 (C≡CH), 74.9 (C≡CH), 64.6 (Ar-O-CH_2), 62.0 (N-O-CH_2), 56.3 (OCH_3).

*2.2.2.12. 2-phenyl-2H-chromene-3-carbaldehyde O-prop-2-yn-1-yl oxime (**8l**).* Brownish yellow Solid (85%), Melting Point: 111-112°C; ^1H NMR (400 MHz, $CDCl_3$) δ_H (ppm): 7.85 (s, 1H, HC=N), 7.41-7.38 (m, 2H, Ar-

H), 7.26-7.23 (m, 3H, Ar-H), 7.16-7.12 (m, 1H, Ar-H), 7.01 (dd, $J_{12} = 1.6$ Hz, $J_{13} = 7.2$ Hz, 1H, Ar-H), 6.89- 6.85 (m, 1H, Ar-H), 6.82-6.79 (m, 2H, Ar-H), 6.33 (s, 1H, Ar-O-CH), 4.61(s, 2H, N-O-CH_2), 2.42 (t, $J = 2.4$ Hz, 1H); ^{13}C NMR (100 MHz, $CDCl_3$) δ_C (ppm): 153.3 (Ar-C), 148.7 (HC=N), 139.2 (Ar-C), 130.9 (Ar-C), 128.7 (Ar-C), 128.2 (Ar-C), 128.2 (Ar-C), 128.18 (Ar-C), 127.5 (Ar-C), 127.3 (Ar-C), 121.4 (Ar-C), 116.7 (Ar-C), 79.2 (C≡CH), 74.9 (C≡CH), 74.7 (Ar-O-CH), 61.9 (N-O-CH_2).

*2.2.2.13. 8-ethoxy-2-phenyl-2H-chromene-3-carbaldehyde O-prop-2-yn-1-yl oxime (**8m**).* Pale Yellow Solid (78%), Melting Point: 112-113°C; ^{1}H NMR (400 MHz, $CDCl_3$) δ_H (ppm): 7.90 (s, 1H, HC=N), 7.47-7.42 (m, 2H, Ar-H), 7.26-7.20 (m, 3H, Ar-H), 6.82-6.78 (m, 3H, Ar-H), 6.75-6.70 (m, 1H, Ar-H), 6.43 (s, 1H, Ar-O-CH), 4.67 (s, 2H, N-O-CH_2), 4.06-3.99 (m, 2H, OCH_2), 2.44 (t, $J = 2.4$ Hz, 1H, C≡CH), 1.36 (t, $J = 7.6$ Hz, 3H, CH_3); ^{13}C NMR (100 MHz, $CDCl_3$) δ_C (ppm): 148.9 (Ar-C), 147.5 (HC=N), 142.9 (Ar-C), 139.1 (Ar-C), 128.9 (Ar-C), 128.4 (Ar-C), 128.1 (Ar-C), 127.0 (Ar-C), 122.5 (Ar-C), 121.1 (Ar-C), 119.9 (Ar-C), 115.8, 79.1 (C≡CH), 74.7 (C≡CH), 74.5 (Ar-O-CH), 64.9 (OCH_2), 61.9 (N-O-CH_2), 14.8 (CH_3).

*2.2.2.14. 6-bromo-2-phenyl-2H-chromene-3-carbaldehyde O-prop-2-yn-1-yl oxime (**8n**).* White Solid (72%), Melting Point: 116-117°C; ^{1}H NMR (400 MHz, $CDCl_3$) δ_H (ppm): 7.84 (s, 1H, HC=N), 7.38-7.34 (m, 2H, Ar-H), 7.28-7.24 (m, 3H, Ar-H), 7.23-7.20 (m, 2H, Ar-H), 6.72 (s, 1H, Ar-H), 6.70-6.68 (m, 1H), 6.33 (s, 1H, Ar-O-CH), 4.61 (s, 2H, N-O-CH_2), 2.42 (t, $J = 2.4$ Hz, 1H, C≡CH); ^{13}C NMR (100 MHz, $CDCl_3$) δ_C (ppm): 152.2 (Ar-C), 148.2 (HC=N), 138.6 (Ar-C), 133.2 (Ar-C), 129.7 (Ar-C), 129.3 (Ar-C), 128.5 (Ar-C), 128.3 (Ar-C), 127.3 (Ar-C), 123.3 (Ar-C), 118.5 (Ar-C), 113.3 (Ar-C), 79.0 (C≡CH), 75.2 (C≡CH), 74.8 (Ar-O-CH), 62.0 (N-O-CH_2).

*2.2.2.15. 6,8-dichloro-2-phenyl-2H-chromene-3-carbaldehyde O-prop-2-yn-1-yl oxime (**8o**).* Light Yellow Solid (83%), Melting Point: 114-115°C; ^{1}H NMR (400 MHz, $CDCl_3$) δ_H (ppm): 7.91 (s, 1H, HC=N), 7.41-7.38 (m, 2H, Ar-H), 7.29-7.25 (m, 3H, Ar-H), 7.18 (d, $J = 2.4$ Hz, 1H, Ar-H), 6.98 (d, $J = 2.8$ Hz, 1H, Ar-H), 6.72 (s, 1H, Ar-H), 6.49 (s, 1H, Ar-O-CH), 4.64 (s, 2H, N-O-CH_2), 2.43 (t, $J = 2.0$ Hz, 1H, C≡CH); ^{13}C NMR (100 MHz, $CDCl_3$) δ_C (ppm): 148.1 (Ar-C), 147.7 (HC=N), 137.9 (Ar-C), 130.4 (Ar-C), 130.3 (Ar-C), 128.5 (Ar-C), 128.3 (Ar-C), 127.0 (Ar-C), 126.8 (Ar-C), 126.1 (Ar-C), 125.3 (Ar-C), 123.9 (Ar-C), 122.6 (Ar-C), 78.9 (C≡CH), 75.3 (C≡CH), 74.9 (Ar-O-CH), 62.2 (N-O-CH_2).

2.2.3. Procedure for synthesis of 2H-chromene-1,2,3-triazolyl glycoconjugates (10a-w)

An oven-dried 10 ml microwave vial was charged with *O*-propargylated chromene derivatives **8a-o** (1 equiv.), sugar azide (1.1 equiv.), sodium ascorbate (0.4 equiv.), and a solvent mixture of CH_3CN and H_2O (2:1 ratio, 2.5 ml). The reaction mixtures were stirred for 2-3 min at room temperature. Then, $CuSO_4.5H_2O$ (0.3 equiv.) was added to it and further stirred for 5 min. Thereafter, the reaction mixtures were microwaved at 100 W pressure and 80°C temperature for 20 min. After completion of the reaction (monitoring by TLC), the reaction mixture was cooled to room temperature and adding ice-cooled water precipitation occurs. The precipitate was filtered and washed with water repeatedly to obtain pure compounds **10a-w** with good to excellent yield (68-98%). The synthesised products were characterised by ^{1}H, ^{13}CNMR, HRMS spectral analysis and confirmed by single crystal X-ray diffraction technique (**10a**).

*2.2.3.1. 5-((4-(((((2H-chromen-3-yl)methylene)amino)oxy)methyl)-1H-1,2,3-triazol-1-yl)methyl)-2,2-dimethyltetrahydrofuro[2,3-d][1,3]dioxol-6-yl 4-methylbenzenesulfonate (**10a**).* Light brown solid (91%), Melting Point: 151-152°C; ^{1}H NMR (400 MHz, $CDCl_3$) δ_H (ppm): 7.83 (d, $J = 8.4$ Hz, 2H, Ar-H), 7.78 (s, 1H, HC=N), 7.67 (s, 1H, Triazole-H), 7.40 (d, $J = 8$ Hz, 2H, Ar-H), 7.17-7.14 (m, 1H, Ar-H), 7.05-7.02 (m, 1H, Ar-H), 6.89-6.86 (m, 1H, Ar-H), 6.82 (d, $J = 8.4$ Hz, 1H, Ar-H), 6.57 (s, 1H, Ar-H), 5.96 (d, $J = 3.6$ Hz, 1H, HC-O), 5.22 (s, 2H, N-O-CH_2), 5.03 (s, 2H, Ar-O-CH_2), 4.87 (d, $J = 2.8$ Hz, 1H, HC-O), 4.69 (d, $J = 3.6$ Hz, 1H), 4.60-4.54 (m, 1H, CH_2), 4.50 (dd, $J_{12} = 3.2$ Hz, $J_{13} = 12.6$ Hz, 1H, HC-O), 4.41-4.37 (m, 1H, HC-O), 2.48 (s, 3H, CH_3), 1.39 (s, 3H, CH_3), 1.25 (s, 3H, CH_3); ^{13}C NMR (100 MHz, $CDCl_3$) δ_C (ppm): 154.6 (Ar-C), 148.2 (HC=N), 146.2 (Ar-C), 144.4 (Triazole-C), 132.3 (Ar-C), 130.5 (Ar-C), 130.4 (Ar-C), 128.5 (Triazole-C), 128.0 (Ar-C), 127.6 (Ar-C), 126.6 (Ar-C), 124.6 (Ar-C), 121.7 (Ar-C), 121.6 (Ar-C), 115.9 (Ar-C), 112.9 (Ar-C), 104.8 (O-CH-O), 83.3 (HC-O), 81.9 (HC-O), 77.6 (HC-O), 67.6 (N-O-CH_2), 64.3 (Ar-O-CH_2), 49.1 (CH_2, O-C-O), 26.5 (CH_3), 26.2 (CH_3), 21.9 (CH_3); HRMS (ESI) calculated for $C_{28}H_{30}N_4O_8S$ $[M + H]^+$ 583.1864, found 583.1879.

*2.2.3.2. 5-((4-(((((8-methoxy-2H-chromen-3-yl)methylene)amino)oxy)methyl)-1H-1,2,3-triazol-1-yl)methyl)-2,2-dimethyltetrahydrofuro[2,3-d][1,3]dioxol-6-yl 4-methylbenzenesulfonate (**10b**).* Brownish yellow solid (94%), Melting Point: 133-134°C; ^{1}H NMR (400 MHz, $CDCl_3$) δ_H (ppm): 7.76 (d, $J = 8.4$ Hz, 2H, Ar-H), 7.71 (s, 1H, HC=N), 7.58 (s, 1H, Triazole-H), 7.33 (d, $J = 6.8$ Hz, 2H, Ar-H), 6.83- 6.74 (m, 2H, Ar-H), 6.61 (dd, $J_{12} = 2.4$ Hz, $J_{13} = 6.4$ Hz, 1H, Ar-H), 6.49 (s, 1H, Ar-H,), 5.89 (d, $J = 3.6$ Hz, 1H, HC-O), 5.16 (s, 2H, N-O-CH_2), 5.02 (s, 2H, Ar-O-CH_2), 4.80 (d, $J = 2.8$ Hz, 1H, HC-O), 4.63 (d, $J = 3.6$ Hz, 1H), 4.51- 4.48 (m, 1H, CH_2), 4.40 (dd, $J_{12} = 3.2$ Hz, $J_{13} = 14$ Hz, 1H, HC-O), 4.33-4.28 (m, 1H, HC-O), 3.81 (s, 3H, OCH_3), 2.41 (s, 3H, CH_3), 1.32 (s, 3H, CH_3), 1.18 (s, 3H, CH_3); ^{13}C NMR (100 MHz, $CDCl_3$) δ_C (ppm): 147.9 (Ar-C), 147.7 (HC=N), 146.1 (Ar-C), 143.4 (Triazole-C), 132.3 (Ar-C), 130.4 (Ar-C), 128.3 (Triazole-C), 127.9 (Ar-C), 126.6 (Ar-C), 124.5 (Ar-C), 122.3 (Ar-C), 121.2 (Ar-C), 119.7 (Ar-C), 113.1 (Ar-C), 112.9 (Ar-C), 104.8 (O-CH-O), 83.2 (HC-O), 81.8 (HC-O), 77.5 (HC-O), 67.6 (N-O-CH_2), 64.5 (Ar-O-CH_2), 56.1 (OCH_3), 48.9 (CH_2, O-C-O), 26.4 (CH_3), 26.1 (CH_3), 21.7 (CH_3); HRMS (ESI) calculated for $C_{29}H_{32}N_4O_9S$ $[M + H]^+$ 613.197, found 613.1993.

*2.2.3.3. 5-((4-(((((6-bromo-2H-chromen-3-yl)methylene)amino)oxy)methyl)-1H-1,2,3-triazol-1-yl)methyl)-2,2-dimethyltetrahydrofuro[2,3-d][1,3]dioxol-6-yl 4-methylbenzenesulfonate (**10c**).* Yellow solid (77%), Melting Point: 117-118°C; ^{1}H NMR (400 MHz, $CDCl_3$) δ_H (ppm): 7.82 (d, $J = 8.4$ Hz, 2H, Ar-H), 7.76 (s, 1H, HC=N), 7.68 (s, 1H, Triazole-H), 7.39 (d, $J =$ Hz, 2H, Ar-H), 7.21 (dd, $J_{12} = 2.0$ Hz, $J_{13} = 8.4$ Hz, 1H, Ar-H), 7.13 (d, $J = 2.0$ Hz, 1H, Ar-H), 6.69 (d, $J = 8.4$ Hz, 1H, Ar-H), 6.48 (s, 1H, Ar-H), 5.95 (d, $J = 4.0$ Hz, 1H, HC-O), 5.22 (s, 2H, N-O-CH_2), 5.02 (s, 2H, Ar-O-CH_2), 4.88 (d, $J = 3.2$ Hz, 1H, HC-O), 4.67 (d, $J = 3.6$ Hz, 1H), 4.59- 4.56 (m, 1H, CH_2), 4.51 (dd, $J_{12} = 4.2$ Hz, $J_{13} = 14.4$ Hz, 1H, HC-O), 4.43-4.37 (m, 1H, HC-O), 2.48 (s, 3H, CH_3), 1.39 (s, 3H, CH_3), 1.25 (s, 3H, CH_3); ^{13}C NMR (100 MHz, $CDCl_3$) δ_C (ppm): 153.4 (Ar-C), 147.5 (HC=N), 146.0 (Ar-C), 132.6 (Ar-C), 132.1 (Ar-C), 130.8 (Ar-C), 130.3 (Ar-C), 129.6 (Ar-C), 128.7 (Triazole-C), 127.8 (Ar-C), 127.5 (Ar-C), 126.7 (Ar-C), 123.3 (Ar-C), 121.7 (Ar-C), 117.5 (Ar-C), 113.1 (Ar-C), 112.7 (Ar-C), 104.6 (O-HC-O), 83.0 (HC-O), 81.7 (HC-O), 77.4 (HC-O), 67.5 (N-O-CH_2), 64.3 (Ar-O-CH_2), 48.8 (CH_2, O-C-O), 26.3 (CH_3), 26.0 (CH_3), 21.7 (CH_3); HRMS (ESI) calculated for $C_{28}H_{29}BrN_4O_8S$ $[M + H]^+$ 661.0969, found 661.0999 and $[M + H + 2]^+$ 663.0977.

*2.2.3.4. 5-((4-(((((6-bromo-8-methoxy-2H-chromen-3-yl)methylene)amino)oxy)methyl)-1H-1,2,3-triazol-1-yl)methyl)-2,2-dimethyltetrahydrofuro[2,3-d][1,3]dioxol-6-yl 4-methylbenzenesulfonate (**10d**).* Yellow solid (80%), Melting Point: 127-128 °C; ^{1}H NMR (400 MHz, $CDCl_3$) δ_H (ppm): 7.82 (d, $J = 6.4$ Hz, 2H, Ar-H), 7.76 (s, 1H, HC=N), 7.65 (s, 1H, Triazole-H), 7.39 (d, $J = 8.4$ Hz, 2H, Ar-H), 6.91-6.90 (m, 1H, Ar-H), 6.81-6.79 (m, 1H, Ar-H), 6.46 (s, 1H, Ar-H), 5.95 (d, $J = 3.6$ Hz, 1H, HC-O), 5.22 (s, 2H, N-O-CH_2), 5.06 (s, 2H, Ar-O-CH_2), 4.86 (d, $J = 2.8$ Hz, 1H, HC-O), 4.68 (d, $J = 4.4$ Hz, 1H), 4.57- 4.54 (m, 1H, CH_2), 4.50-4.46 (m, 1H, HC-O), 4.39-4.34 (m, 1H, HC-O), 3.85 (s, 3H, OCH_3), 2.48 (s, 3H, CH_3), 1.38 (s, 3H, CH_3), 1.24 s, 3H, CH_3); ^{13}C NMR (100 MHz,

$CDCl_3$) δ_C (ppm): 148.4 (Ar-C), 147.6 (HC=N), 146.1 (Ar-C), 144.1 (Triazole-C), 142.5 (Ar-C), 132.2 (Ar-C), 130.4 (Ar-C), 127.9 (Triazole-C), 127.6 (Ar-C), 126.8 (Ar-C), 124.5 (Ar-C), 123.5 (Ar-C), 121.9 (Ar-C), 115.9 (Ar-C), 112.9 (Ar-C), 112.8 (Ar-C), 104.7 (O-CH-O), 83.1 (HC-O), 81.7 (HC-O), 77.5 (HC-O), 67.6 (N-O-CH_2), 64.6 (Ar-O-CH_2), 56.3 (OCH_3), 48.9 (CH_2, O-C-O), 26.4 (CH_3), 26.1 (CH_3), 21.7 (CH_3); HRMS (ESI) calculated for $C_{29}H_{31}BrN_4O_9S$ $[M + H]^+$ 691.1075, found 691.1066.

*2.2.3.5. (2S,3S,4S,5S,6S)-2-(4-(((((2H-chromen-3-yl)methylene)amino) oxy)methyl)-1H-1,2,3-triazol-1-yl)-6-(acetoxymethyl)tetrahydro-2H-pyran-3,4,5-triyl triacetate (**10e**).* Light brown solid (91%), Melting Point: 191-192°C; ^{1}H NMR (400 MHz, $CDCl_3$) δ_H (ppm): 7.79-7.78 (m, 2H, HC=N, Triazole-H), 7.22-6.81 (m, 4H, Ar-H), 6.58 (s, 1H, Ar-H), 5.89 (d, J = 6.8 Hz, 1H, CH), 5.46-5.41 (m, 3H, HC-O), 5.24 (s, 2H, N-O-CH_2), 5.03 (s, 2H, Ar-O-CH_2), 4.30-3.90 (m, 3H, CH, O-CH_2), 2.07 (s, 6H, CH_3, CH_3), 2.02 (s, 3H, CH_3), 1.86 (s, 3H, CH_3); ^{13}C NMR (100 MHz, $CDCl_3$) δ_C (ppm): 170.5 (C=O), 169.9 (C=O), 169.3 (C=O), 168.8 (C=O), 154.5 (Ar-C), 148.2 (HC=N), 145.0 (Triazole-C), 130.3 (Ar-C), 128.5 (Triazole-C), 127.5 (Ar-C), 126.4 (Ar-C), 121.6 (Ar-C), 121.5 (Ar-C), 121.4 (Ar-C), 115.9 (Ar-C), 85.7 (CH), 75.1 (CH), 72.6 (HC-O), 70.0 (HC-O), 67.6 (HC-O), 67.3 (N-O-CH_2), 64.2 (Ar-O-CH_2), 61.4 (O-CH_2), 20.6 (CH_3), 20.5 (CH_3, CH_3), 20.1 (CH_3); HRMS (ESI) calculated for $C_{27}H_{30}N_4O_{11}$ $[M + H]^+$ 587.1991, found 587.1974.

*2.2.3.6. (2S,3S,4S,5S,6S)-2-(acetoxymethyl)-6-(4-(((((8-methoxy-2H-chromen-3-yl)methylene)amino)oxy)methyl)-1H-1,2,3-triazol-1-yl)tetrahydro-2H-pyran-3,4,5-triyl triacetate (**10f**).* Light brown solid (98%), Melting Point: 194-195°C; ^{1}H NMR (400 MHz, $CDCl_3$) δ_H (ppm): 7.80-7.79 (m, 2H, HC=N, Triazole-H), 6.85-6.82 (m, 2H, Ar-H,), 6.70-6.67 (m, 1H, Ar-H), 6.57 (s, 1H, Ar-H), 5.87 (d, J = 9.2 Hz, 1H, CH), 5.47-5.39 (m, 1H, HC-O), 5.26-5.19 (m, 3H, HC-O, N-O-CH_2), 5.10 (s, 2H, Ar-O-CH_2), 4.29 (dd, J_{12} = 5.2 Hz, J_{13} = 12.8 Hz, 1H, CH), 4.19-4.13 (m, 1H), 4.02-3.96 (m, 1H, O-CH_2), 3.87 (s, 3H, OCH_3), 2.07 (s, 3H, CH_3), 2.06 (s, 3H, CH_3), 2.03 (s, 3H, CH_3), 1.85 (s, 3H, CH_3); ^{13}C NMR (100 MHz, $CDCl_3$) δ_C (ppm): 170.5 (C=O), 169.9 (C=O), 169.3 (C=O), 168.8 (C=O), 148.1 (HC=N), 147.8(Ar-C), 144.9 (Triazole-C), 143.4 (Ar-C), 128.4 (Triazole-C), 126.6 (Ar-C), 122.3 (Ar-C), 121.4 (Ar-C), 121.2 (Ar-C), 119.8 (Ar-C), 113.2 (Ar-C), 85.7 (CH), 75.2 (CH), 72.6 (HC-O), 70.1 (HC-O), 67.7 (HC-O), 67.4 (N-O-CH_2), 64.5 (Ar-O-CH_2), 61.5 (O-CH_2), 56.1 (OCH_3), 20.6 (CH_3), 20.5 (CH_3, CH_3), 20.1 (CH_3); HRMS (ESI) calculated for $C_{28}H_{32}N_4O_{12}$ $[M + H]^+$ 617.2097, found 617.2101.

*2.2.3.7. (2S,3S,4S,5S,6S)-2-(acetoxymethyl)-6-(4-(((((8-ethoxy-2H-chromen-3-yl)methylene)amino)oxy)methyl)-1H-1,2,3-triazol-1-yl)tetrahydro-2H-pyran-3,4,5-triyl triacetate (**10g**).* Light Yellow solid (92%), Melting Point: 185-186°C; ^{1}H NMR (400 MHz, $CDCl_3$) δ_H (ppm): 7.80-7.79 (m, 2H, HC=N, Triazole-H), 6.81-6.80 (m, 2H, Ar-H), 6.68-6.63 (m, 1H, Ar-H), 6.56 (s, 1H, Ar-H), 5.87 (d, J = 8.8 Hz, 1H, CH), 5.48-5.39 (m, 2H, HC-O), 5.27-5.19 (m, 3H, N-O-CH_2, HC-O), 5.09 (s, 2H, Ar-O-CH_2), 4.31-3.99 (m, 5H, CH, O-CH_2, OCH_2), 2.07 (s, 6H, CH_3, CH_3), 2.02 (s, 3H, CH_3), 1.85 (s, 3H, CH_3), 1.44 (t, J = 6.8 Hz, 3H, CH_3); ^{13}C NMR (100 MHz, $CDCl_3$) δ_C (ppm): 170.5 (C=O), 169.9 (C=O), 169.3 (C=O), 168.3 (C=O), 148.1 (HC=N), 147.0 (Ar-C), 144.9 (Triazole-C), 130.9 (Ar-C), 128.8 (Ar-C), 128.5 (Triazole-C), 126.4 (Ar-C), 121.5 (Ar-C), 121.1 (Ar-C), 119.8 (Ar-C), 114.7 (Ar-C), 85.7 (CH), 75.1 (CH), 72.6 (HC-O), 70.1 (HC-O), 67.6 (HC-O), 67.4 (N-O-CH_2), 64.6 (Ar-O-CH_2), 64.4 (OCH_2), 61.4 (O-CH_2), 20.6 (CH_3), 20.5 (CH_3), 20.1 (CH_3), 14.8 (CH_3); HRMS (ESI) calculated for $C_{29}H_{34}N_4O_{12}$ $[M + H]^+$ 631.2253, found 631.2252.

*2.2.3.8. (2S,3S,4S,5S,6S)-2-(acetoxymethyl)-6-(4-(((((6-nitro-2H-chromen-3-yl)methylene)amino)oxy)methyl)-1H-1,2,3-triazol-1-yl)tetrahydro-2H-pyran-3,4,5-triyl triacetate (**10h**).* Redish brown solid (92%), Melting Point: 179-180°C; ^{1}H NMR (400 MHz, $CDCl_3$) δ_H (ppm): 8.05-8.03 (m, 1H, Ar-H), 7.94-7.80 (m, 2H, HC=N, Triazole-H), 6.87 (d, J = 9.2 Hz, 1H, Ar-H), 6.59 (s, 1H, Ar-H), 5.89 (d, J = 8.4 Hz, 1H, CH), 5.46-5.40 (m, 2H, Ar-H A), 5.31-5.21 (m, 3H, N-O-CH_2, HC-O), 5.18 (s, 2H, Ar-O-CH_2), 4.32-4.27 (m, 2H, O-CH_2), 4.14 (d, J = 12.4 Hz, 1H, CH), 4.02-3.99 (m, 1H, CH-O), 2.07 (s, 6H, CH_3, CH_3), 2.02 (s, 3H, CH_3), 1.86 (s, 3H, CH_3); ^{13}C NMR (100 MHz, $CDCl_3$) δ_C (ppm): 170.5 (C=O), 169.8 (C=O), 169.4 (C=O), 168.9 (C=O), 159.6 (Ar-C), 147.3 (HC=N), 144.7 (Triazole-C), 141.9 (Ar-C), 130.9 (Ar-C), 128.0 (Triazole-C), 126.0 (Ar-C), 122.9 (Ar-C), 121.4 (Ar-C), 121.1 (Ar-C), 116.3 (Ar-C), 85.7 (CH), 75.1 (CH), 72.5 (HC-O), 70.1 (HC-O), 67.6 (N-O-CH_2), 65.5 (HC-O), 65.3 (Ar-O-CH_2), 61.5 (O-CH_2), 20.6 (CH_3), 20.5 (CH_3), 20.5 (CH_3), 20.1 (CH_3); HRMS (ESI) calculated for $C_{27}H_{29}N_5O_{13}$ $[M + H]^+$ 632.1847, found 632.1840.

*2.2.3.9. (2S,3S,4S,5S,6S)-2-(4-(((((3H-benzo[f]chromen-2-yl)methylene)amino)oxy)methyl)-1H-1,2,3-triazol-1-yl)-6-(acetoxymethyl)tetrahydro-2H-pyran-3,4,5-triyl triacetate (**10i**).* Deep brown solid (93%), Melting Point: 193-194°C; ^{1}H NMR (400 MHz, $CDCl_3$) δ_H (ppm): 8.01-7.67 (m, 6H, Ar-H, HC=N, Triazole-H), 7.52-7.34 (m, 2H, Ar-H), 7.08 (d, J = 8.0 Hz, 1H, Ar-H), 5.89 (d, J = 8.8 Hz, 1H, CH), 5.49-5.40 (m, 2H, HC-O), 5.27-5.22 (m, 3H, N-O-CH_2, HC-O), 5.12 (s, 2H, Ar-O-CH_2), 4.32-4.28 (m, 1H, CH), 4.15 (d, J = 12.4 Hz, 1H), 4.01-3.99 (m, 1H, O-CH_2), 2.07 (s, 6H, CH_3, CH_3), 2.02 (s, 3H, CH_3), 1.86 (s, 3H, CH_3); ^{13}C NMR (100 MHz, $CDCl_3$) δ_C (ppm): 170.5 (C=O), 169.9 (C=O), 169.3 (C=O), 168.9 (C=O), 153.4 (Ar-C), 148.6 (HC=N), 145.1 (Triazole-C), 130.8 (Ar-C), 129.9 (Ar-C), 129.3 (Ar-C), 128.7 (Triazole-C), 127.1 (Ar-C), 124.7 (Ar-C), 124.6 (Ar-C), 124.0 (Ar-C), 121.4 (Ar-C), 121.0 (Ar-C), 117.5 (Ar-C), 114.7 (Ar-C), 85.7 (CH), 75.1 (CH), 72.6 (HC-O), 70.0 (HC-O), 67.6 (HC-O), 67.4 (N-O-CH_2), 64.1 (Ar-O-CH_2), 61.5 (O-CH_2), 20.6 (CH_3), 20.5 (CH_3, CH_3), 20.1 (CH_3); HRMS (ESI) calculated for $C_{31}H_{32}N_4O_{11}$ $[M + H]^+$ 637.2148, found 637.2145.

*2.2.3.10. (2S,3S,4S,5S,6S)-2-(acetoxymethyl)-6-(4-(((((6-chloro-2H-chromen-3-yl)methylene)amino)oxy)methyl)-1H-1,2,3-triazol-1-yl)tetrahydro-2H-pyran-3,4,5-triyl triacetate (**10j**).* Pale yellow solid (73%), Melting Point: 181-182°C; ^{1}H NMR (400 MHz, $CDCl_3$) δ_H (ppm): 7.79-7.77 (m, 2H, HC=N, Triazole-H), 7.11-7.07 (m, 1H, Ar-H), 7.00-6.99 (m, 1H, Ar-H), 6.75 (d, J = 8.8 Hz, 1H, Ar-H), 6.50 (s, 1H, Ar-H), 5.88 (d, J = 8.4 Hz, 1H, CH), 5.47-5.40 (m, 2H, HC-O), 5.26-5.21 (m, 3H, N-O-CH_2, HC-O), 5.02 (s, 2H, Ar-O-CH_2), 4.32-4.27 (m, 1H, CH), 4.14 (d, J = 11.6 Hz, 1H), 4.02-3.98 (m, 1H, O-CH_2), 2.07 (s, 3H, CH_3), 2.06 (s, 3H, CH_3), 2.02 (s, 3H, CH_3), 1.85 (s, 3H, CH_3); ^{13}C NMR (100 MHz, $CDCl_3$) δ_C (ppm): 170.5 (C=O), 169.9 (C=O), 169.3 (C=O), 168.9 (C=O), 153.0 (Ar-C), 147.8 (HC=N), 144.9 (Triazole-C), 129.8 (Ar-C), 127.6 (Triazole-C), 127.1 (Ar-C), 126.8 (Ar-C), 126.2 (Ar-C), 122.7 (Ar-C), 121.4 (Ar-C), 117.2 (Ar-C), 85.7 (CH), 75.1 (CH), 72.6 (HC-O), 70.0 (HC-O), 67.6 (HC-O), 67.4 (N-O-CH_2), 64.3 (Ar-O-CH_2), 61.5 (O-CH_2), 20.6 (CH_3), 20.5 (CH_3, CH_3), 20.1 (CH_3); HRMS (ESI) calculated for $C_{27}H_{29}ClN_4O_{11}$ $[M + H]^+$ 621.1601, found 621.1600 and $[M + H + 2]^+$ 623.1586.

*2.2.3.11. (2S,3S,4S,5S,6S)-2-(acetoxymethyl)-6-(4-(((((6-bromo-2H-chromen-3-yl)methylene)amino)oxy)methyl)-1H-1,2,3-triazol-1-yl)tetrahydro-2H-pyran-3,4,5-triyl triacetate (**10k**).* Light brown solid (81%), Melting Point: 188-189°C; ^{1}H NMR (400 MHz, $CDCl_3$) δ_H (ppm): 7.79-7.77 (m, 2H, HC=N, Triazole-H), 7.24-7.18 (m, 1H, Ar-H), 7.15- 7.13 (m, 1H, Ar-H), 6.70 (d, J = 8.8 Hz, 1H, Ar-H), 6.49 (s, J = Hz, 1H, Ar-H), 5.88 (d, J = 8.8 Hz, 1H, CH), 5.47-5.40 (m, 2H, HC-O), 5.25-5.22 (m, 3H, N-O-CH_2, HC-O), 5.02 (s, 2H, Ar-O-CH_2), 4.29 (dd, J_{12} = 4.8 Hz, J_{13} = 14.6 Hz, 1H, CH), 4.15- 4.12 (m, 1H), 4.02-3.99 (m, 1H, O-CH_2), 2.07 (s, 3H, CH_3), 2.06 (s, 3H, CH_3), 2.02 (s, 3H, CH_3), 1.85 (s, 3H, CH_3); ^{13}C NMR (100 MHz, $CDCl_3$) δ_C (ppm): 170.5 (C=O), 169.8 (C=O), 169.4 (C=O), 168.9 (C=O), 153.5 (Ar-C), 147.8 (HC=N), 144.9 (Triazole-C), 132.7 (Ar-C), 129.7 (Ar-C), 127.6 (Triazole-C), 126.9 (Ar-C), 123.4 (Ar-C), 121.4 (Ar-C), 117.6 (Ar-C), 113.4 (Ar-C), 85.7 (CH), 75.1 (CH), 72.6 (HC-O), 70.0 (HC-O), 67.6 (HC-O), 67.5 (N-O-CH_2), 64.3 (Ar-O-CH_2),

61.5 (O-CH_2), 20.7 (CH_3), 20.5 (CH_3, CH_3), 20.1 (CH_3); HRMS (ESI) calculated for $C_{27}H_{29}BrN_4O_{11}$ $[M + H]^+$ 665.1096, found 665.1094, and $[M + H + 2]^+$ 667.1083.

*2.2.3.12. (2S,3S,4S,5S,6S)-2-(acetoxymethyl)-6-(4-(((((8-bromo-6-chloro-2H-chromen-3-yl)methylene)amino)oxy)methyl)-1H-1,2,3-triazol-1-yl)tetrahydro-2H-pyran-3,4,5-triyl triacetate (**10l**).* Pale yellow solid (86%), Melting Point: 185-186°C; ^{1}H NMR (400 MHz, $CDCl_3$) δ_H (ppm): 7.79-7.78 (m, 2H, HC=N, Triazole-H), 7.35 (s, 1H, Ar-H), 6.96 (d, J = 2.4 Hz, 1H, Ar-H), 6.47 (s, 1H, Ar-H), 5.88 (d, J = 8.8 Hz, 1H, CH), 5.47-5.40 (m, 2H, HC-O), 5.27-5.22 (m, 3H, N-O-CH_2, HC-O), 5.13 (s, 2H, Ar-O-CH_2), 4.30 (dd, J_{12} = 4.8 Hz, J_{13} = 12.4 Hz, 1H, CH), 4.15 (d, J = 12.0 Hz, 1H), 4.02-3.99 (m, 1H, O-CH_2), 2.07 (s, 3H, CH_3), 2.06 (s, 3H, CH_3), 2.03 (s, 3H, CH_3), 1.86 (s, 3H, CH_3); ^{13}C NMR (100 MHz, $CDCl_3$) δ_C (ppm): 170.5 (C=O), 169.9 (C=O), 169.3 (C=O), 168.9 (C=O), 149.9 (Ar-C), 147.3 (HC=N), 144.7 (Triazole-C), 132.7 (Ar-C), 128.2 (Triazole-C), 126.4 (Ar-C), 126.3 (Ar-C), 126.0 (Ar-C), 123.6 (Ar-C), 121.5 (Ar-C), 110.3 (Ar-C), 85.7 (CH), 75.2 (CH), 72.6 (HC-O), 70.1 (HC-O), 67.6 (HC-O), 67.5 (N-O-CH_2), 65.1 (Ar-O-CH_2), 61.5 (O-CH_2), 20.7 (CH_3), 20.5 (CH_3, CH_3), 20.1 (CH_3); HRMS (ESI) calculated for $C_{27}H_{28}BrClN_4O_{11}$ $[M + H]^+$ 699.0706, found 699.0703, $[M + H + 2]^+$ 701.0678 and $[M + H + 4]^+$ 703.0673.

*2.2.3.13. (2S,3S,4S,5S,6S)-2-(acetoxymethyl)-6-(4-(((((6,8-dichloro-2H-chromen-3-yl)methylene)amino)oxy)methyl)-1H-1,2,3-triazol-1-yl)tetrahydro-2H-pyran-3,4,5-triyl triacetate (**10m**).* Brownish white solid (68%), Melting Point: 176-177°C; ^{1}H NMR (400 MHz, $CDCl_3$) δ_H (ppm): 7.79-7.78 (m, 2H, HC=N, Triazole-H), 7.19-7.16 (m, 1H, Ar-H), 6.92 (d, J = 1.6 Hz, 1H, Ar-H), 6.48 (s, 1H, Ar-H), 5.88 (d, J = 8.8 Hz, 1H, CH), 5.47-5.39 (m, 2H, HC-O), 5.25-5.22 (m, 3H, N-O-CH_2, HC-O), 5.13 (s, 2H, Ar-O-CH_2), 4.30 (dd, J_{12} = 4.8 Hz, J_{13} = 12.4 Hz, 1H, CH), 4.14 (d, J = 11.6 Hz, 1H), 4.02-3.99 (m, 1H, O-CH_2), 2.07 (s, 3H, CH_3), 2.06 (s, 3H, CH_3), 2.02 (s, 3H, CH_3), 1.86 (s, 3H, CH_3); ^{13}C NMR (100 MHz, $CDCl_3$) δ_C (ppm): 170.5 (C=O), 169.9 (C=O), 169.3 (C=O), 168.9 (C=O), 148.8 (Ar-C), 147.3 (HC=N), 144.7 (Triazole-C), 129.9 (Ar-C), 128.2 (Triazole-C), 126.3 (Ar-C), 125.9 (Ar-C), 125.4 (Ar-C), 123.6 (Ar-C), 121.7 (Ar-C), 121.5 (Ar-C), 85.7 (CH), 75.1 (CH), 72.6 (HC-O), 70.1 (HC-O), 67.6 (HC-O), 67.5 (N-O-CH_2), 64.9 (Ar-O-CH_2), 61.4 (O-CH_2), 20.6 (CH_3), 20.5 (CH_3, CH_3), 20.1 (CH_3); HRMS (ESI) calculated for $C_{27}H_{28}Cl_2N_4O_{11}$ $[M + H]^+$ 655.1212, found 655.1210 and $[M + H + 2]^+$ 657.1189.

*2.2.3.14. (2S,3S,4S,5S,6S)-2-(acetoxymethyl)-6-(4-(((((6,8-dibromo-2H-chromen-3-yl)methylene)amino)oxy)methyl)-1H-1,2,3-triazol-1-yl)tetrahydro-2H-pyran-3,4,5-triyl triacetate (**10n**).* Brownish yellow solid (88%), Melting Point: 194-195°C; ^{1}H NMR (400 MHz, $CDCl_3$) δ_H (ppm): 7.79-7.78 (m, 2H, HC=N, Triazole-H), 7.49-7.48 (m, 1H, Ar-H), 7.14-7.10 (m, 1H, Ar-H), 6.47 (s, 1H, Ar-H), 5.88 (d, J = 8.8 Hz, 1H, CH), 5.48-5.39 (m, 2H, HC-O), 5.27-5.22 (m, 3H, N-O-CH_2, HC-O), 5.14 (s, 2H, Ar-O-CH_2), 4.30 (dd, J_{12} = 4.8 Hz, J_{13} = 12.4 Hz, 1H, CH), 4.15 (d, J = 12.0 Hz, 1H), 4.02-3.98 (m, 1H, O-CH_2), 2.08 (s, 3H, CH_3), 2.07 (s, 3H, CH_3), 2.03 (s, 3H, CH_3), 1.86 (s, 3H, CH_3); ^{13}C NMR (100 MHz, $CDCl_3$) δ_C (ppm): 170.5 (C=O), 169.9 (C=O), 169.3 (C=O), 168.9 (C=O), 150.3 (Ar-C), 147.3 (HC=N), 144.7 (Triazole-C), 135.3 (Ar-C), 128.9 (Ar-C), 128.2 (Triazole-C), 126.2 (Ar-C), 124.1 (Ar-C), 121.4 (Ar-C), 113.3 (Ar-C), 110.7 (Ar-C), 85.7 (CH), 75.2 (CH), 72.6 (HC-O), 70.1 (HC-O), 67.6 (HC-O), 67.5 (N-O-CH_2), 65.1 (Ar-O-CH_2), 61.5 (O-CH_2), 20.7 (CH_3), 20.5 (CH_3, CH_3), 20.1 (CH_3); HRMS (ESI) calculated for $C_{27}H_{28}Br_2N_4O_{11}$ $[M + H]^+$ 745.0181, found 745.0182 $[M + H + 2]^+$ 747.0168.

*2.2.3.15. (2S,3S,4S,5S,6S)-2-(acetoxymethyl)-6-(4-(((((6-bromo-8-methoxy-2H-chromen-3-yl)methylene)amino)oxy)methyl)-1H-1,2,3-triazol-1-yl)tetrahydro-2H-pyran-3,4,5-triyl triacetate (**10o**).* Yellow solid (90%), Melting Point: 187-188°C; ^{1}H NMR (400 MHz, $CDCl_3$) δ_H (ppm): 7.78-7.77 (m, 2H, HC=N, Triazole-H), 6.90 (s, 1H, Ar-H), 6.82 (s, 1H, Ar-H), 6.47 (s, 1H, Ar-H), 5.87 (d, J = 8.8 Hz, 1H, CH), 5.46-5.38 (m, 2H, HC-O), 5.24-5.18 (m, 3H, N-O-CH_2, HC-O), 5.08 (s, 2H, Ar-O-CH_2), 4.31-4.27 (m, 1H, CH), 4.15-3.98 (m, 2H, O-CH_2), 3.85 (s, 3H, OCH_3), 2.07 (s, 3H, CH_3), 2.06 (s, 3H, CH_3), 2.02 (s, 3H, CH_3), 1.85 (s, 3H, CH_3); ^{13}C NMR (100 MHz, $CDCl_3$) δ_C (ppm): 170.5 (C=O), 169.9 (C=O), 169.3 (C=O), 168.8 (C=O), 148.5 (Ar-C), 147.7 (HC=N), 144.8 (Triazole-C), 142.5 (Ar-C), 127.5 (Triazole-C), 126.9 (Ar-C), 123.4 (Ar-C), 121.9 (Ar-C), 121.4 (Ar-C), 116.0 (Ar-C), 112.9 (Ar-C), 85.7 (CH), 75.1 (CH), 72.6 (HC-O), 70.1 (HC-O), 67.6 (HC-O), 67.5 (N-O-CH_2), 64.5 (Ar-O-CH_2), 61.5 (O-CH_2), 56.3 (O-CH_3), 20.6 (CH_3), 20.5 (CH_3, CH_3), 20.1 (CH_3); HRMS (ESI) calculated for $C_{28}H_{31}BrN_4O_{12}$ $[M + H]^+$ 695.1202, found 695.1200.

*2.2.3.16. (2S,3S,4S,5S,6S)-2-(acetoxymethyl)-6-(4-(((((2-phenyl-2H-chromen-3-yl)methylene)amino)oxy)methyl)-1H-1,2,3-triazol-1-yl)tetrahydro-2H-pyran-3,4,5-triyl triacetate (**10p**).* Light brown solid (93%), Melting Point: 192-193°C; ^{1}H NMR (400 MHz, $CDCl_3$) δ_H (ppm): 7.85-784 (m, 1H, Ar-H), 7.41-7.30 (m, 6H, HC=N, Triazole-H, Ar-H), 7.18-7.07 (m, 2H, Ar-H), 6.92-6.83 (m, 1H, Ar-H), 6.81-6.56 (m, 2H, Ar-H), 6.32 (d, J = 13.2 Hz, 1H, CH), 5.79-5.76 (m, 1H, HC-O), 5.57-5.04 (m, 5H, Ar-O-CH, N-O-CH_2, HC-O), 4.34-4.23 (m, 1H, CH), 4.17-4.10 (m, 1H), 3.99-3.95 (m, 1H, O-CH_2), 2.07 (s, 3H, CH_3), 2.06 (s, 3H, CH_3), 2.04 (s, 3H, CH_3), 1.84 (s, 3H, CH_3); ^{13}C NMR (100 MHz, $CDCl_3$) δ_C (ppm): 170.5 (C=O), 169.9 (C=O), 169, .4 (C=O), 168.8 (C=O), 152.9 (Ar-C), 148.5 (HC=N), 145.1 (Ar-C), 144.9 (Triazole-C), 139.1 (Ar-C), 130.8 (Ar-C), 128.7 (Ar-C), 128.4 (Triazole-C), 127.9 (Ar-C), 127.5 (Ar-C), 121.5 (Ar-C), 121.4 (Ar-C), 116.7 (Ar-C), 85.5 (CH), 75.0 (CH), 72.7 (Ar-O-CH), 72.6 (HC-O), 70.1 (HC-O), 69.8 (HC-O), 67.6 (N-O-CH_2), 61.5 (O-CH_2), 20.7 (CH_3), 20.5 (CH_3, CH_3), 20.1 (CH_3); HRMS (ESI) calculated for $C_{33}H_{34}N_4O_{11}$ $[M + H]^+$ 663.2304, found 663.2302.

*2.2.3.17. (2S,3S,4S,5S,6S)-2-(acetoxymethyl)-6-(4-(((((8-ethoxy-2-phenyl-2H-chromen-3-yl)methylene)amino)oxy)methyl)-1H-1,2,3-triazol-1-yl)tetrahydro-2H-pyran-3,4,5-triyl triacetate (**10q**).* Greenish yellow solid (87%), Melting Point: 188-189°C; ^{1}H NMR (400 MHz, $CDCl_3$) δ_H (ppm): 7.90-7.88 (m, 1H, Ar-H), 7.49-7.40 (m, 3H, HC=N, Triazole-H, Ar-H), 7.34-7.29 (m, 3H, Ar-H), 6.81-6.77 (m, 3H, Ar-H), 6.75-6.71 (m, 1H, Ar-H), 6.42 (d, J = 8.0 Hz, 1H, CH), 5.79-5.75 (m, 1H, HC-O), 5.42-5.21 (m, 3H, Ar-O-CH, HC-O), 5.17 (s, 2H, N-O-CH_2), 4.32-4.26 (m, 1H), 4.18-4.08 (m, 1H, O-CH_2), 4.07-3.97 (m, 3H, CH, OCH_2), 2.07 (s, 3H, CH_3), 2.06 (s, 3H, CH_3), 2.03 (s, 3H, CH_3), 1.86 (s, 3H, CH_3); ^{13}C NMR (100 MHz, $CDCl_3$) δ_C (ppm): 170.5 (C=O), 169.9 (C=O), 169.4 (C=O), 168.8 (C=O), 148.7 (Ar-C), 147.5 (HC=N), 145.1 (Triazole-C), 142.6 (Ar-C), 138.9 (Ar-C), 128.9 (Ar-C), 128.2 (Triazole-C), 127.3 (Ar-C), 122.5 (Ar-C), 121.5 (Ar-C), 121.4 (Ar-C), 121.1 (Ar-C), 119.9 (Ar-C), 116.0 (Ar-C), 115.8 (Ar-C), 85.6 (CH), 75.0 (CH), 72.7 (Ar-O-CH), 72.6 (HC-O), 70.1 (HC-O), 69.9 (HC-O), 67.6 (N-O-CH_2), 64.9 (OCH_2), 61.5 (O-CH_2), 20.7 (CH_3), 20.5 (CH_3, CH_3), 20.1 (CH_3), 14.8 (CH_3); HRMS (ESI) calculated for $C_{35}H_{38}N_4O_{12}$ $[M + H]^+$ 707.2566, found 707.2565.

*2.2.3.18. (2S,3S,4S,5S,6S)-2-(acetoxymethyl)-6-(4-(((((6-bromo-2-phenyl-2H-chromen-3-yl)methylene)amino)oxy)methyl)-1H-1,2,3-triazol-1-yl)tetrahydro-2H-pyran-3,4,5-triyl triacetate (**10r**).* Pale yellow solid (77%), Melting Point: 184-185°C; ^{1}H NMR (400 MHz, $CDCl_3$) δ_H (ppm): 7.84-7.83 (m, 1H, Ar-H), 7.41-7.31 (m, 6H, HC=N, Triazole-H, Ar-H), 7.22-7.18 (m, 2H, Ar-H), 6.73 (d, J = 2.8 Hz, 1H, Ar-H), 6.66 (d, J = 8.4 Hz, 1H, Ar-H), 6.34-6.30 (m, 1H, CH), 5.80-5.77 (m, 1H, HC-O), 5.56-5.06 (m, 5H, Ar-O-CH, N-O-CH_2, HC-O), 4.30-4.24 (m, 1H, CH), 4.16-4.11 (m, 1H), 4.02-3.86 (m, 1H, O-CH_2), 2.08 (s, 3H, CH_3), 2.07 (s, 3H, CH_3), 2.03 (s, 3H, CH_3), 1.86 (s, 3H, CH_3); ^{13}C NMR (100 MHz, $CDCl_3$) δ_C (ppm): 170.5 (C=O), 169.9 (C=O), 169.4 (C=O), 168.9 (C=O), 151.9 (Ar-C), 148.1 (HC=N), 145.0 (Triazole-C), 138.5 (Ar-C), 133.2 (Ar-C), 129.7 (Ar-C), 128.7 (Ar-C), 128.5 (Triazole-C), 127.3 (Ar-C), 121.4 (Ar-C), 121.3 (Ar-C), 118.6 (Ar-C), 113.4 (Ar-C), 85.6 (CH), 75.0 (CH), 72.9 (Ar-O-CH), 72.8 (HC-O), 70.6 (HC-O), 70.5 (HC-O), 67.6

Table 1
Crystallographic data and refinement parameters of compound **10a**.

Parameter	Compound 10a
CCDC No.	2314962
Empirical formula	$C_{28}H_{30}N_4O_8S_1$
Formula weight [g/mol]	582.62
Temperature [K]	295.15
Crystal system	triclinic
Space group	P1(No. 1)
Cell lengths (a, b, c) [Å]	6.0527(2), 9.7411(3), 13.5541(4)
Cell angle (α, β, γ) [°]	107.539(3), 101.265(3), 99.698(3)
Cell volume (V) [$Å^3$]	724.90(4)
R-factor [%]	4.49
T_{min}, T_{max}	0.6976, 1.0000
Z	1
ρ_{calc} [g/cm^3]	1.332
μ [mm^{-1}]	1.466
Absorption correction	Multi-scan
Scan method	ω and φ
F (000)	380
Crystal size [mm^3]	0.2 × 0.3 × 0.35
Radiation [mm]	CuKα (λ = 1.54184)
2Θ range for data collection [°]	7.088 to 156.806
Index ranges (h, k, l)	-7 ≤ h ≤ 7, -12 ≤ k ≤ 12, -17 ≤ l ≤ 15
Reflections collected	11275
Independent reflections	4489 [R_{int} = 0.0406, R_{sigma} = 0.0298]
Data/restraints/parameters	4489/3/374
Goodness-of-fit on F^2	1.143
Final R indexes [I≥2σ (I)]	R_1 = 0.0376, wR_2 = 0.1137
Final R indexes [all data]	R_1 = 0.0400, wR_2 = 0.1163
Largest diff. peak/hole [e $Å^{-3}$]	0.21/-0.23
Flack parameter	0.137(15)

(N-O-CH_2), 61.5 (O-CH_2), 20.7 (CH_3), 20.5 (CH_3, CH_3), 20.1 (CH_3); HRMS (ESI) calculated for $C_{33}H_{33}BrN_4O_{11}$ $[M + H]^+$ 741.1409, found 741.1407 and $[M + H + 2]^+$ 743.1394.

*2.2.3.19. (2S,3S,4S,5S,6S)-2-(acetoxymethyl)-6-(4-(((((6,8-dichloro-2-phenyl-2H-chromen-3-yl)methylene)amino)oxy)methyl)-1H-1,2,3-triazol-1-yl)tetrahydro-2H-pyran-3,4,5-triyl triacetate (**10s**).* Redish brown solid (75%), Melting Point: 187-188°C; ^{1}H NMR (400 MHz, $CDCl_3$) δ_H (ppm): 7.91-7.90 (m, 1H, Ar-H), 7.45-7.31(m, 6H, HC=N, Triazole-H, Ar-H), 7.17 (d, *J* = 2.8 Hz, 1H, Ar-H), 6.99-6.98 (m, 1H, Ar-H), 6.74-7.72 (m, 1H, Ar-H), 6.47 (d, *J* = 11.6 Hz, 1H, CH), 5.81- 5.77 (m, 1H, HC-O), 5.47-5.17 (m, 5H, Ar-O-CH, N-O-CH_2, HC-O), 4.34-4.22 (m, 1H, CH), 4.16-4.09 (m, 1H), 4.01-3.96 (m, 1H, O-CH_2), 2.07 (s, 3H, CH_3), 2.06 (s, 3H, CH_3), 2.03 (s, 3H, CH_3), 1.86 (s, 3H, CH_3); ^{13}C NMR (100 MHz, $CDCl_3$) δ_C (ppm): 170.5 (C=O), 169.9 (C=O), 169.4 (C=O), 168.8 (C=O), 147.9 (Ar-C), 147.5 (HC=N), 144.8 (Triazole-C), 137.9 (Ar-C), 130.2 (Ar-C), 128.5 (Triazole-C), 127.2 (Ar-C), 126.8 (Ar-C), 126.1 (Ar-C), 125.3 (Ar-C), 122.6 (Ar-C), 121.5 (Ar-C), 121.4 (Ar-C), 85.6 (CH), 75.3 (CH), 75.0 (HC-O), 73.4 (Ar-O-CH), 70.6 (HC-O), 70.1 (HC-O), 67.6 (N-O-CH_2), 60.4 (O-CH_2), 20.7 (CH_3), 20.5 (CH_3, CH_3), 20.1 (CH_3); HRMS (ESI) calculated for $C_{33}H_{32}Cl_2N_4O_{11}$ $[M + H]^+$ 731.1525, found 731.1523 and $[M + H + 2]^+$ 733.1505.

*2.2.3.20. 8-methoxy-2H-chromene-3-carbaldehyde O-((1-((6-(benzyloxy)-2,2-dimethyltetrahydrofuro[2,3-d][1,3]dioxol-5-yl)methyl)-1H-1,2,3-triazol-4-yl)methyl) oxime (**10t**).* Light yellow solid (72%), Melting Point: 117-118°C; ^{1}H NMR (400 MHz, $CDCl_3$) δ_H (ppm): 7.77 (s, 1H, HC=N), 7.61 (s, 1H, Triazole-H), 7.37-7.29 (m, 5H, Ar-H), 6.86-6.80 (m, 2H, Ar-H), 6.68 (dd, J_{12} = 2.4 Hz, J_{13} = 6.4 Hz, 1H, Ar-H), 6.55 (s, 1H, Ar-H), 5.98 (d, *J* = 4.0 Hz, 1H, HC-O), 5.23 (s, 2H, N-O-CH_2), 5.08 (s, 2H, Ar-O-CH_2), 4.75-4.64 (m, 3H, CH_2, HC-O), 4.56-4.47 (m, 3H, O-CH_2, HC-O), 3.98 (d, *J* = 2.8 Hz, 1H, HC-O), 3.88 (s, 3H, OCH_3), 1.41 (s, 3H, CH_3), 1.29 (s, 3H, CH_3); ^{13}C NMR (100 MHz, $CDCl_3$) δ_C (ppm): 147.9 (Ar-C), 147.7 (HC=N), 143.9 (Triazole-C), 143.3 (Ar-C), 136.8 (Ar-C), 128.7 (Ar-C), 128.3 (Triazole-C), 128.2 (Ar-C), 127.9 (Ar-C), 126.6 (Ar-C), 124.4 (Ar-C), 122.3 (Ar-C), 121.2 (Ar-C), 119.7 (Ar-C), 113.0 (Ar-C), 112.1 (Ar-C), 105.2 (O-CH-O), 81.9 (HC-O), 81.5 (HC-O), 78.8 (HC-O), 71.9 (OCH_2), 67.6 (N-O-CH_2), 64.5 (Ar-O-CH_2), 56.1 (OCH_3), 49.3 (CH_2, O-C-O), 26.7 (CH_3), 26.1 (CH_3); HRMS (ESI) calculated for $C_{29}H_{32}N_4O_7$ $[M + H]^+$ 549.2351, found 549.2397.

*2.2.3.21. 6-nitro-2H-chromene-3-carbaldehyde O-((1-((6-(benzyloxy)-2,2-dimethyltetrahydrofuro[2,3-d][1,3]dioxol-5-yl)methyl)-1H-1,2,3-triazol-4-yl)methyl) oxime (**10u**).* Brownish yellow solid (84%), Melting Point: 111-112°C; ^{1}H NMR (400 MHz, $CDCl_3$) δ_H (ppm): 8.08-7.99 (m, 1H, Ar-H), 7.92-7.91 (m, 1H, Ar-H), 7.78 (s, 1H, HC=N), 7.37- 7.31 (m, 5H, Triazole-H, Ar-H), 6.85 (d, *J* = 9.2 Hz, 1H, Ar-H), 6.56 (s, 1H, Ar-H), 5.97 (d, *J* = 3.6 Hz, 1H, HC-O), 5.23 (s, 2H, N-O-CH_2), 5.15 (S, 2H, Ar-O-CH_2), 4.77-4.65 (m, 3H, CH_2, HC-O), 4.54-3.83 (m, 3H, O-CH_2, HC-O), 3.99 (d, *J* = 2.8 Hz, 1H, HC-O), 1.40 (s, 3H, CH_3), 1.28 (s, 3H, CH_3); ^{13}C NMR (100 MHz, $CDCl_3$) δ_C (ppm): 159.5 (Ar-C), 146.9 (HC=N),

Table 2
Exploring the reaction condition for the synthesis of novel 2*H*-chromene-1,2,3-triazolyl glycoconjugates.

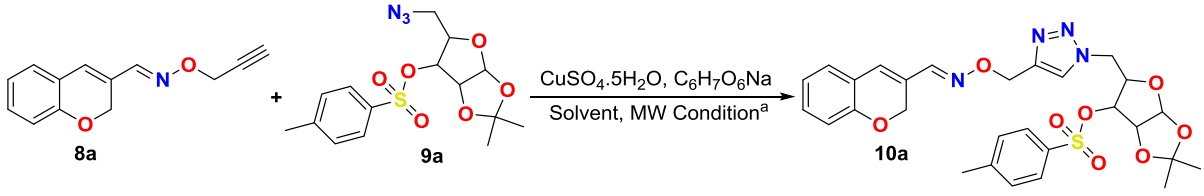

Entry	Solvent	Equiv. of sugar azide (9a)	Equiv. of catalyst ($CuSO_4.5H_2O$)	Equiv. of base ($C_6H_7O_6Na$)	Temperature	Power	Time	Yield[b]
1	EtOH	1.0	0.2	0.3	70°C	100W	15 min	nr
2	DCM	1.0	0.2	0.3	70°C	100W	15 min	nr
3	THF	1.0	0.2	0.3	70°C	100W	15 min	nr
4	CH_3CN	1.0	0.2	0.3	70°C	100W	15 min	48%
5	Toluene	1.0	0.2	0.3	80°C	100W	15 min	trace
6	DMF	1.0	0.2	0.3	80°C	100W	15 min	38%
7	CH_3CN/H_2O (1:1)	1.0	0.2	0.3	80°C	100W	15 min	63%
8	CH_3CN/H_2O (1:1)	1.1	0.3	0.4	80°C	100W	15 min	79%
9[a]	**CH_3CN/H_2O (2:1)**	**1.1**	**0.3**	**0.4**	**80°C**	**100W**	**20 min**	**91%**
10	CH_3CN/H_2O (2:1)	1.1	0.3	0.4	90°C	120W	20 min	85%
11	DMF/H_2O (2:1)	1.1	0.3	0.4	90°C	100W	20 min	52%
12	DMF/H_2O (2:1)	1.1	0.3	0.4	90°C	120W	25 min	56%

[a] Standard Condition: *O*-propargylated chromene (**8a**, 1.0 equiv.), Sugar azide (**9a**, 1.1 equiv.), Copper sulphate as catalyst (0.3 equiv.), Sodium ascorbate as base (0.2 equiv.), Power (100 W), time (20 min), Temperature (80°C), CH_3CN/H_2O (2:1; 2.5 ml).
[b] Isolated yield; nr: no reaction.

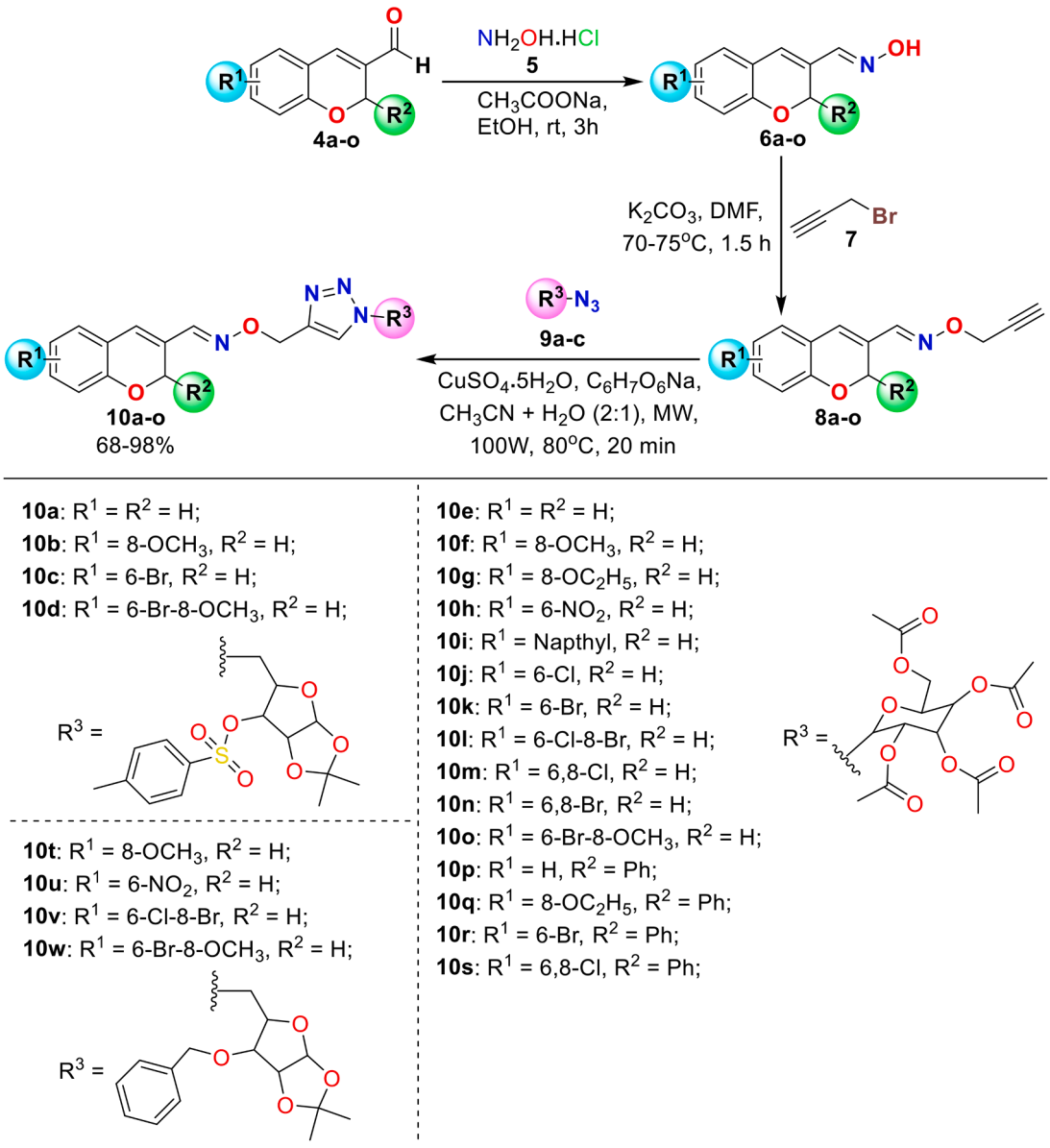

Scheme 1. Synthetic pathway of 2*H*-chromene-1,2,3-triazolyl glycoconjugates **10a-w**.

143.7 (Triazole-C), 141.8 (Ar-C), 136.7 (Ar-C), 128.6 (Ar-C), 128.3 (Triazole-C), 128.0 (Ar-C), 127.9 (Ar-C), 125.9 (Ar-C), 125.7 (Ar-C), 124.4 (Ar-C), 122.8 (Ar-C), 121.1 (Ar-C), 116.1 (Ar-C), 112.1 (Ar-C), 105.2(O-CH-O), 81.9 (HC-O), 81.5 (HC-O), 78.8 (HC-O), 71.9 (OCH_2), 67.8 (N-O-CH_2), 65.3 (Ar-O-CH_2), 49.4 (CH_2, O-C-O), 26.6 (CH_3), 26.1 (CH_3); HRMS (ESI) calculated for $C_{28}H_{29}N_5O_8$ $[M + H]^+$ 564.2096, found 564.2100.

*2.2.3.22. 8-bromo-6-chloro-2H-chromene-3-carbaldehyde O-((1-((6-(benzyloxy)-2,2-dimethyltetrahydrofuro[2,3-d][1,3]dioxol-5-yl)methyl)-1H-1,2,3-triazol-4-yl)methyl) oxime (**10v**).* Pale Yellow solid (74%), Melting Point: 120-121°C; ^{1}H NMR (400 MHz, $CDCl_3$) δ_H (ppm): 7.76 (s, 1H, HC=N), 7.63 (s, 1H, Triazole-H), 7.38-7.32 (m, 6H, Ar-H), 6.95 (d, J = 2.4 Hz, 1H, Ar-H), 6.44 (s, 1H, Ar-H), 5.98 (d, J = 3.6 Hz, 1H, HC-O), 5.23 (s, 2H, N-O-CH_2), 5.12 (s, 2H, Ar-O-CH_2), 4.75-4.64 (m, 3H, CH_2, HC-O), 4.56-4.48 (m, 3H, O-CH_2, HC-O), 3.99 (d, J = 2.8 Hz, 1H, HC-O), 1.39 (s, 3H, CH_3), 1.29 (s, 3H, CH_3); ^{13}C NMR (100 MHz, $CDCl_3$) δ_C (ppm): 149.8 (Ar-C), 147.0 (HC=N), 143.8 (Triazole-C), 136.7 (Ar-C), 132.6 (Ar-C), 128.7 (Ar-C), 128.4 (Ar-C), 128.3 (Triazole-C), 127.9 (Ar-C), 126.1 (Ar-C), 126.0, 124.5 (Ar-C), 112.2 (Ar-C), 110.2 (Ar-C), 105.2 (O-CH-O), 81.9 (HC-O), 81.6 (HC-O), 78.8 (HC-O), 71.9 (OCH_2), 67.8 (N-O-CH_2), 65.2 (Ar-O-CH_2), 49.4 (CH_2, O-C-O), 26.7 (CH_3), 26.1 (CH_3); HRMS (ESI) calculated for $C_{28}H_{28}BrClN_4O_6$ $[M + H]^+$ 631.0961, found 631.0965 and $[M + H + 2]^+$ 633.0943.

*2.2.3.23. 6-bromo-8-methoxy-2H-chromene-3-carbaldehyde O-((1-((6-(benzyloxy)-2,2-dimethyltetrahydrofuro[2,3-d][1,3]dioxol-5-yl)methyl)-1H-1,2,3-triazol-4-yl)methyl) oxime (**10w**).* Brownish white solid (81%), Melting Point: 115-116°C; ^{1}H NMR (400 MHz, $CDCl_3$) δ_H (ppm): 7.76 (s, 1H, HC=N), 7.61 (s, 1H, Triazole-H), 7.37-7.32 (m, 5H, Ar-H), 6.90 (d, J = 1.6 Hz, 1H, Ar-H), 6.81 (d, J = 2.0 Hz, 1H, Ar-H), 6.46 (s, 1H, Ar-H), 5.97 (d, J = 4.0 Hz, 1H, HC-O), 5.23 (s, 2H, N-O-CH_2), 5.07 (s, 2H, Ar-O-CH_2), 4.74-4.64 (m, 3H, CH_2, HC-O), 4.55- 4.47 (m, 3H, O-CH_2, HC-O), 3.98 (d, J = 3.2 Hz, 1H, HC-O), 3.86 (s, 3H, OCH_3), 1.41 (s, 3H, CH_3), 1.30 (s, 3H, CH_3); ^{13}C NMR (100 MHz, $CDCl_3$) δ_C (ppm): 148.5 (Ar-C), 147.5 (HC=N), 143.9 (Triazole-C), 142.5 (Ar-C), 136.8 (Ar-C), 128.7 (Ar-C), 128.3 (Triazole-C), 127.9 (Ar-C), 127.6 (Ar-C), 126.8 (Ar-C), 121.9 (Ar-C), 115.9 (Ar-C), 112.1 (Ar-C), 105.2 (O-CH-O), 81.9 (HC-O), 81.5 (HC-O), 78.8 (HC-O), 71.9 (OCH_2), 67.8 (N-O-CH_2), 64.6 (Ar-O-CH_2), 56.3 (OCH_3), 49.4 (CH_2, O-C-O), 26.6 (CH_3), 26.1 (CH_3); HRMS

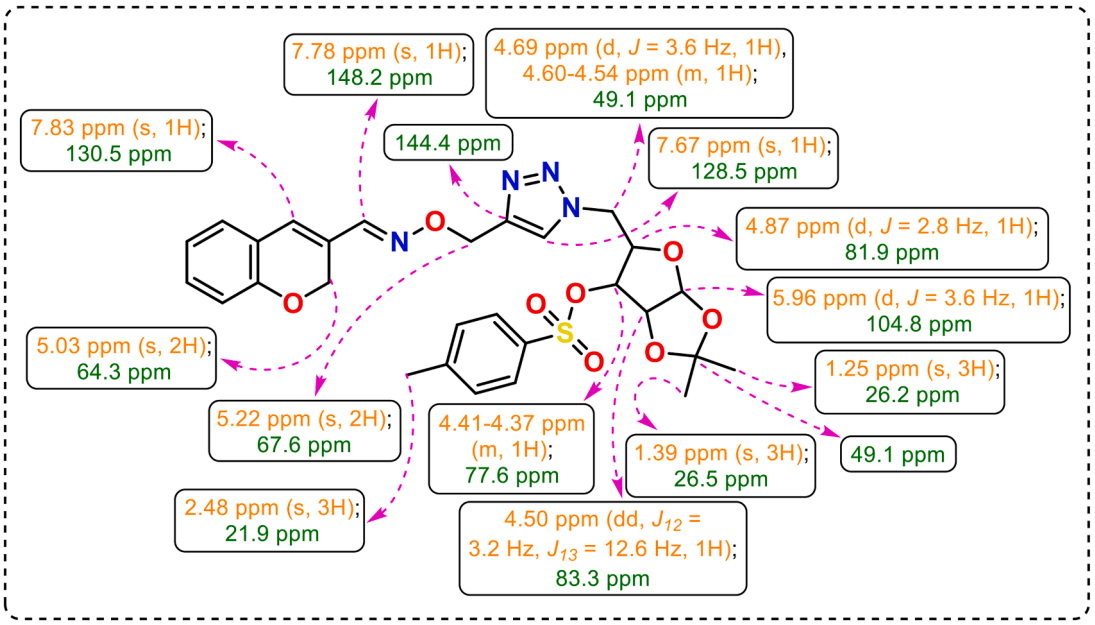

Fig. 3. ^{1}H and ^{13}C NMR data of synthesized compound **10a**.

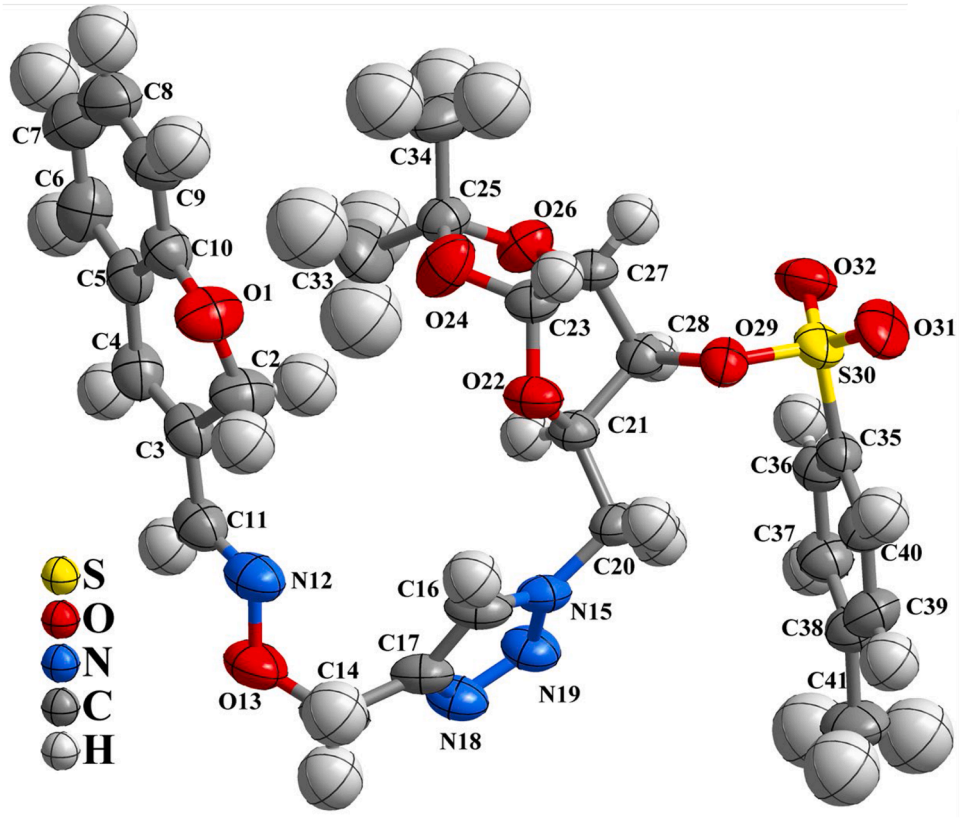

Fig. 4. The ORTEP diagram of the compound **10a** with 50% ellipsoidal probability (**CCDC: 2314962**).

(ESI) calculated for $C_{29}H_{31}BrN_4O_7$ $[M+H]^+$ 627.1456, found 627.1459.

2.3. X-ray crystallographic studies

2.3.1. Crystal growth development

The pure single crystal of compound **10a** was grown from acetone and hexane (1:2) solvent mixture solution using slow evaporation technique or vapor diffusion method at room temperature.

2.3.2. Single crystal data collection, data reduction, structure solution, and structure refinement

A good quality light brown coloured single-crystal has been picked through a thing glass fibre loop with parabar oil (adhesive) and mounted on Rigaku XtaLab-II Super-Nova single-crystal X-ray diffractometer with misfocused copper Kα X-ray source with a graphite monochromator. The intensity data were recorded at 295.15 K with graphite-monochromatized copper Kα radiation (λ = 1.54184 Å). The data

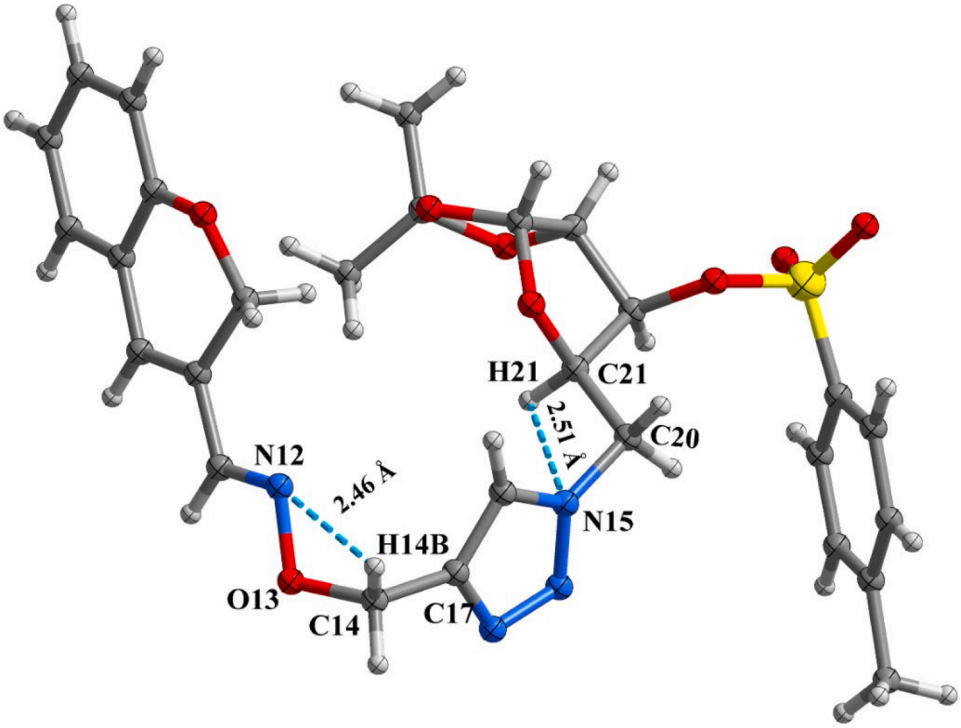

Fig. 5. Compound 10a with intramolecular hydrogen bonding.

Table 3
Intramolecular hydrogen bonding contacts in compound **10a**.

D-H···A	D-H (Å)	H···A (Å)
C14-H14B···N12	0.97	2.46
C21-H21···N15	0.98	2.51

were collected at room temperature at ω/φ scan mode for Lorentz-polarization and absorption effects. A total of 11,275 reflections were measured experimentally out of which 4,489 were treated as independent reflections. The data collection, data reduction and absorption correction were carried out using the program Crysalispro [55]. The structure of the compound was solved via SHELXT in the intrinsic phase method [56] using the OLEX2 software [57]. It showed all the non-hydrogenic atoms were perfectly assigned. Empirical absorption corrections were done using spherical harmonics, implemented in the SCALE3 ABSPACK scaling algorithm [58]. All the assigned atoms are refined with SHELXL [56]. Again, the SHELXTL-PLUS package of programs is used for Full-matrix least-squares structure refinement against $|F^2|$ [59]. The hydrogen atoms are added to the non-hydrogen atoms and held in a riding mode. Finally, anisotropic thermal parameters for non-hydrogen atoms and isotropic thermal parameters for hydrogen atoms are employed. The crystallographic data and refinement parameters of compound **10a** are listed in Table 1.

2.4. Biological activity evaluations

2.4.1. In vitro anticancer activity

2.4.1.1. Cell culture. Two human breast cancer adenocarcinoma cell lines (MCF-7 and MDA-MB-231) [35,60], one human lung cancer cell line (A549) [61], and one human embryonic kidney cell line (HEK) [62] were procured from the National Centre for Cell Science Pune, India. The cells were maintained in Dulbecco's Modified Eagle Medium (DMEM) supported with 10% Fetal Bovine Serum (FBS) and 1%

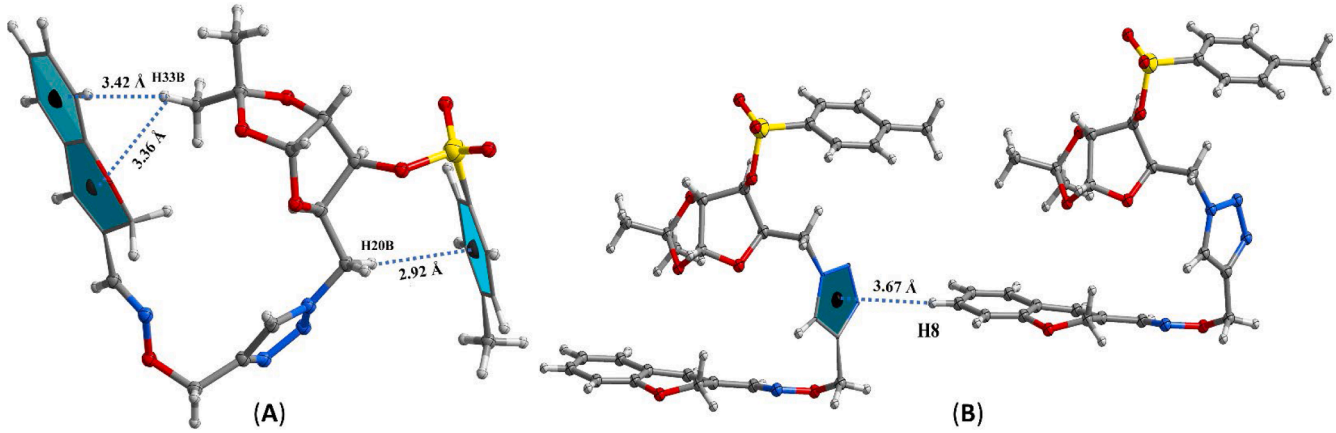

Fig. 6. (A) Intramolecular and (B) intermolecular C-H···π interactions within compound 10a.

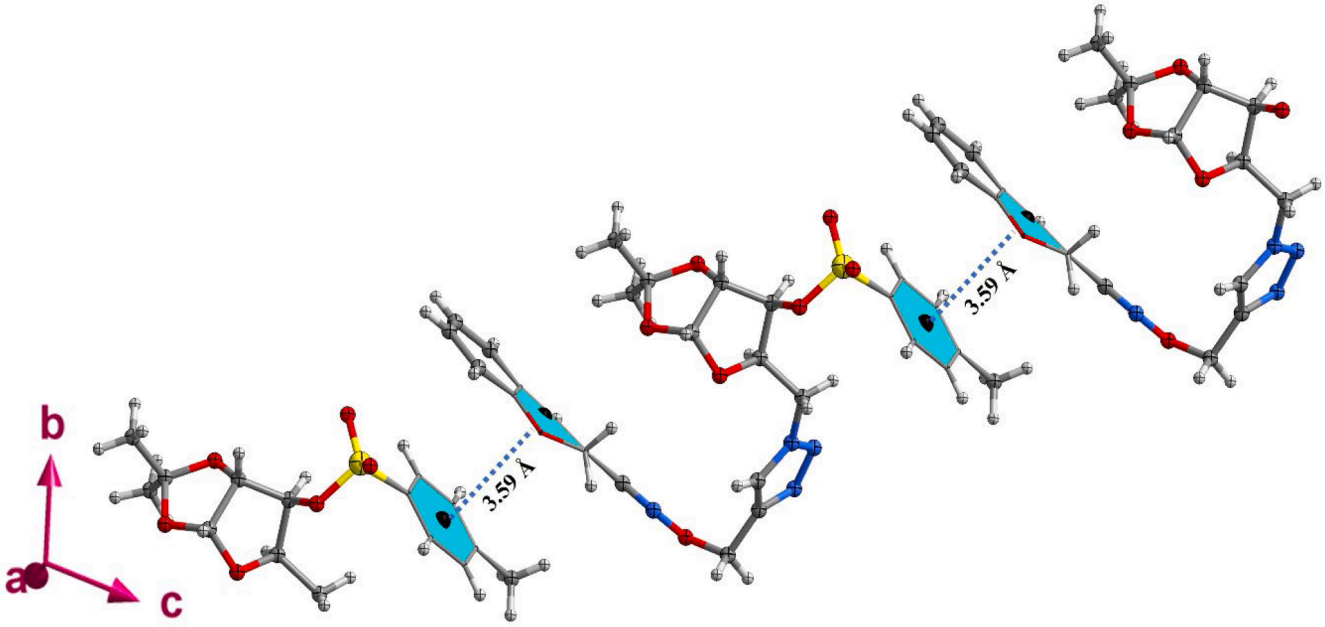

Fig. 7. π-π stacking interactions within compound 10a propagating along the crystallographic b-direction with a glide plane in the bc-plane.

antibiotic-antimycotic solution and placed in an incubator at 37°C with 5% CO_2.

2.4.1.2. Cytotoxicity MTT assay. The MTT assay is based on the capability of the cells to covert the yellow MTT salt (3-[4,5-dimethylthiazol-2-yl]-2,5 diphenyl tetrazolium bromide) to purple formazan crystals through the mitochondrial dehydrogenase enzyme and the mitochondrial activity are interpreted as an indicator of cell viability [63-65]. In brief, the cells were initially plated in a 96-well plate at a seeding density of 5000 cells per well in 100 µL of complete media containing 10% FBS and allowed to grow for overnight. Then cells were exposed to desire concentrations of compounds **10a-w** (5 µM, 10 µM, 20 µM, 50 µM, 75 µM, 100 µM) and incubated for 72 h at 37°C with 5% CO_2. After the incubation period, the spent medium was removed and MTT reagent was added to the each well, which were then further incubated for 4 h in the CO_2 incubator. The formazan crystals were dissolved using DMSO, and the absorbance at 570 nm was measured using a micro plate reader. Cells treated with complete media alone were considered the control. To calculate the percentage of cell viability, the following formula was used:

% of viability = [**Mean absorbance of the test sample** / **Mean absorbance of the control**] × 100

The experiments were conducted in triplicate, and the data is presented as mean ± standard deviation (n = 3).

2.4.1.3. Morphological observation. To determine the cellular and morphological changes on MCF-7, cells were cultivated in 6-well culture plate for 24 h at 37 °C and treated with the IC_{50} concentration of **10t** for respective time period. After completion of 24 h incubation, cells were washed with PBS, and stained with Hoechst 33342/PI solution (1:1, V/V) at room temperature for 15 min with light protected condition [65,66]. The imaging was done using Inverted microscope (Model: Nikon ECLIPSE T_S2R).

2.4.2. In vitro antibacterial activity

2.4.2.1. Preparation of microorganism tests. The *in vitro* antibacterial activity of all the newly prepared compounds were evaluated using agar well diffusion method and macrodilution method against two pathogenic bacteria strains *Escherichia coli* (Gram -ve) and *Staphylococcus aureus* (Gram + ve). Antibacterial tests were conducted in the exponential growth phase from fresh cultures (24 hours). The opacity of the bacterial interruptions in physiological sterile water was equivalent to 0.5 McFarland (a bacterial concentration projected at 10^6 CFU/ml) [39].

2.4.2.2. Agar well diffusion method. In this well-known method, agar plates placed on Petri dishes are seeded with a standardized amount of the target microorganism using sterilized cotton swabs. After inoculation, wells were bored into the solidified agar surfaces on the Petri dishes by the use of 6 mm sterile corkborer. Various concentrations of 1.0, 5.0, 10.0, and 20.0 µg/ml were added in 0.1% DMSO were introduced to the well. Then, the bacteria were cultured in agar nutrient and incubated at 37°C for 24 h. The standard drug Gentamicin served as the positive control and DMSO was taken as the negative control which did not produce any significant zone of inhibition. Any extending of inhibition zone around the wells, even a small diameter, was considered as a positive result [36,38,39]. All tests were conducted in duplicate.

2.4.2.3. Macrodilution method. The minimum inhibitory concentration (MIC) for all the tested compounds was calculated using well-established macrodilution method [39,47]. Initially, seven sterile test tubes were prepared by autoclaving, and each was filled with 1 ml of sterile nutrient broth (NB) medium. Subsequently, 1 ml of the tested compound was added to the first tube and thoroughly mixed to ensure a bubble-free solution. Serial dilution was then carried out by transferring 1 ml of the solution from the first tube to the second, and so on, until the seventh tube was reached. Afterwards, 10 µl of a bacterial suspension with a

Table 4
IC_{50} Values of **10a-w** Compounds on four different cell lines

Sl. No.	Compounds	IC_{50} (Mean±SD) μM			
		HEK	MCF-7	MDA-MB-231	A549
1	**10a**	411.43 ± 2.61	58.87 ± 0.71	91.90 ± 1.09	36.66 ± 1.56
2	**10b**	180.54 ± 2.26	45.76 ± 1.01	106.62 ± 0.93	46.16 ± 1.66
3	**10c**	191.04 ± 1.96	42.47 ± 1.73	153.51 ±1.34	91.59 ± 1.96
4	**10d**	147.04 ± 2.17	19.31 ± 0.7	93.76 ± 1.15	117.1 ± 2.07
5	**10e**	162.0 ± 2.21	30.31 ± 0.88	99.10 ± 0.32	56.23 ± 1.75
6	**10f**	455.42 ± 2.66	67.46 ± 2.05	167.73 ± 0.71	133.8 ± 2.13
7	**10g**	202.91 ± 2.31	25.33 ± 0.49	46.92 ±1.87	29.62 ± 1.47
8	**10h**	170.4 ± 2.23	20.21 ± 0.38	32.66 ±1.02	44.72 ± 1.65
9	**10i**	507.33 ± 2.71	31.8 ± 2.31	43.42 ±1.17	40.89 ± 1.61
10	**10j**	259.62 ± 2.41	25.28 ± 0.23	42.18 ± 0.37	82.35 ± 1.92
11	**10k**	192.32 ± 1.92	56.81 ± 0.01	49.03 ± 0.87	82.55 ± 2.28
12	**10l**	111.51 ± 2.05	23.4 ± 0.91	31.89 ±0.94	52.79 ± 1.72
13	**10m**	424.81 ± 2.63	34.38 ± 0.24	41.56 ± 0.49	64.45 ± 1.81
14	**10n**	155.0 ± 2.19	18.57 ± 0.70	31.83 ± 0.91	48.96 ± 1.69
15	**10o**	90.54 ± 1.96	25.33 ± 0.38	47.8 ± 1.03	64.24 ± 1.81
16	**10p**	121.14 ±2.05	79.80 ± 1.34	80.83 ± 0.33	123.7 ± 2.09
17	**10q**	193.64 ± 2.29	50.33 ± 1.41	65.15 ± 0.56	39.38 ± 1.59
18	**10r**	376.83 ± 2.58	26.09 ± 1.28	37.67 ± 0.60	57.14 ± 1.76
19	**10s**	329.32 ± 2.52	56.81 ± 1.44	90.83 ± 0.88	110.82 ± 2.05
20	**10t**	244.74 ± 2.39	6.90 ± 0.24	51.72 ± 0.91	42.14 ± 2.09
21	**10u**	169.81 ± 2.23	12.49 ± 0.37	65.47 ± 1.040	82.63 ± 1.92
22	**10v**	202.83 ± 2.31	7.45 ± 0.31	55.59 ± 0.94	87.86 ± 1.94
23	**10w**	140.62 ± 2.15	15.39 ± 0.81	26.87 ± 0.83	66.16 ± 1.82

concentration of 1.5×10^6 CFU/ml (colony forming unit) diluted inoculums of bacterial interruption adjusted with McFarland 0.5 standard was added in all test tubes and incubated at 37°C for 24 h after proper mixing. For the negative control, 1 ml of sterile NB media and 10 μl of the 1.5×10^6 CFU/ml diluted bacterial suspension were added to the M + I (medium + inoculums) test tube to observe bacterial growth in the presence of medium. Similarly, for the positive control, 1 ml of diluted antibacterial compound and sterile NB media were added to the M + AC (medium + antibacterial compound) test tube to assess the transparency of the solution. Additionally, 1 ml of sterile NB medium was added to the blank control test tube M (medium) to verify the sterility of the medium and equipment. All these control test tubes were then incubated at 37°C for 24 h.

2.5. Computational studies

2.5.1. Quantum chemical and electronic structure investigations

The quantum chemical calculations and structural relaxation of three different triazoles were performed using the Gaussian 09 program package at exchange-correlation functional Beckee-3-Lee-Yang-Parr (B3LYP) and basis set 6-311++G(d,p) [67-69]. The optimized structure geometry, Frontier molecular orbital (FMO) analysis, and Molecular electrostatic potential (MEP) analysis were calculated with this method. The Gauss View 6.0 program was used to obtained graphical representations [70]. Electronic structure investigations (Average local ionization energy analysis, Topological analysis and Reduced density gradient analysis) were performed using the Multiwfn 3.8 program package [71].

2.5.2. In silico molecular docking investigations

Drug designing plays a crucial role in pharmaceutical industry. Molecular docking is a most prominent method for structure-based drug design that simulates molecular interactions and forecasts the binding affinities between receptors and ligands [72]. All the compounds **10a-w** were analysed with molecular docking investigations using the AutoDock 4.2.0 software package, the programme is with multiple mainstay capability, offers rapid speed, better accuracy, and easy to use [73]. The selection of a protein must possess drug-ability to be considered a viable drug target. A druggable protein is characterized by its ability to form favourable interactions with small drug-like molecules, whether naturally occurring or external and hence, it possesses a binding site. These binding sites are anticipated to possess special attributes that facilitate the drug-like molecule's ability to bind with high affinity at a particular pose. For a protein to be considered as a potential therapeutic target, it must be associated with drug-disease process, as is the case with all pharmacological targets [74]. The selection and prioritization of target proteins for this study based on a disease and data mining methods by searching through literature and databases, by which we obtained docking results with a greater number of proteins like HER2, BDR4, EGFR tyrosine kinase, DNA topoisomerase IIa, BCL-2 receptors for anticancer activities [35,75-79] and peptide deformylase, dihydropteroate synthase receptors for antibacterial activities [38,43,80,81]. But, our synthesised compounds **10a-w** showed good binding affinity towards the proteins, which we have chosen from the protein data bank (PDB) by its codes namely 1G2A (Gram negative anti-bacterial protein), 1Q1Y (Gram positive anti-bacterial protein), 2W3L (Lung cancer protein), and 1ZXN (Breast cancer protein) [78-81]. The crystal structures of the selected proteins were determined using the X-ray diffraction (XRD) method, with a resolution of 1.75 Å (for 1G2A), 1.90 Å (for 1Q1Y), 2.10 Å (for 2W3L), and 2.51 Å (for 1ZXN) respectively. The macromolecule underwent a process where water molecules and heteroatoms were removed and polar hydrogens were added to it. The ligands were drawn using Chemdraw Ultra 16.0 software and saved in MDL file format, then transformed into PDB format using PyMOL software. The target molecule and the ligands were both imported into PyRx, and the CASTp 3.0 web server was utilized to forecast the active sites of the target molecule [82]. The obtained molecular docking results were visualized through PyMOL and BIOVIA Discovery Studio 2024.

2.5.3. In silico ADMET and pharmacokinetic properties predictions

Using a methodology adopted from Rocha et al. [83], the *in silico* ADMET predictions of four potent compounds **10a, 10b, 10t** and **10v** was carried out using web-based software ADMETlab 3.0 (https://admetlab3.scbdd.com/). The potentially blocking fragments of the ion transport channels in the cardiac hERG system (human ether-a-go-go-related gene) were predicted by the structure-activity relationship models of the web-based software LABMOL (http://predherg.labmol.com.br/) and the median lethal dose (LD_{50}) and Toxicity class were predicted by a web-based software ProTox-3.0 (ttps://comptox.charite.de/protox3/index.php/) [84].

3. Results and discussion

3.1. Chemistry

3.1.1. Synthesis

Our initial investigative work started with the discovery of the

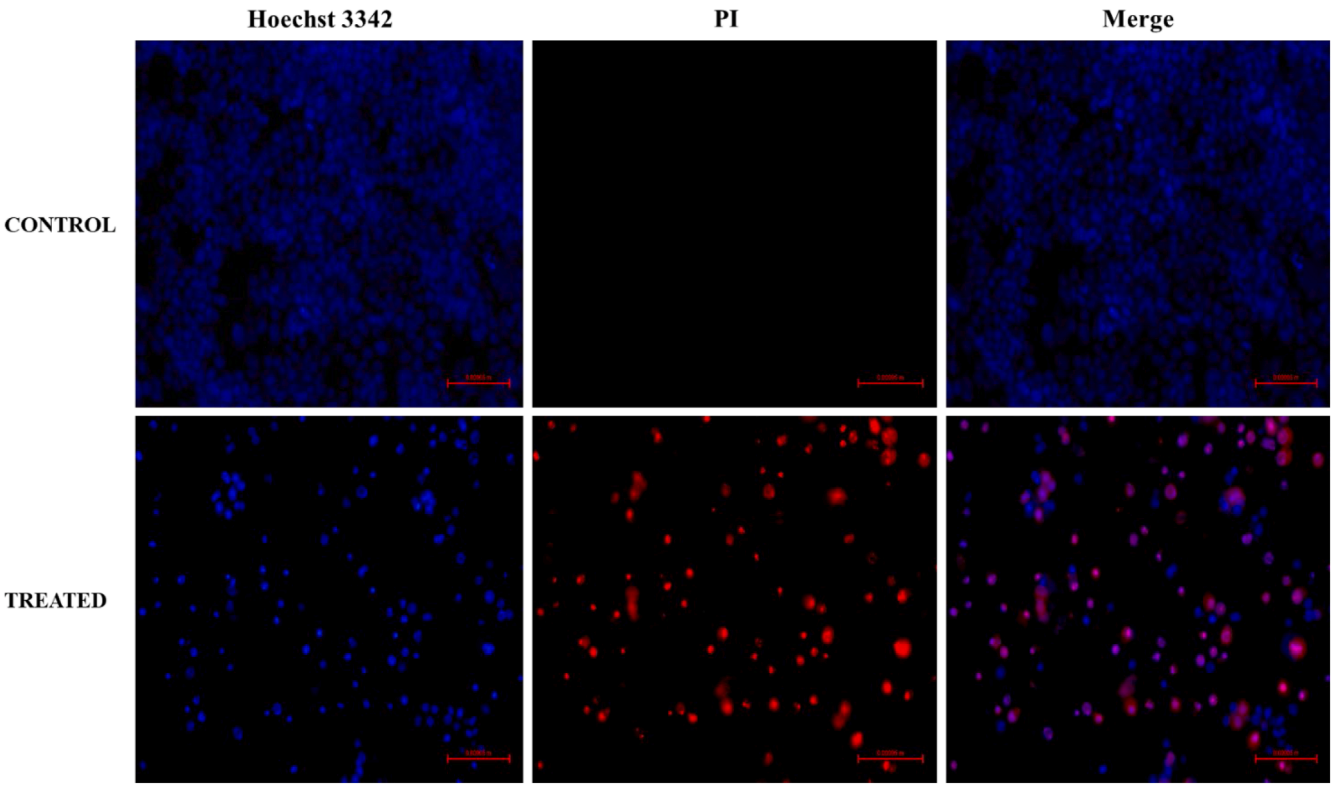

Fig. 8. Hoechst 3342/PI dye shows the normal and dead cells. MCF-7 cells treated with **10t** for 24 h and stained with Hoechst 33342/PI dye (Original magnification 20x).

feasible strategy and optimization conditions for the synthesis of 2*H*-chromene-1,2,3-triazolyl glycoconjugates. First the 2*H*-chromene-3-carbaldehydes **4a-o** were prepared by the reaction of salicylaldehydes **1a-k** and acrolein **2**/ cinnamaldehyde **3** in the presence of K_2CO_3/pyrrolidine [51,52]. In the subsequent step, 2*H*-chromene-3-carbaldehyde oximes **6a-o** were synthesised by the reaction of 2*H*-chromene-3--carbaldehydes and Hydroxyl amine hydrochloride in presence of sodium acetate [53]. Further, the 2*H*-chromene based aldoximes **6a-o** were reacted with propargyl bromide in presence of potassium carbonate to obtain 2*H*-chromene-3-carbaldehyde *O*-prop-2-yn-1-yl oximes **8a-o** [54]. The sugar azides **9a-c** were prepared following previously reported procedures [85-87]. All the synthesized molecules were successfully characterized by ^{1}H NMR and ^{13}C NMR. After the successful synthesis of these two significant parent pharmacophores, we moved towards the synthesis of the hybrid molecules by Click reaction method using copper sulphate as a catalyst, sodium ascorbate as base, and altering different parameters including time, power, temperature, and solvent mediums.

As indicated in Table 2, following the micro wave irradiation technique (Condition: 100W, 70°C, 15 min) the screening was started by the reaction of 1.0 equivalent *O*-propargylated chromene derivative **8a** with 1.0 equivalent of tosyl-protected sugar azide **9a** in presence 0.3 equiv. copper sulphate, 0.2 equivalent of sodium ascorbate, and different solvents (EtOH, DCM, THF); unfortunately, no reaction was observed under these conditions (Table 2, Entries **1**-**3**). However, a 48% yield of desired product was achieved when the reaction was monitored in CH_3CN (Entry **4**). Then, the structure of synthesized compound **10a** was characterized by ^{1}H, ^{13}C NMR, HRMS, and X-ray crystallographic analysis.

Thereafter, the reaction was monitored in toluene with increasing temperature to 80°C, resulting a trace amount of product (Entry **5**). The reaction was then tested by switching to DMF under the same condition and resulted in an inferior yield of 38% (Entry **6**). While using the combination of solvents such as CH_3CN and H_2O in a 1:1 ratio, the yield of the product improved to 63% (Entry **7**). By increasing the equivalent of azide from 1.0 to 1.1 equivalent and equivalent of base from 0.3 to 0.4 a good yield of 79% was obtained (Entry **8**). After increasing the reaction time from 15 min to 20 min as well as ratio of CH_3CN and H_2O solvent mixture from 1:1 to 2:1 gave an excellent yield (91%) of the product (Entry **9**). Increasing the power and temperature, the yield was further decreased (Entry **10**). Furthermore, the reaction was tested in a more polar solvent medium (mixture of DMF and H_2O in 2:1 ratio) at 100W, 90°C, 20 min but the yield was reduced to 52% (Entry **11**). The reaction was again studied by increasing power from 100W to 120W and time from 20 min to 25 min, but the yield increased to 56% (Entry **12**).

After getting the ideal reaction condition for synthesis, we proceeded to explore the efficiency and versatility of the protocol using several substituents in *O*-propargylated 2*H*-chromene ring containing electron-withdrawing as well as electron-donating groups **8a-o**. These were reacted with three different sugar azides **9a-c** and afford 23 new 2*H*-chromene-1,2,3-triazolyl glycoconjugates **10a-w** in good to excellent yields 68-98% (Scheme 1). The structures of all synthesised compounds **10a-w** were confirmed by ^{1}H NMR, ^{13}C NMR, and HRMS spectral data. After successful synthesis of the desired products, we further proceeded for their anti-bacterial as well as anti-cancer activities study.

3.1.2. *Characterization of compound 10a*

The series of chromene-1,2,3-triazolyl glycoconjugates (**10a**-**w**) were synthesized using *O*-propargylated chromene derivatives and sugar azides as shown in Scheme 1. The structure of all synthesized compounds was established basing on different spectral methods. The aromatic and aliphatic protons the compound **10a** are confirmed by ^{1}H NMR. In the ^{1}H NMR spectra the compound **10a**, a singlet peak appears at δ_H 5.03 ppm attributed to the 2*H*-chromene (-O-CH_2) protons, a singlet peak at δ_H 7.78 ppm indicates that azomethine (HC=N) proton, and a singlet peak appears at δ_H 5.22 ppm for N-O-CH_2 protons. A singlet peak appears at δ_H 7.67 ppm indicates the presence of triazole ring proton. Two doublet peaks (at δ_H 5.96 ppm and δ_H 4.87 ppm), one doublet of doublet peak (at δ_H 4.50 ppm) and one multiplet peak (at δ_H 4.41-4.37 ppm) indicates the HC-O protons of glycosyl ring. Similarly,

Table 5
Ligand-protein binding energies scores, various amino acid residues binding interactions with interaction type with distance of potent anti-cancer agents **10t** and **10v**.

Compounds	*Anti-breast cancer* (PDBID: 1ZXN)		*Anti-lung Cancer* (PDBID: 2W3L)	
	Binding Energy Score (kcal/mol)	Interaction Type and Amino acid Residues with Distance(Å)	Binding Energy Score (kcal/mol)	Interaction Type and Amino acid Residues with Distance(Å)
10t	-10.6	π-Alkyl: Arg 70 (4.86 Å), Ala 64 (5.02 Å); Alkyl: Ile 113 (4.02 Å), Ile 5 (4.03 Å), Arg 4 (4.14 Å); C-H bond: Ser 121 (2.83 Å), Ile 5 (3.03 Å); π-σ: Ile 186 (3.80 Å)	-9.9	π-Donor: Arg 81 (2.61 Å); Alkyl: Met 50 (4.58 Å); C-H Bond: Asp 46 (2.62 Å), Leu 72 (2.46 Å); π-Anion: Tyr 43 (4.94 Å), Asp 46 (4.94 Å); π-Alkyl: Arg 81 (4.55 Å), Leu 72 (5.20 Å), Ala 84 (4.49 Å); π-π-T-Shaped: Phe 47 (5.10 Å)
10v	-10.2	π-Alkyl: Ala 64 (5.06 Å), Arg 70 (5.21 Å), Tyr 6 (4.74 Å, 4.55 Å), Ile 5 (4.96 Å); Alkyl: Arg 4 (4.33 Å), Ile 113 (3.65 Å, 4.39 Å); Conventional-H Bond: Asn 122 (2.40 Å); π-Donor: Asn 122 (2.81 Å); Amide π-Stacked: Asp 66 (4.74 Å)	-9.7	π-Alkyl: Phe 39 (5.02 Å), Ala 84 (4.52 Å); π-π-T-Shaped: Phe 39 (5.32 Å, 4.85 Å); Alkyl: Met 50 (5.40 Å), Val 68 (6.68 Å), Val 83 4.04 Å), Arg 42 (4.23 Å); C-H Bond: Glu 71 (2.56 Å); Conventional-H Bond: Arg 81 (2.60 Å, 2.13 Å, 1.99 Å)

three singlets at δ_H 2.48 ppm, 1.39 ppm and 1.25 ppm indicate the presence of methyl (CH_3) protons of tosyl-protected glycosyl ring. The necessary information about the carbon skeleton of the product **10a** was provided by ^{13}C NMR spectra. The carbon of azomethine group appears at δ_C 148.2 ppm and O-CH_2 Carbon of chromene ring appears at δ_C 64.3 ppm. The two carbons of triazole ring observed at δ_C 144.4 ppm and 128.5 ppm. In the tosyl-protected glycosyl ring of the compound three carbons of methyl groups appeared at δ_C 26.5 ppm, 26.2 ppm and 21.9 ppm respectively. All the protons and carbons of the synthesized compound **10a** were found in their respective positions (Fig. 3). Further, the formation structure of the compound **10a** was confirmed by HRMS spectral data (Molecular ion peak appeared at m/z 583.1879 compared to the calculated value of 583.1864). In addition to these, a single crystal X-ray diffraction was recorded to unambiguously determine the structure of compound **10a** (**CCDC: 2314962**) [88] as shown in Fig. 4.

3.1.3. *Crystal structure description and Intermolecular interactions*

The structural resolution revealed that the synthesized compound **10a** has been crystallized in the *triclinic* crystal system with the non-centrosymmetric space group P1. The unit cell parameters obtained by least-squares refinement method are: $a = 6.0527(2)$ Å, $b = 9.7411(3)$ Å, $c = 13.5541(4)$ Å, $\alpha = 107.539(3)^\circ$, $\beta = 101.265(3)^\circ$, $\gamma = 99.698(3)^\circ$, V = 724.90(4) $Å^3$ and the absorption coefficient is $\mu = 1.466$ mm^{-1} (Table 1). In the structure of compound **10a**, the oxygen atom O13 that is attached to the azomethine group is connected to the triazole moiety at the sp^3 hybridized C14 carbon atom. The sp^3 hybridization of C14 and C20 carbon atoms brings flexibility to the compound and again intramolecular hydrogen bonding between C14-H···N12 (2.46 Å) and C21-H···N15 (2.51 Å) leads to folding in compound **10a** (Fig. 5, Table 3).

3.1.4. *Supramolecular self-assembly in compound 10a*

The compound **10a** is stabilized by a combination of intramolecular and intermolecular C-H···π and π-π stacking interactions (Figs. 6 and 7). In Fig. 6A, the hydrogen H33B of glycosyl ring is in contact with the centroids of benzene ring with a separation distance of 3.42 Å and pyran ring with a separation distance of 3.36 Å of the chromene moiety through intra molecular C-H···π interactions. Also, another intramolecular interaction seen between the H20B hydrogen and benzene ring of tosyl-protected scaffold with a distance of 2.92 Å. Similarly, during the crystal packing of compounds an intermolecular interaction found between the centroids of triazole ring and H8 hydrogen of chromene ring with a separation distance of 3.67 Å (Fig. 6B). Furthermore, it was assumed that the folding of compound **10a** may be for the presence of C-H···π intramolecular interactions.

Moreover, the packing in compound **10a** is such that each individual compound has two weak π···π interactions within the benzene ring centroid of tosyl-protected glycosyl moiety and pyran ring centroid of chromene moiety which forms a chain that runs along the crystallographic *b*-axis with a glide plane in the *bc*-plane (Fig. 7).

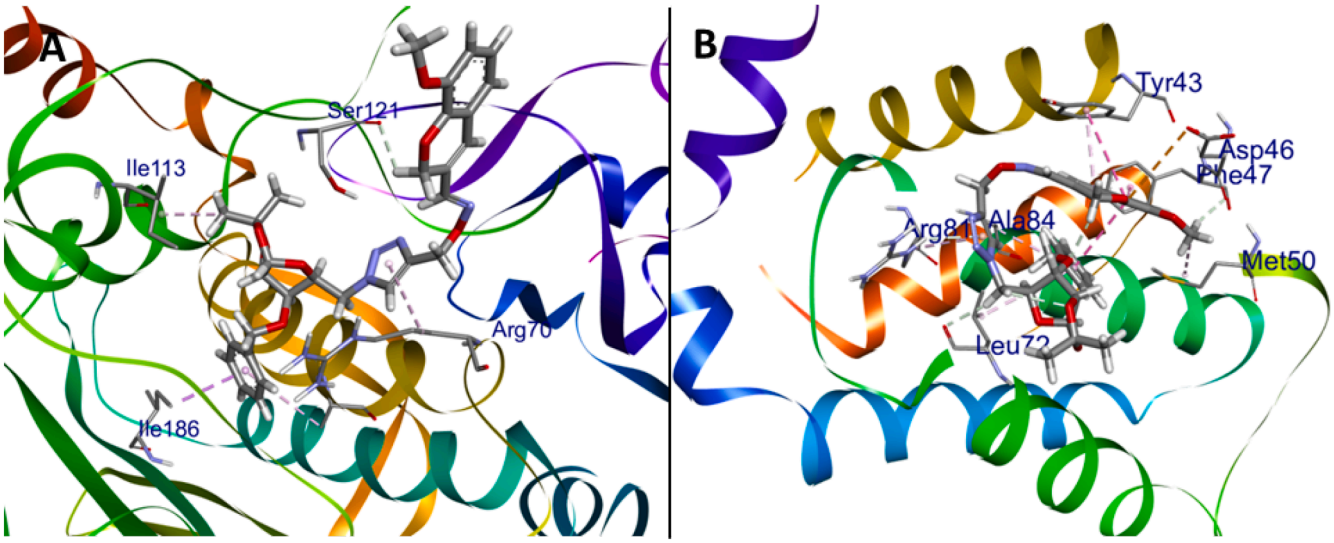

Fig. 9. 3D representation for the docking interaction of compound **10t** with DNA Topoisomerase IIA (**A**) and the apoptosis regulator BCL-2 (**B**). In the docked complex, protein represents as flat ribbon and the compound **10t** as stick model with amino acid residue interactions.

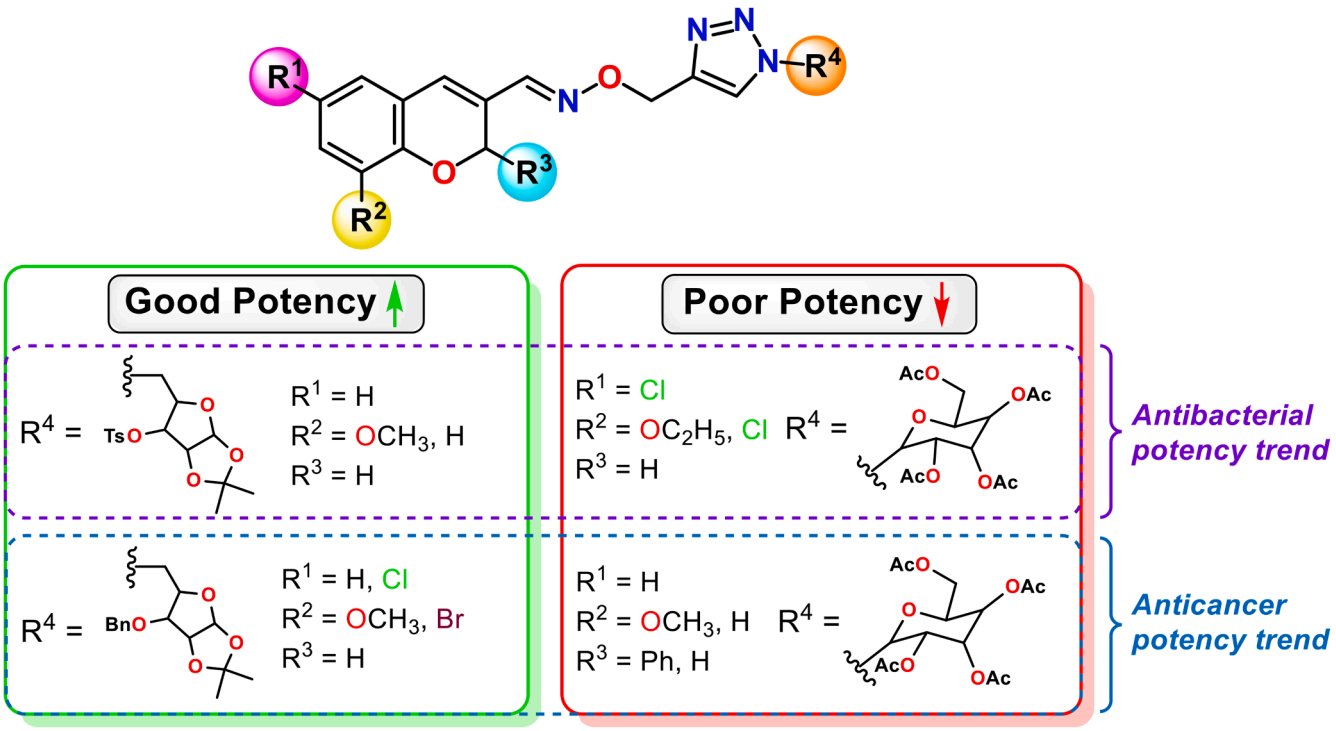

Fig. 10. Structure-activity relationships (SARs) analysis of 2*H*-chromene-1,2,3-triazolyl glycoconjugates **10a-w**.

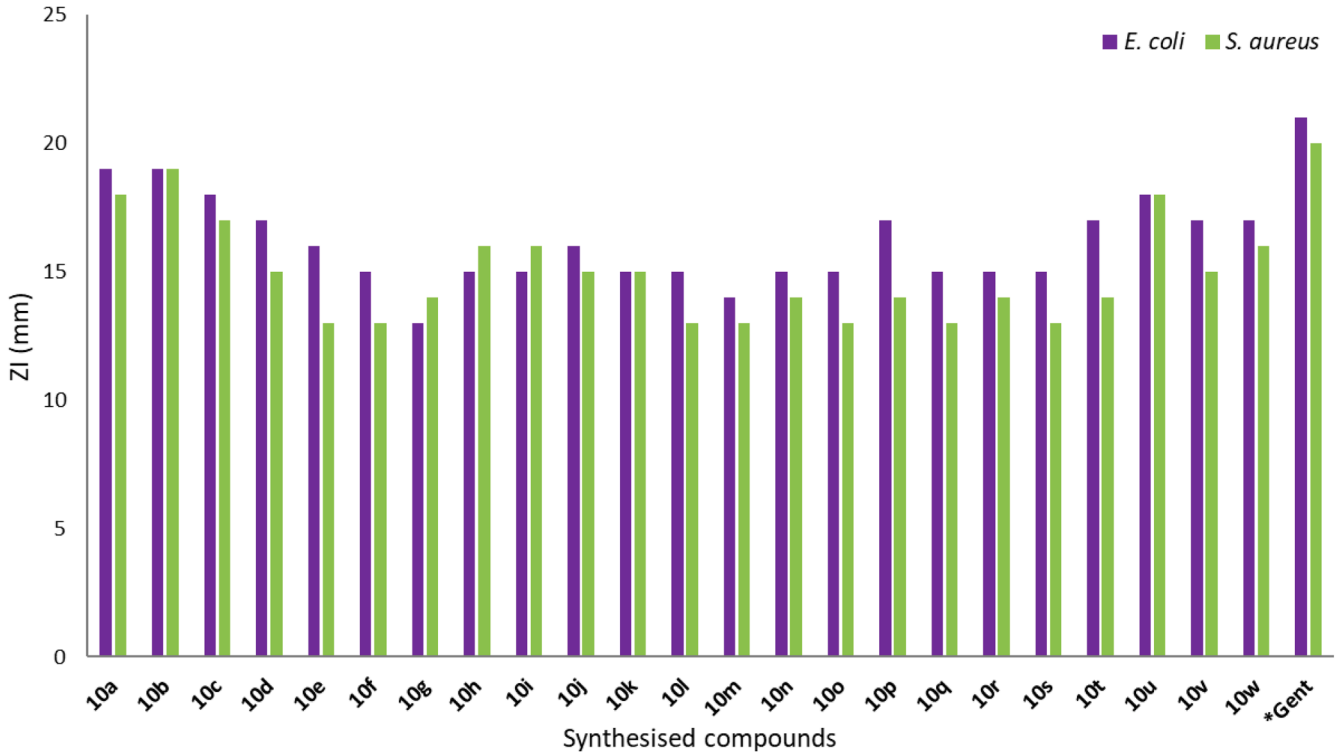

Fig. 11. The inhibitory antimicrobial action by zone of inhibition (ZI) assay of the synthesised 2*H*-chromene-1,2,3-triazolyl glycoconjugates **10a-w** assessed with reference drug Gentamicin.

3.2. Biological evaluations and molecular docking studies

3.2.1. Anticancer assay

3.2.1.1. In vitro cytotoxicity study. The cytotoxicity analysis of synthesized compounds **10a-w** were performed using MTT assay [63,64] on two human breast adenocarcinoma cell lines (MCF-7 and MDAMB-231) [35,60], one lung cancer cell line (A549) [61], in addition to a noncancerous cell line (HEK) [55]. IC_{50} values of these compound were calculated using GraphPad Prism. The experiments were conducted in triplicate and the data is presented as Mean IC_{50} values ± standard deviation (n = 3). The pursual of results of anticancer evaluation as

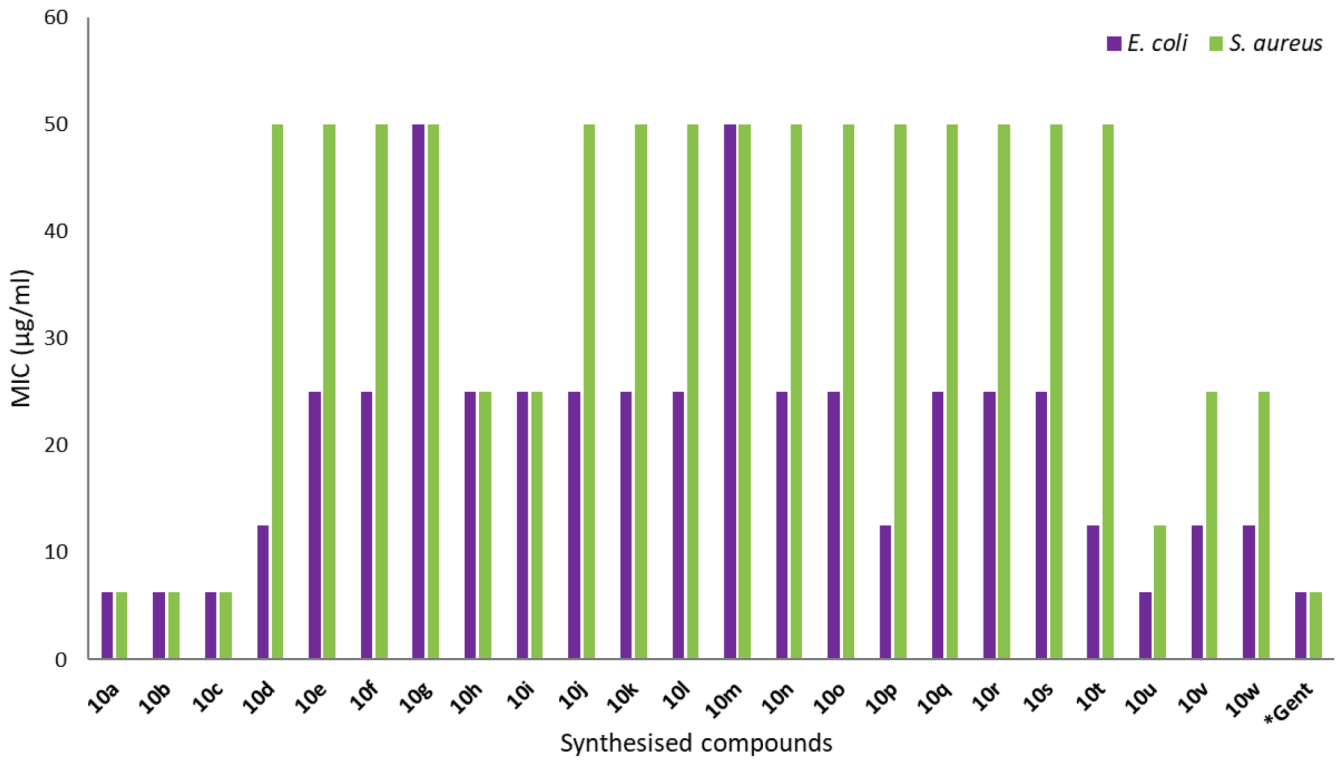

Fig. 12. The minimal inhibitory concentration (MIC) assay of the synthesised 2*H*-chromene-1,2,3-triazolyl glycoconjugates **10a-w** assessed with reference drug Gentamicin.

depicted in Table 4 revealed that all the derivatives showed dose dependent proliferation inhibition against human cancer cell lines. It was observed that in MCF-7 cell line the triazole compounds exhibited better activity as compared to other two cancer cell lines. Amongst them, the compounds **10t** ($IC_{50} = 6.90 \pm 0.24$ μM), **10v** ($IC_{50} = 7.45 \pm 0.31$ μM), **10u** ($IC_{50} = 12.49 \pm 0.37$ μM), and **10w** ($IC_{50} = 15.39 \pm 0.81$ μM) were found as the most active against MCF7. However, the remaining compounds exhibited inadequate inhibitory activity against the tested cell lines.

3.2.1.2. Hoechst 33342/PI double staining. Hoechst 33342/PI double staing study was used to determine the normal and death cells [65,66], The nuclei of normal cell show light blue where as the apoptotic cells can be stained in to brillant blue and red light (Fig. 8). In experiment the untreated group nulei were stained with blue and no red appear in image. In presence of compound **10t**, the cell number is dramatically reduced and containing number of apoptotic and necrotic cells, it can be concluded that the **10t** compund inhibit MCF-7 cell growth significantly.

3.2.2. Molecular docking analysis of anticancer proteins

3.2.2.1. Molecular docking analysis of antibreast cancer protein (PDB ID: 1ZXN). The docking outcomes for the synthesized 2*H*-chromene-1,2,3-triazolyl glycoconjugates **10a-w** against anti-breast cancer protein Human DNA Topoisomerase IIA (PDB ID: 1ZXN) target reflected a good binding energy ranged from -6.7 to -10.6 kcal/mol (Table 5, Table S5). The findings of this investigation revealed that all compounds commonly showed various binding interactions like conventional H-bonds, π-anion interactions, alkyl, Van der Waals interactions, π-cation interactions, π-donor hydrogen bonds, π-alkyl, π-σ bond, and π-π-stacked interactions with amino acid residues are shown in Table S5. Among all docked compounds, **10t** exhibited the highest binding energy -10.6 kcal/mol and π-alkyl interactions with Arg 70, Ala 64; C-H bond interactions with Ile 55, Ser 121; alkyl interactions with Arg 40, Ile 113; and π-σ interaction with Ile 186 respectively. The 3D image showing amino acid residue interactions of compound **10t** is as shown in Fig. 9, and the 2D images of all investigated compounds are as displayed in Fig. S29-S51.

3.2.2.2. Molecular docking analysis of anti-lungs cancer protein (PDB ID: 2W3L). The crystal structures of Chimaeric BCL-2-xL (PDB ID: 2W3L) was docked with the synthesised compounds **10a-w**. The binding energies of all docked compounds **10a-w** ranged from -6.3 to -9.6 kcal/mol (Table S5). In this series of compounds, the **10t** was found with the highest binding energy (-9.6 kcal/mol) owing to the good stability and strong interactions like alkyl, C-H bond, π-anion, π-π-stacked, π-alkyl, and π-donor (Table 5). The 3D visualisation of amino acid residual interactions with compound **10t** was illustrated in Figs. 9, and 2D images of all synthesised compounds are given in Fig. S29-S51.

3.2.3. Anti-cancer Structure-Activity Relationships (SARs)

We further established the structure activity relationships (SAR) according to the *in vitro* anticancer assay results (MCF 7 cell line) and *in silico* molecular docking of all the compounds **10a-w**. Notably, the compound **10t** having $R^1 = R^3 = H$, $R^2 = OCH_3$, R^4 = benzyl-protected sugar and the compound **10t** having R^1 = Cl, R^2 = Br, R^3 = H, R^4 = benzyl-protected sugar, exhibited significant anticancer effects against MCF-7 cell line with IC_{50} value of 6.90 ± 0.24 μM and 7.45 ± 0.31 μM respectively. Additionally, the computational analysis revealed that compound **10t** exhibited the most favorable binding interaction with both breast cancer and lung cancer proteins. Conversely, the presence of $R^1 = R^2 = H$, R^3 = Ph, R^4 = acetyl-protected sugar in the compound **10p** and the compound **10f** containing $R^1 = R^3 = H$, $R^2 = OCH_3$, R^4 = acetyl-protected sugar, demonstrated the lowest anticancer activity among all tested compounds, with weak binding interactions against cancer protein (Fig. 10).

3.2.4. Antibacterial assay

In the present study, pathogenic bacteria like *Methicillin-resistant Staphylococcus aureus* (MRSA) and *E. coli* were chosen due to their

Table 6
Ligand-protein binding energies scores, various amino acid residues binding interactions with interaction type with distance of potent anti-bacterial agents **10a** and **10b**.

Compounds	*E. coli* (PDB ID: 1G2A)		*S. aureus* (PDB ID: 1Q1Y)	
	Binding Energy Score (kcal/mol)	Interaction Type and Amino acid Residues with Distance(Å)	Binding Energy Score (kcal/mol)	Interaction Type and Amino acid Residues with Distance(Å)
10a	-8.9	π-Alkyl: Val 16 (5.03 Å), Cys 129 (4.90 Å), His 132 (4.85 Å); Alkyl: Val 138 (5.42 Å), Val 16 (4.80 Å), Lys 18 (4.34 Å), Ile 44 (4.55 Å); C-H Bond: Glu 42 (2.23 Å), (2.61 Å), (2.67 Å); π-Cation: Arg 97 (3.43Å); π-σ: Ile 44 (3.82 Å); π-π-Stacked: His 132 (4.84 Å); π-Anion: Glu 88 (4.66 Å)	-8.8	π-π-T-Shaped: His 154 (5.08 Å); π-σ: Val 151 (3.84 Å); Alkyl: Val 151 (5.41 Å), Val 159 (4.54 Å), Arg 56 (4.51 Å); C-H Bond: Gly 110 (3.51 Å), Ser 57 (2.98 Å); π–Donor: Arg 56 (2.80 Å); π-Alkyl: Arg 56 (4.45 Å); Conventional-H Bond: Asn 117 (2.14 Å)
10b	-9.5	π-Alkyl: Val 16 (4.49 Å),Val 138 (4.60 Å), His 132 (4.23 Å), Ile 44 (5.40 Å); π-π-Stacked: His 132 (5.70 Å); Alkyl: Val 16 (4.85 Å), Ile 128 (5.49 Å), Cys 129 (4.26 Å), Leu 91 (4.50 Å), (4.03 Å); C-H Bond: Ser 63 (2.77 Å),Val 62 (2.92 Å); Conventional-H Bond: Gly 89 (3.24Å); π-Donor: Gly 89 (4.66 Å)	-9.3	π-Alkyl: Val 151 (4.65 Å); π-π-Stacked: His 154 (4.2 Å); Alkyl: Val 59 (4.79 Å); C-H Bond: Gly 60 (2.96 Å), Thr 107 (2.92 Å), Glu 185 (2.32 Å); Conventional-H Bond: Ser 57 (2.61Å); π-Anion: Glu 185 (3.34Å)

frequent involvement in various infections, significant clinical relevance and prevalence. For instance, MRSA is commonly associated with conditions like bacteremia, infective endocarditis, and skin and soft-tissue infections, particularly following breaches in skin or mucosal barriers. It is a leading cause of hospital-acquired infections and is known for its resistance to multiple antibiotics, posing a serious public health challenge [89,90]. Meanwhile, *E. coli* is a major cause of diarrhea, urinary tract infections, respiratory illness and foodborne illnesses, with rising antibiotic resistance being a critical concern [91]. Additionally, it contributes to extraintestinal diseases like pneumonia, bacteremia, and abdominal infections such as spontaneous bacterial peritonitis [92,93].

All the newly synthesized scaffolds were screened for their *in vitro* antibacterial activity against a Gram-positive bacterium (*S. aureus*), as well as a Gram-negative bacterium (*E. coli*) with the concurrent study of minimum inhibitory concentration (MIC) and zone of inhibition (ZI). Gentamicin was taken as standard drug for the bacterial strain evaluations. As depicted in Figs. 11 and 12, all the synthesized compounds **10a-w** exhibited significant variations in the MIC and ZI assay values ranging from 13 mm to 19 mm and 6.5 μg/ml to 50 μg/ml for both *E. coli* and *S. aureus* in comparison to the standard antibacterial drug Gentamicin with ZI values of 21 mm, 20 mm and MIC assay of 6.25 μg/ml, 12.5 μg/ml respectively. Among all the tested compounds, tosyl-protected glycosyl containing compounds **10a, 10b**, and **10c** exhibited the most potent antibacterial activity with a MIC value of 6.25 μg/ml against both bacterial strains. The compound **10b** showed the highest zone of inhibition of 19 mm against both *E. coli* and *S. aureus*. On the other hand, acetyl-protected sugar containing compounds **10g** and **10m** displayed a weakest antibacterial activity with a MIC of 50 μg/ml against both gram-positive and gram-negative bacterial strains.

3.2.5. *Molecular docking analysis of antibacterial proteins*

3.2.5.1. Gram -ve antibacterial protein (PDB ID: 1G2A). The crystal structure of *Escherichia coli* peptide deformylase complex was docked with the synthesised compounds **10a-w**. The binding energies of all docked compounds **10a-w** ranged from -6.5 to -9.5 kcal/mol (Table S4). The findings of this investigation revealed that all compounds commonly showed various binding interactions like conventional H-bonds, π-cation interactions, π-donor hydrogen bonds, Van der waals interactions, π-anion interactions, π-π-stacked, π-alkyl, alkyl, and π-σ interactions with amino residues are shown in Fig. S6-S28. Among all

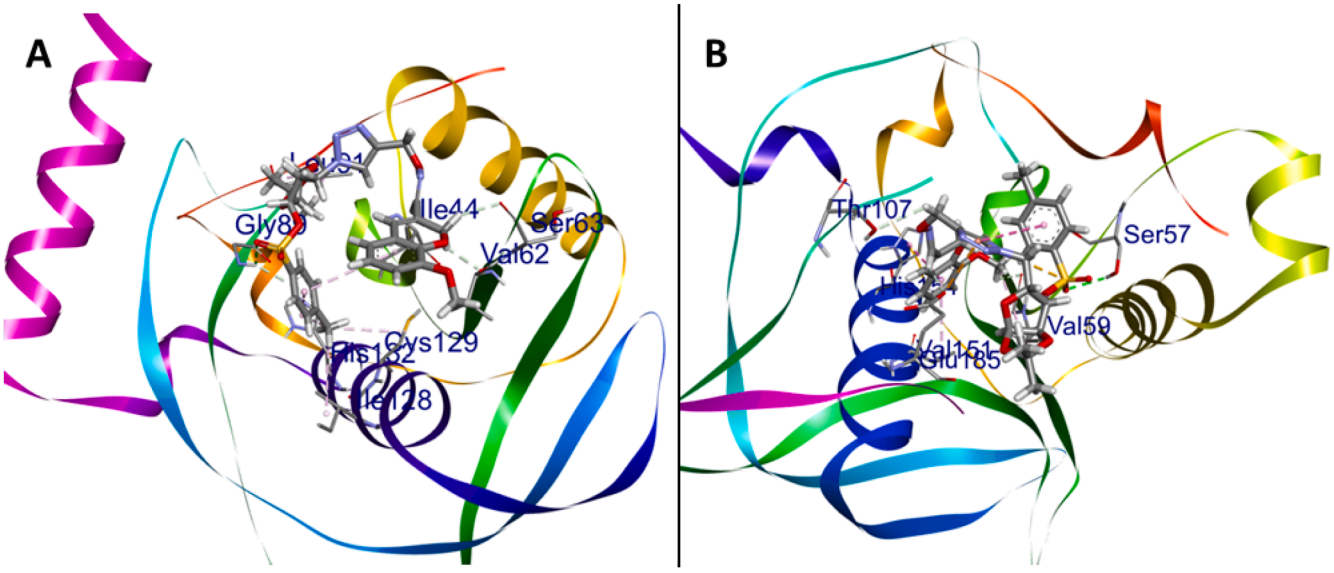

Fig. 13. 3D representation for the docking interaction of compound **10b** with *E. coli* Peptide deformylase (**A**) and with *S. aureus* Peptide deformylase (**B**). In the docked complex, protein represents as flat ribbon and the compound **10b** as stick model with amino acid residue interactions.

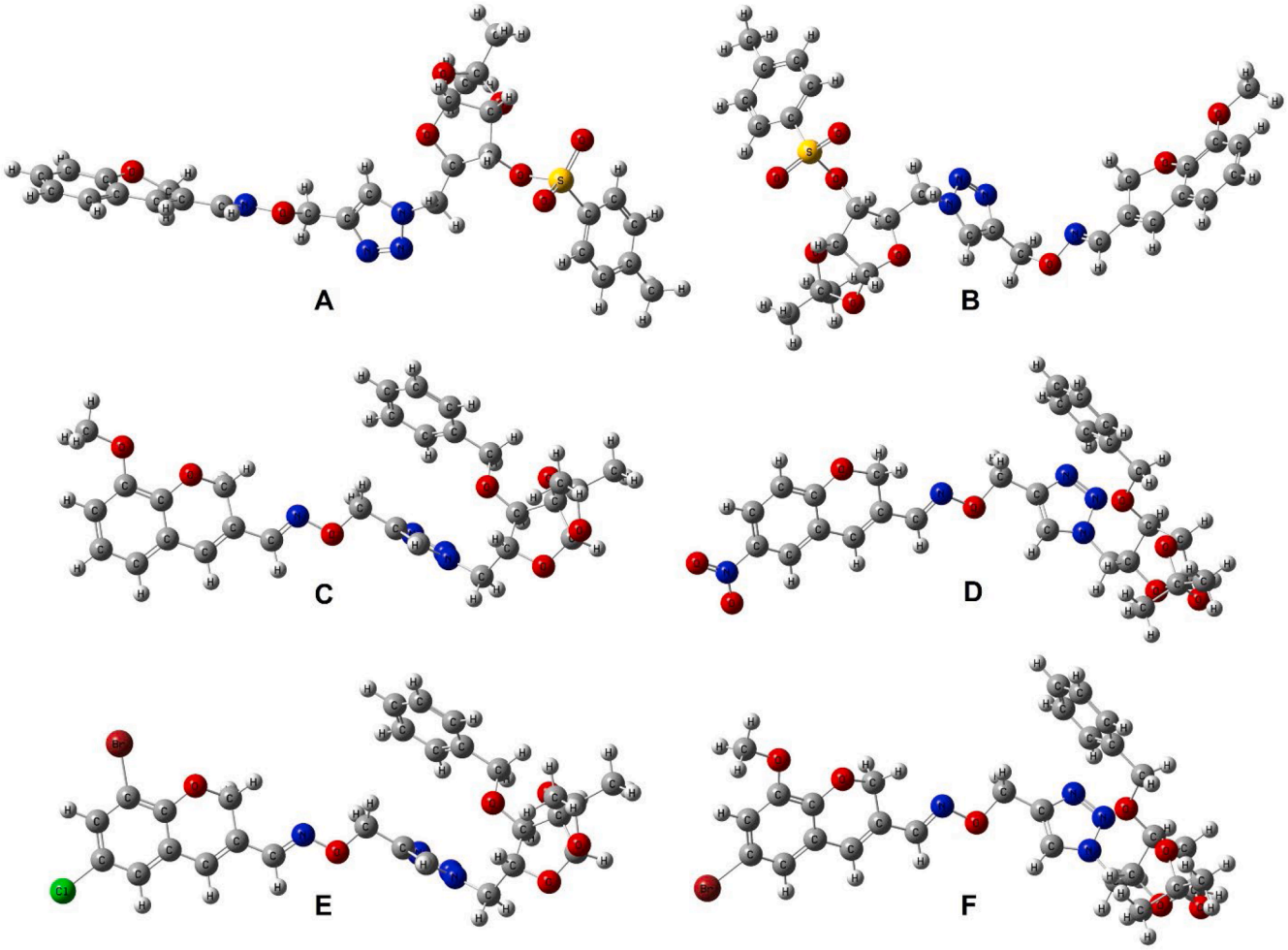

Fig. 14. The ball and stick model of optimized molecular structure of **10a** (**A**), **10b** (**B**), **10t** (**C**), **10u** (**D**), **10v** (**E**) and **10w** (**F**).

Table 7
FMO properties of 2*H*-chromene-1,2,3-triazolyl glycoconjugates **10a-w**.

Compounds	Energy of molecular properties										
	E_{LUMO} (eV)	E_{HOMO} (eV)	ΔEg (eV)	I (eV)	A (eV)	χ (eV)	μ (eV)	η (eV)	S (eV^{-1})	ω (eV)	N (eV^{-1})
10a	-2.7064	-5.5015	2.7951	5.5015	2.7064	4.1040	-4.1040	1.3976	0.3578	6.0258	0.1660
10b	-2.6672	-5.3450	2.6778	5.3450	2.6672	4.0061	-4.0061	1.3389	0.3734	5.9933	0.1669
10c	-2.2046	-4.9072	2.7026	4.9072	2.2046	3.5559	-3.5559	1.3513	0.3700	4.6787	0.2137
10d	-2.2346	-4.8762	2.6416	4.8762	2.2346	3.5554	-3.5554	1.3208	0.3786	4.7852	0.2090
10e	-1.4397	-5.1521	3.7124	5.1521	1.4397	3.2959	-3.2959	1.8562	0.2694	2.9262	0.3417
10f	-1.3660	-5.0403	3.6743	5.0403	1.3660	3.2031	-3.2031	1.8371	0.2722	2.7924	0.3581
10g	-1.3244	-5.0348	3.7105	5.0348	1.3244	3.1796	-3.1796	1.8552	0.2695	2.7247	0.3670
10h	-2.5507	-5.8308	3.2800	5.8308	2.5507	4.1908	-4.1908	1.6400	0.3049	6.3721	0.1569
10i	-1.6155	-4.9263	3.3108	4.9263	1.6155	3.2709	-3.2709	1.6554	0.3020	3.2315	0.3095
10j	-1.6520	-5.3725	3.7205	5.3725	1.6520	3.5122	-3.5122	1.8603	0.2688	3.3156	0.3016
10k	-1.5997	-5.3156	3.7159	5.3156	1.5997	3.4577	-3.4577	1.8580	0.2691	3.2174	0.3108
10l	-1.8305	-5.5508	3.7203	5.5508	1.8305	3.6906	-3.6906	1.8601	0.2688	3.6612	0.2731
10m	-1.9429	-5.6071	3.6642	5.6071	1.9429	3.7750	-3.7750	1.8321	0.2729	3.8891	0.2571
10n	-1.7812	-5.4942	3.7129	5.4942	1.7812	3.6377	-3.6377	1.8565	0.2693	3.5640	0.2806
10o	-1.5010	-5.1864	3.6854	5.1864	1.5010	3.3437	-3.3437	1.8427	0.2713	3.0336	0.3296
10p	-1.6318	-5.3154	3.6835	5.3154	1.6318	3.4736	3.4736	1.8418	0.2715	3.2756	0.3053
10q	-1.4931	-5.2237	3.7306	5.2237	1.4931	3.3584	-3.3584	1.8653	0.2681	3.0233	0.3308
10r	-1.7570	-5.4596	3.7026	5.4596	1.7570	3.6083	-3.6083	1.8513	0.2701	3.5164	0.2844
10s	-2.0386	-5.7254	3.6868	5.7254	2.0386	3.8820	-3.8820	1.8434	0.2712	4.0876	0.2446
10t	-1.6142	-5.3638	3.7496	5.3638	1.6142	3.4890	-3.4890	1.8748	0.2667	3.2465	0.3080
10u	-2.0830	-5.8245	3.7415	5.8245	2.0830	3.9537	-3.9537	1.8707	0.2673	4.1780	0.2393
10v	-2.0180	-5.7793	3.7613	5.7793	2.0180	3.8987	-3.8987	1.8807	0.2659	4.0411	0.2475
10w	-1.4639	-5.1967	3.7328	5.1967	1.4639	3.3303	-3.3303	1.8664	0.2679	2.9713	0.3366

Mathematical Description: Energy of LUMO = E_{LUMO}; Energy of HOMO = E_{HOMO}; Energy Gap (ΔEg) = E_{LUMO}-E_{HOMO}; Ionization Potential (I) = − E_{HOMO}; Electron Affinity (A) = − E_{LUMO}; Electronegativity (χ) = − (E_{LUMO} + E_{HOMO})/2; Chemical potential (μ) = (E_{LUMO} + E_{HOMO})/2; Global Hardness (η) = (E_{LUMO} − E_{HOMO})/2; Global Softness (S) = 1/2η; Global Electrophilicity index (ω) = μ^2/2η; Global Nucleophilicity index (N) = 1/ω

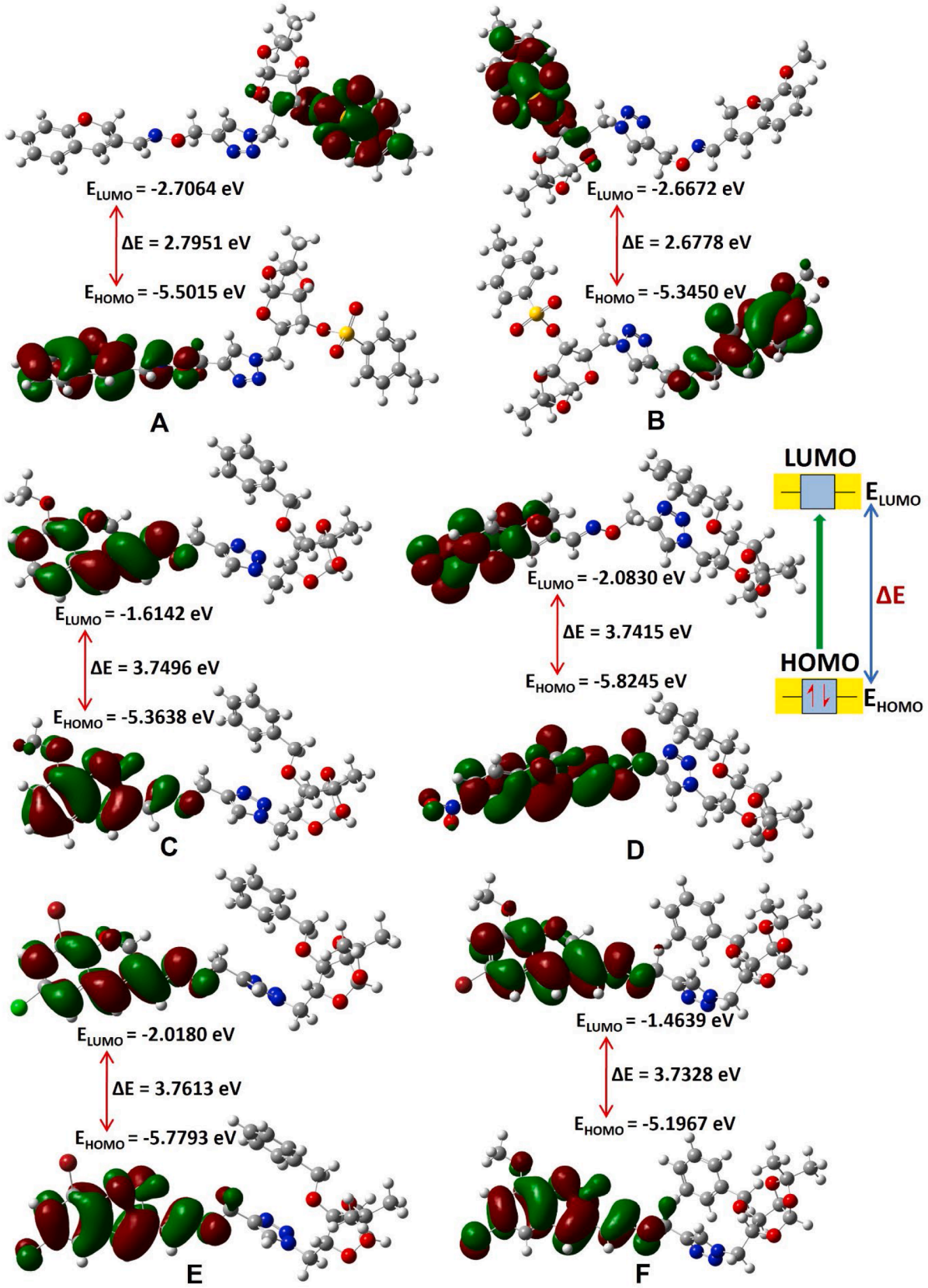

Fig. 15. HOMO-LUMO surface maps of optimized molecular structure of 2*H*-chromene-1,2,3-triazolyl glycoconjugates **10a** (**A**), **10b** (**B**), **10t** (**C**), **10u** (**D**), **10v** (**E**) and **10w** (**F**).

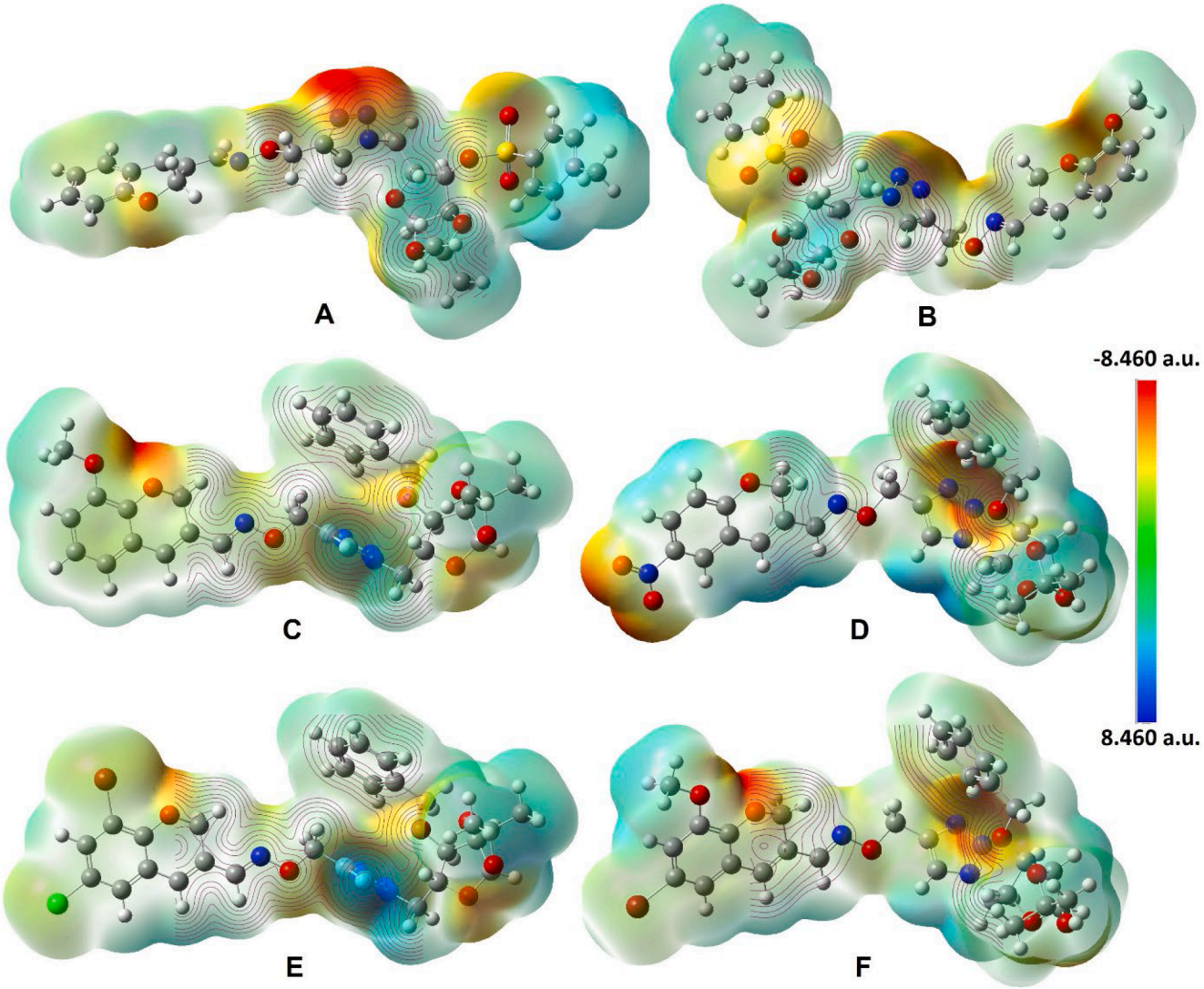

Fig. 16. Molecular electrostatic potential (MEP) with electrostatic contour plots of the investigated compounds **10a** (**A**), **10b** (**B**), **10t** (**C**), **10u** (**D**), **10v** (**E**) and **10w** (**F**).

docked compounds, **10b** exhibited the highest binding energy -9.5 kcal/mol and π-alkyl interactions with Val 16, Val 138, His 132, Ile 44; π-π-stacked interactions with His 132; C-H bond interactions with Ser 63, Val 62; conventional-H bond interactions Gly 89; and π-Donor interactions Gly 89 respectively (Table 6). The 3D image with amino acid residue interactions of compound **10b** is as shown in Fig. 13, all the 2D images of other compounds are as displayed in Fig. S6-S28.

3.2.5.2. Gram +ve antibacterial protein (PDB ID: 1Q1Y). The crystal structures of peptide deformylase from *Staphylococcus aureus* complex was docked with the synthesised compounds **10a-w**. The binding energies of all docked compounds **10a-w** ranged from -5.7 to -9.3 kcal/mol (Table S4). In this series of compounds, **10b** exhibited the highest binding energy (-9.3 kcal/mol) and amino acid residual interactions with interaction with π-alky, π-π-stacked, alkyl, Van der waals interactions C-H bond, conventional-H Bond, and π-anion (Table 6 and Fig. 13). All the docking results are as shown in Table S4 and also the 2D images are given in Fig. S6-S28.

3.2.6. Antibacterial Structure-Activity Relationships (SARs)

After a detailed analysis of the *in vitro* antibacterial activity and *in silico* molecular docking of all the compounds **10a-w**, the structure-activity relationship was outlined. Remarkably, the synthesised compound **10a** containing $R^1 = R^2 = R^3 = H$, R^4 = tosyl-protected sugar and the compound **10b** containing $R^1 = R^3 = H$, $R^2 = OCH_3$, R^4 = tosyl-protected sugar, showed the most potent antibacterial activity against both *E. coli* and *S. aureus* strains, with a minimal inhibitory concentration MIC of 6.25 μg/mL respectively. Additionally, the computational analysis revealed that compound **10b** exhibited the most favourable binding interaction with peptide deformylase of both Gram-negative (*E. coli*) and Gram-positive (*S. aureus*) bacteria, with binding energies of -9.5 kcal/mol and -9. kcal/mol, respectively. Likewise, **10a** demonstrated good interactions with both bacterial strains, displaying binding energies of -8.9 kcal/mol with *E. coli*, and -8.8 kcal/mol with *S. aureus*, respectively. Conversely, the compounds **10g** containing $R^1 = R^3 = H$, $R^2 = OC_2H_5$, R^4 = acetyl-protected sugar and the presence of $R^1 = R^2 =$ Cl, R^2 = H, R^4 = acetyl-protected sugar in the synthesised compound **10m** demonstrated the lowest antibacterial activity among all tested compounds, with lowest binding interactions against both bacterial strain proteins (Fig. 10).

3.3. Density functional theory investigation

3.3.1. Molecular geometry

The potent compounds **10a, 10b, 10t, 10u, 10v,** and **10w** among the series of synthesized 2*H*-chromene-1,2,3-triazolyl glycoconjugates went

Table 8
Physiochemical properties and medicinal chemistry data of compounds **10a, 10b, 10t, 10u, 10v**, and **10w** calculated using Admetlab 3.0 software.

	10a	10b	10t	10u	10v	10w	Recommended limit
Physicochemical Property							
MW	582.18	612.19	548.23	563.20	630.09	626.14	100 to 600 g/mol
logP	4.58	4.42	2.932	2.821	4.314	3.722	0 to 3 log octanol/water
logS	-5.94	-5.81	-4.59	-4.39	-5.80	-5.417	-4 to 0.5 mol/l
logD	3.79	3.62	3.458	3.25	3.823	3.686	1 to 3
nHA	12	13	11	13	10	11	0 to 12
nHD	0	0	0	0	0	0	0 to 7
TPSA	132.59	141.82	107.68	141.59	98.45	107.68	0 to 140 $Å^2$
nRot	9	10	10	10	9	10	0 to 11
nRing	1	1	1	1	1	1	0 to 6
MaxRing	10	10	10	10	10	10	0 to 18
nRig	34	34	32	33	32	32	0 to 30
nHet	13	14	11	13	12	12	1 to 15
fChar	0	0	0	0	0	0	-4 to 4
%ABS	63.26%	60.07%	71.85%	60.15%	75.04%	71.85%	
Medicinal Chemistry							
SA Score	4.46	4.54	4.00	4.00	4.00	4.00	≤ 6
NP Score	-0.31	-0.20	-0.116	-0.419	-0.319	-0.133	-5 to 5
Lipinski Rule (nViol)	Rejected (02)	Rejected (02)	Rejected (02)	Rejected (02)	Accepted (01)	Rejected (02)	MW $\leq$ 500, logP $\leq$ 5, nHA $\leq$ 10, nHD $\leq$ 5, nViol $\leq$ 1
Pfizer Rule	Accepted	Accepted	Accepted	Accepted	Accepted	Accepted	logP $\leq$ 3, TPSA $\geq$ 75 $Å^2$
Golden Triangle	Rejected	Rejected	Rejected	Rejected	Rejected	Rejected	200 $\leq$ MW $\leq$ 500, -2 $\leq$ logD $\leq$ 3

Abbreviations: MW = Molecular weight (in g/mol), nHA = Number of hydrogen bond acceptor, nHD = Number of hydrogen bond donor, TPSA = Topological polar surface area (in $Å^2$), nRig = Number of rigid bonds, nRing = Number of rings, MaxRing = Number of atoms in the biggest ring, %ABS = Percentage absorption, nViol = Number of violations

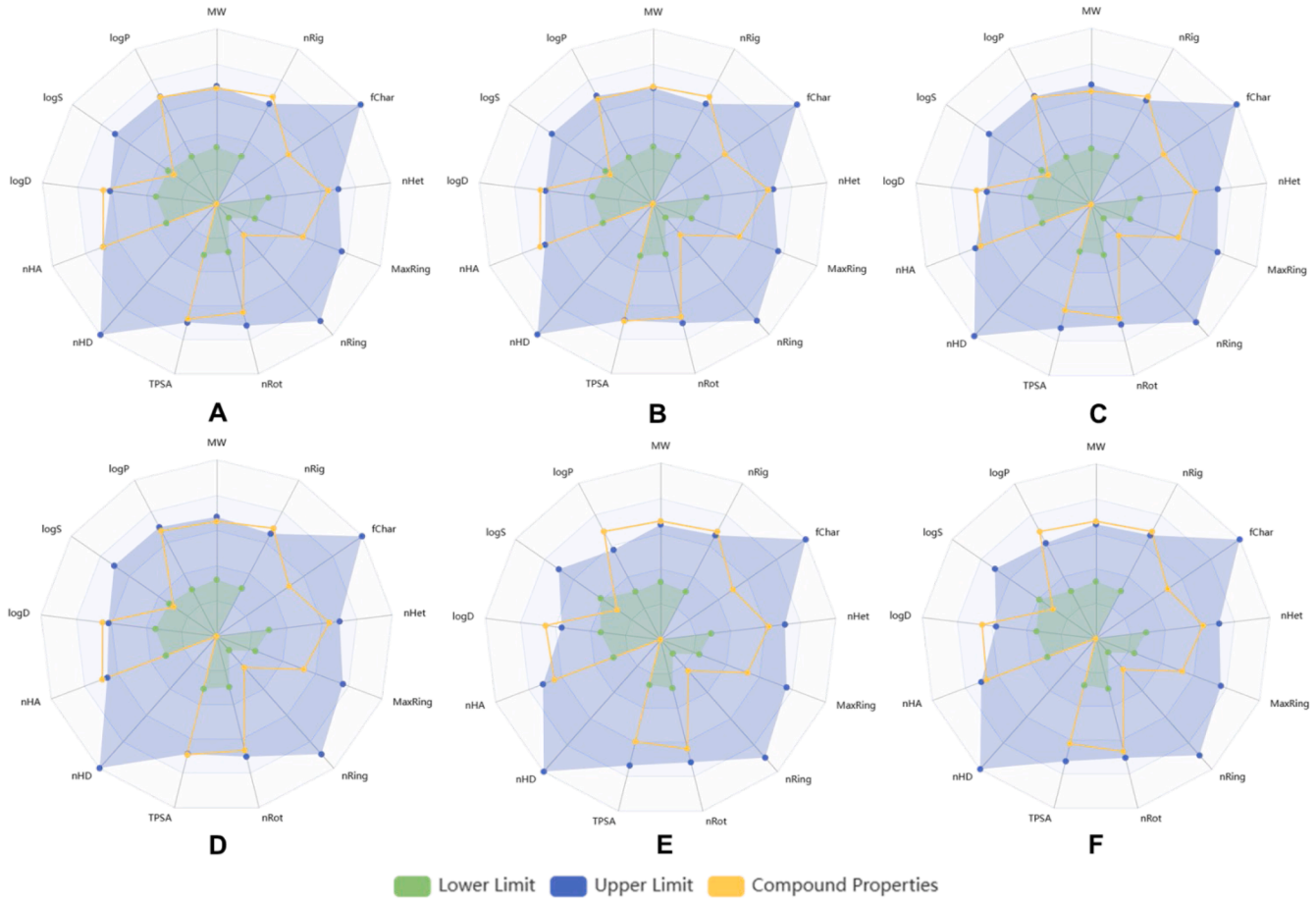

Fig. 17. Radar chart of the physicochemical properties of the compounds **10a** (**A**), **10b** (**B**), **10t** (**C**), **10u** (**D**), **10v** (**E**), **10w** (**F**) showing the *in-silico* measurements of the descriptors MW, nRig, fChar, nHet, MaxRig, nRing, nRot, TPSA, nHD, nHA, LogD, LogS, LogP.

Table 9
ADMET Properties data of compounds **10a, 10b, 10t, 10u, 10v**, and **10w** calculated using Admetlab 3.0 software.

ADMET	10a	10b	10t	10u	10v	10w	Recommended Limit
Absorption							
Caco-2 Permeability	-5.152	-5.210	-5.006	-5.064	-4.937	-5.068	$\geq$ -5.15 log unit
MDCK Permeability	-4.852	-4.922	-4.771	-4.742	-4.696	-4.754	$\leq 20 \times 10^{-6}$ cm/s
Pgp-inhibitor	0.164	0.131	0.168	0.053	0.190	0.413	0 to 0.5
Pgp-substrate	0.009	0.013	0.005	0.001	0.001	0.001	0 to 0.5
HIA	0.0	0.0	0.001	0.0	0.0	0.0	
$F_{50\%}$	0.055	0.025	0.227	0.210	0.013	0.006	
Distribution							
PPB	91.50%	91.72%	89.795%	94.127%	93.064%	97.435%	$\leq$ 90%
BBB	0.949	0.866	0.978	0.585	0.931	0.997	$<$ 0.5
VD	0.436	0.414	0.193	0.150	0.055	0.017	0.04 to 20 l/kg
Fu	1.688%	2.14%	5.91%	4.56%	1.939%	2.152	5 to 20%
Metabolism							
CYP1A2 inhibitor	0.001	0.003	0.061	0.026	0.588	0.254	0 to 0.5
CYP1A2 substrate	0.0	0.001	0.032	0.001	0.001	0.001	0 to 0.5
CYP2C19 inhibitor	0.870	0.849	0.846	0.583	0.980	0.985	0 to 0.5
CYP2C19 substrate	0.987	0.991	0.92	0.486	0.132	0.562	0 to 0.5
CYP2C9 inhibitor	0.920	0.948	0.669	0.320	0.961	0.988	0 to 0.5
CYP2C9 substrate	0.298	0.173	0.063	0.038	0.001	0.003	0 to 0.5
CYP2D6 inhibitor	0.071	0.111	0.043	0.012	0.061	0.553	0 to 0.5
CYP2D6 substrate	0.010	0.049	0.542	0.177	0.004	0.149	0 to 0.5
CYP3A4 inhibitor	0.923	0.930	0.227	0.039	0.113	0.096	0 to 0.5
CYP3A4 substrate	0.999	0.996	0.993	0.962	0.992	0.973	0 to 0.5
Excretion							
CL	2.309	3.718	5.346	5.233	4.516	4.572	5 to 15 ml/min/kg
$T_{1/2}$	0.045	0.771	0.939	0.841	1.029	1.164	$>$ 4h
Toxicity							
hERG Blocker	Safe (80.16%)	Safe (75.75%)	Safe (84.67%)	Safe (81.54%)	Safe (87.70%)	Safe (76.70%)	
DILI	0.994	0.997	0.976	0.999	0.996	0.987	$<$ 0.5
Carcinogenicity	0.932	0.951	0.924	0.935	0.887	0.935	$<$ 0.5
Skin Sensitization	0.239	0.288	0.314	0.724	0.593	0.400	$<$ 0.5
LD_{50}	1000	1000	3750	1000	3750	3750	above 2000 mg/kg
Toxicity Class	4	4	5	4	5	5	Class 5 and 6

MDCK = Apparent permeability in Madin-Darby canine kidney cells, HIA = Human intestinal absorption, VD = Volume of distribution, $F_{50\%}$ = 50% Bioavailability, PPB = Plasma protein binding, BBB = Blood-Brain Barrier, PGP = Plasma glycoprotein, CL = Clearance, DILI = Drug-induced liver injury, hERG = human ether-a-go-go-related gene, $T_{1/2}$ = Half-life period, LD_{50} = The median lethal dose.

through full DFT geometry optimization, as the conformational characteristics significantly affect the chemical and physical properties of the compound. The optimised molecular structures were as displayed in Fig. 14.

3.3.2. *Frontier molecular orbital (FMO) analysis*

Frontier Molecular Orbital (FMO) analysis is a theoretical method employed in quantum chemistry to comprehend the reactivity, chemical responses, stability, electronic characteristics, and optical properties of organic molecules [94]. The energy difference between these Highest Occupied Molecular Orbital (HOMO) and Lowest Unoccupied Molecular Orbital (LUMO), known as the HOMO-LUMO energy gap (ΔE_g), predicts the reactivity and kinetic stability of the molecule [95]. A minimal ΔE_g value indicates significant intramolecular charge transfer along a conjugated pathway from the electron donor to the acceptor. Consequently, molecules with smaller ΔEg value tend to exhibit higher chemical reactivity and polarizability, but lower kinetic stability. Whereas, large ΔEg value implies high kinetic stability, less chemical reactivity and less polarizability, because adding electrons to a high-lying LUMO orbital and removing electrons from a low-lying HOMO orbital is energetically unfavorable, making it difficult to form the activated complex for any potential reaction [96].

Table 7 displays the 2*H*-chromene-1,2,3-triazolyl glycoconjugates (**10a-w**) exhibited HOMO and LUMO energy values ranging from -5.8308 eV to -4.8762 eV and -2.7064 eV to -1.3244 eV respectively. The calculated energy gaps (ΔEg) were from 2.6416 eV to 3.7613 eV. In our research, compound **10v** is the most stable molecule with ΔEg value 3.7613 eV. As depicted in Fig. 15 A-F, the molecular orbitals analysis of most potent compounds (**10a, 10b, 10t, 10u, 10v**, and **10w**) revealed that the HOMO cloud predominantly localized over the 2*H*-Chromene ring and with lesser coverage extending to the adjacent acyclic rings. Whereas in compound **10a** and **10b** (Fig. 15 A and B) the LUMO cloud is primarily concentrated on the tosyl-protected glycosyl ring and in compound **10t** and **10v** (Fig. 15 C-F) focused on 2*H*-chromene ring, with marginal extension towards the adjacent acyclic rings. Among the potent compounds, compound **10v** has high kinetic stability and low chemical reactivity.

For understanding the electrical and chemical characteristics of the investigated compounds, as well as their optimization for specific applications, depend on evaluating their FMO properties. In computational chemistry, electronegativity(χ), electrophilicity index(ω), hardness (η), softness (S) etc. are some of the most often used chemical global reactivity descriptors. A chemical with a low value of ω is considered a nucleophile, whereas a compound with a high value of ω is considered a good electrophile [97]. Koopman's theorem was often used in FMO property estimations [98]. The FMO properties of the examined compounds are shown in Table 7.

The global electrophilicity index (ω) for all the compounds are determined to be 2.7247 eV to 6.3721 eV. A higher electrophilicity index value suggests a stronger capacity to bind to biomolecules and behave as an electrophilic species [99]. As indicated in Table 5, the lower value of chemical softness and higher value of hardness of the molecule suggested that all the synthesized compounds exhibit predominantly hard in nature. The electronic chemical potential (μ) having lower calculated values indicates that the investigated compounds are stable with good polarizability [100]. The higher level of resonance, strong polarizability, and promoting stability of the compounds were further confirmed by Average Local Ionization Energy (ALIE), Electron Localization Function (ELF), Local Orbital Locator (LOL), and Reduced Density Gradient (RDG) color-filled plots analysis of some potent

compounds (**10a, 10b, 10t** and **10v**) were illustrated in Fig. S52, S53, S54 and S55 (supporting Information) [101-104].

3.3.3. Molecular electrostatic potential (MEP) analysis

The molecular electrostatic potential (MEP) is a highly instructive characteristic for discerning the reactive sites within a molecule, distinguishing between electrophilic and nucleophilic reactivity. It depicts the electrostatic field generated by the nuclei and electrons of the molecule in its surrounding space. The color-coded graphs exhibit a rainbow-like appearance, characterized by the division of multiple zones by distinct colours; each color code represents the electrostatic potential present at the molecule's surface [105,106]. The prospective value spectrum is delineated as follows: red, orange, yellow, green, and blue. The colors red and blue are indicative of regions that are abundant in electrons and deficient in electrons, signifying electrophilic and nucleophilic behavior respectively. Neutral regions are depicted in green color, indicating a zero electrostatic potential. As shown in Fig. 16, the color-coded MEP with contour diagrams for the investigated compounds were derived from their optimized structures. Our investigation exploits MEP maps ranging from -8.460 a.u. to 8.460 a.u. on an electron density iso-surface of 0.0004 a.u. In our findings, regions of pronounced negativity are observed above the oxygen atoms in the chromene as well as glycosyl rings, suggesting them as probable sites for electrophilic attack. The presence of positive areas around each hydrogen atom indicates their suitability as sites for nucleophilic assault.

Furthermore, the contour lines on these maps delineate the charge distribution within the compounds, with positive charges depicted by yellow lines and negative charges by red lines (Fig. 16). This analysis highlights the triazoles moiety as a hydrogen bond acceptor, affirming the donor-acceptor nature of our molecules due to the presence of electrophilic and nucleophilic interactions. The nitrogen atoms of triazole ring are more electron rich than the other nitrogen atom in the investigated compounds. The positive potential is specifically confined to the H hydrogen atoms of the C-H, whereas the negative potential is mostly focused on the S and N atoms in both compounds, as seen by the MEP plots.

3.4. In silico ADMET properties studies

A successful pharmaceutical candidate needs to show not just effectiveness but also the ability to arrive at its target destination in the body with the required concentration to perform its intended biological function without causing any negative side effects. *In silico* ADMET prediction can be used to find the most promising compounds and minimize late-stage pharmaceutical toxicity. To determine drug-likeness, Admetlab 3.0 software assessed the ADMET (absorption, distribution, metabolism, excretion, and toxicity) features of all synthesized derivatives [107,108]. Calculations are conducted on the physiochemical attributes and medicinal chemistry of some top potent anti-bacterial compounds (**10a, 10b, 10u, 10v**, and **10w**) and anti-cancer compounds (**10t, 10u, 10v**, and **10w**) among the synthesized compounds (Table 8). Lipinski's rule is commonly employed to assess molecular properties crucial for a drug's *in vivo* pharmacokinetics. According to the Lipinski's rule of five, a candidate compound is likely to be orally active if it meets the criteria: (a) molecular weight (MW) is $\leq$ 500 g/mol, (b) octanol water partition coefficient (logP) is $\leq$ 5, (c) hydrogen-bond acceptors (nHA) is $\leq$ 10 (d), hydrogen bond donors (nHD) is $\leq$ 5, and (e) number of violations (nViol) is $\leq$ 1 [89,109-112].

The number of rotatable bonds indicates the molecular flexibility which might impact oral bioavailability; a more flexible molecule may result in less effectiveness when administered orally. Moreover, it has been proposed that the topological polar surface area (TPSA), inversely related to the percentage absorption (%ABS = 109 - 0.345 $\times$ TPSA), could serve as an alternative method for estimating percentage absorption, replacing the need to count hydrogen bonding groups. Compounds possessing a total polar surface area (TPSA) below 140 $Å^2$ and no more than 10 rotatable bonds need to demonstrate high oral bioavailability [108,113].

The TPSA values of compounds **10t, 10v**, and **10w** at 107.68 $Å^2$, 98.45 $Å^2$, and 107.68 $Å^2$ suggest favourable intestinal absorption, whereas compounds **10a, 10b**, and **10u** with values of 132.59 $Å^2$, 141.82 $Å^2$, and 141.59 $Å^2$ respectively, indicate moderate absorption (Table 6). The molecular weights of selected compounds range from 548.23 to 630.09 g/mol, and hydrogen bond acceptor counts range from 10 to 13. These compounds exhibit high permeability, absorption, and membrane transport, along with 9 to 10 rotatable bonds and oral absorption percentages between 60.07% and 75.04%. *In silico* assessments indicate promising activity based on physicochemical property findings indicated that **10t** aligned well with the optimal reference values depicted in its bioavailability radar chart (Fig. 17).

Table 9 comprehends all the ADMET properties of the selected four compounds. It was exposed that outcomes of compounds tended to be either a substrate or inhibitor of plasma glycoprotein (PGP). Plasma protein binding (PPB) is a critical factor in determining the safety of a treatment as a drug. The drugs with low PPB values ($\leq$ 90%) are considerably safer than those with high PPB values, which have a limited therapeutic range. The examined molecules in this study may have a wide therapeutic index, as they exhibited PPB value with safer range. Although prediction showed the compounds have poor Pgp-inhibitors, all the demonstrated compounds have excellent MDCK permeability ranging between -4.922 and -4.696 cm/s with Pgp-substrates. The predicted bioavailability ($F_{50\%}$) score and human intestinal absorption (HIA) of all four compounds shows good results. Also, the blood-brain barrier (BBB) permeability of these molecules is low. The Caco-2 permeability values ranging between -5.210 and -4.937 log unit for metabolism. The prediction showed a lower order of metabolic clearance of CL = 2.309 to 5.346 ml/min/kg with a shorter half-life range of $T_{1/2}$ = 0.045 to 1.164 h. The predicted LD_{50} and toxicity class defined that compound **10t, 10v**, and **10w** came under drug recommendation limit and also all four compounds showed class 4 to 6 toxicity level (Table 9, Fig. S56). According to ADMET analysis, compounds **10a, 10b, 10t, 10u, 10v** and **10w** are anticipated to be safe and might not cause hERG (human ether-a-go-go related gene), DILI, Carcinogenicity and skin sensitization.

4. Conclusion

We have successfully synthesized a novel series of 2*H*-chromene-1,2,3-triazolyl glycoconjugates **10a-w** were synthesized in good to excellent yields (68-98%), via a microwave irradiation technique following Click chemistry protocol. All the synthesized compounds were characterized by ^{1}H NMR, ^{13}C NMR, and HRMS spectroscopic techniques. The crystal of compound **10a** was obtained and its structure was confirmed by single crystal X-ray diffraction method. All synthesized compounds were subjected to *in vitro* antibacterial evaluation against two human pathogenic bacteria, one Gram-positive (*S. aureus*) and one Gram-negative (*E. coli*). Among these, compounds **10a, 10b, 10u, 10v**, and **10w** had remarkable inhibitory action exhibiting ZI value of 15 mm to 19 mm with MIC value of 6.25 μg/ml to 25 μg/ml for *S. aureus* bacterial strain and ZI value of 17 mm to 19 mm with MIC value of 6.25 μg/ml to 12.5 μg/ml for *E. coli* bacterial strain in comparison to the reference drug Gentamicin (MIC value: 6.25 μg/ml; ZI value: 20 mm, 21 mm). Also, the anti-cancer activity of synthesized compounds were evaluated towards two human breast cancer (MCF-7, MDAMB-231) and one lung cancer cell lines (A549). It was observed that in MCF-7 cell line the triazole compounds exhibited better activity as compared to other two cancer cell lines. Compounds **10t, 10u, 10v**, and **10w** showed most potent inhibitory activity against MCF-7 cell line with IC_{50} value 6.90 $\pm$ 0.24 μM, 12.49 $\pm$ 0.37 μM, 7.45 $\pm$ 0.31 μM, and 15.39 $\pm$ 0.81 μM respectively. Notably, compounds **10u, 10v**, and **10w** exhibited promising anticancer as well as antimicrobial activity. The higher negative binding energy of the corresponding compounds **10a, 10b, 10t, 10u,**

10v, and **10w** also supports the significant potency. The molecular structures of these compounds were optimized using DFT at B3LYP/6-311++G (d,p). Among the potent compounds, compound **10v** has high kinetic stability and low chemical reactivity. The overall E_{LUMO} values (-2.7064 eV to -1.3244 eV), E_{HOMO} values (-5.8308 eV to -4.8762 eV), and ΔEg values (2.6416 eV to 3.7613 eV) indicated that the studied compounds have high chemical reactivity and polarizability with low kinetic stability. Additionally, the most potent hybrids showed satisfactory ADMET characteristics. Therefore, it was concluded that compounds **10u, 10v**, and **10w** could be considered as promising dual inhibitors (bearing both anticancer and antimicrobial activities), compounds **10a** and **10b** as potent antibacterial agents and compound **10t** as an effective breast cancer agent which may serve as useful lead compounds for future drug discovery. Moreover, further derivatization or modification could lead to the development of more potent and selective agents.

Supporting Information Summary

Supporting information encompasses the experimental particulars, ^{1}H NMR spectra, ^{13}C NMR spectra, XRD, and HRMS data for all the produced compounds, accompanied by their respective MIC values, ZI values and binding energy.

CRediT authorship contribution statement

Bhabani Shankar Panda: Writing – review & editing, Writing – original draft, Validation, Software, Methodology, Investigation, Formal analysis, Data curation, Conceptualization. **Mohammed Ansar Ahemad:** Methodology, Formal analysis. **Suhasini Mohapatra:** Formal analysis. **Eeshara Naik:** Methodology, Formal analysis. **Sabita Nayak:** Writing – review & editing, Visualization, Validation, Supervision, Resources, Project administration, Methodology, Funding acquisition, Conceptualization. **Seetaram Mohapatra:** Supervision, Project administration, Funding acquisition. **Pradeep Kumar Naik:** Visualization, Validation, Resources, Methodology. **Debdutta Bhattacharya:** Validation, Resources, Methodology. **Chita Ranjan Sahoo:** Software, Methodology, Formal analysis. **Malaya K. Sahoo:** Methodology, Software.

Declaration of competing interest

The authors declare the following financial interests/personal relationships which may be considered as potential competing interests: SABITA NAYAK reports a relationship with Ravenshaw University that includes: employment. There is no conflict of interest. If there are other authors, they declare that they have no known competing financial interests or personal relationships that could have appeared to influence the work reported in this paper.

Data availability

Data will be made available on request.

Acknowledgments

Author BSP would like to thank CSIR (project No. 02(0381)/19/EMR-II) for providing the Senior research fellowship. The author MAA acknowledges LSRB, New Delhi (LSRB/01/15001/M/LSRB-372/BTB/2020) for their financial support. The authors SRM and SM are also thankful to SERB-SURE (project no. SUR/2022/ 000257) for financial support in the form of the research grant. The author EN would like to thank the award of student research fellowship (DST/INSPIRE/IF210313), Department of Science and Technology, Government of India. The authors would also acknowledge Dr. Sarada Srinivas Pati, DES, OSPCB-Bhubaneswar for his support. The author SN acknowledge DST, FIST-New Delhi (SR/FST/CSI-243/2012) for providing NMR facility to Ravenshaw University, Cuttack.

Supplementary materials

Supplementary material associated with this article can be found, in the online version, at doi:10.1016/j.molstruc.2024.139323.

References

[1] U.M. Kocyigit, Y. Budak, M.B. Gurdere, F. Erturk, B. Yencilek, P. Taslimi, I. Gulcin, M. Ceylan, Synthesis of chalcone-imide derivatives and investigation of their anticancer and antimicrobial activities, carbonic anhydrase and acetylcholinesterase enzymes inhibition profiles, Arch. Physiol. Biochem. 124 (2018) 61–68, https://doi.org/10.1080/13813455.2017.1360914.

[2] A.S. Almalki, S. Nazreen, A.M. Malebari, N.M. Ali, A.A. Elhenawy, A. A. Alghamdi, A. Ahmad, S.Y.M. Alfaifi, M.A. Alsharif, M.M. Alam, Synthesis and biological evaluation of 1,2,3-triazole tethered thymol-1, 3, 4-oxadiazole derivatives as anticancer and antimicrobial agents, Pharmaceuticals 14 (2021) 866, https://doi.org/10.3390/ph14090866.

[3] L.O.T. Gainkam, L. Huang, V. Caveliers, M. Keyaerts, S. Hernot, I. Vaneycken, C. Vanhove, H. Revets, P. de Baetselier, T. Lahoutte, Comparison of the biodistribution and tumor targeting of two 99mTc-labeled anti-EGFR nanobodies in mice, using pinhole SPECT/micro-CT, J. Nucl. Med. 49 (2008) 788–795, https://doi.org/10.2967/jnumed.107.048538.

[4] M.F. Hassan, S.A.F. Rostom, M.H. Badr, A.E. Ismail, A.M. Almohammadi, Synthesis of some 1,4,6-trisubstituted-2-oxo-1,2 dihydropyridine-3-carbonitriles and their biological evaluation as cytotoxic and antimicrobial agents, Arch. Pharm. Chem. Life Sci. 348 (2015) 824–834, https://doi.org/10.1002/ardp.201500175.

[5] N. Tavvabi-Kashani, M.V.B. Hasanpour, N.Vahdati-Mashhadian Rahimi, V. R. Askari, Pharmacodynamic, pharmacokinetic, toxicity, and recent advances in Eugenol's potential benefits against natural and chemical noxious agents: A mechanistic review, Toxicon (2024) 107607, https://doi.org/10.1016/j.toxicon.2024.107607.

[6] S.A. Rostom, M.H. Badr, H.A. Abd El Razik, H.M. Ashour, A.E. Abdel Wahab, Synthesis of some pyrazolines and pyrimidines derived from polymethoxy chalcones as anticancer and antimicrobial agents, Archiv Pharm. 344 (2011) 572–587, https://doi.org/10.1002/ardp.201100077.

[7] A. Chokshi, Z. Sifri, D. Cennimo, H. Horng, Global contributors to antibiotic resistance, J. Glob. Infect. Dis. 11 (2019) 36–42, https://doi.org/10.4103/jgid.jgid_110_18.

[8] M. Lomazzi, M. Moore, A. Johnson, M. Balasegaram, B. Borisch, Antimicrobial resistance–moving forward? BMC Public Health 19 (2019) 1–6, https://doi.org/10.1186/s12889-019-7173-7.

[9] C.L. Ventola, The antibiotic resistance crisis: Part 1: causes and threats, Pharm. Ther. 40 (2015) 277–283.

[10] I. Baccelli, Y. Gareau, B. Lehnertz, S. Gingras, J.F. Spinella, S. Corneau, N. Mayotte, S. Girard, M. Frechette, V. Blouin-Chagnon, K. Leveille, I. Boivin, T. MacRae, J. Krosl, C. Thiollier, V.P. Lavallee, E. Kanshin, T. Bertomeu, J. Coulombe-Hunt-ington, C. St-Denis, M.E. Bordeleau, G. Boucher, P.P. Roux, S. Lemieux, M. Tyers, P. Thibault, J. Hebert, A. Marinier, G. Sauvageau, Mubritinib targets the electron transport chain complex I and reveals the landscape of OXPHOS dependency in Acute Myeloid Leukemia, Cancer Cell 36 (2019) 84–99, https://doi.org/10.1016/j.ccell.2019.06.003.

[11] C.C. Blackwell, E.H. Freimer, G.C. Tuke, In Vitro evaluation of the new oral cephalosporin cefatrizine: comparison with other cephalosporins, Antimicrob. Agents Chemother. 10 (1976) 288–292, https://doi.org/10.1128/aac.10.2.288.

[12] C. Corrado, A.M. Flugy, S. Taverna, S. Raimondo, G. Guggino, R. Karmali, G. De Leo, R. Alessandro, Carboxyamidotriazole-orotate inhibits the growth of imatinib-resistant chronic myeloid leukaemia cells and modulates exosomes-stimulated angiogenesis, PLoS One 7 (2012) e42310, https://doi.org/10.1371/journal.pone.0042310.

[13] N.D. Thanh, V.T.N. Bich, P.T.T. Hien, N.T.K. Duyen, N.T. Mai, T.T. Dung, V. N. Toan, H.T.K. Van, D.N. Toan, T.T.T. Van, Efficient click chemistry towards novel 1*H*-1, 2, 3-triazole-tethered 4*H*-chromene-d-glucose conjugates: Design, synthesis and evaluation of in vitro antibacterial, MRSA and antifungal activities, Eur. J. Med. Chem. 167 (2019) 454–471, https://doi.org/10.1016/j.ejmech.2019.01.060.

[14] M. Dhameja, H. Kumar, S. Kurella, A. Uma, P. Gupta, Flavone-1, 2, 3-triazole derivatives as potential α-glucosidase inhibitors: Synthesis, enzyme inhibition, kinetic analysis and molecular docking study, Bioorg. Chem. 127 (2022) 106028, https://doi.org/10.1016/j.bioorg.2022.106028.

[15] L.S. Feng, M.J. Zheng, F. Zhao, D. Liu, 1,2,3-Triazole hybrids with anti-HIV-1 activity, Arch. Pharm. 354 (2021) e2000163, https://doi.org/10.1002/ardp.202000163.

[16] S. Zhang, Z. Xu, C. Gao, Q.C. Ren, L. Chang, Z.S. Lv, L.S. Feng, Triazole derivatives and their anti-tubercular activity, Eur. J. Med. Chem. 138 (2017) 501–513, https://doi.org/10.1016/j.ejmech.2017.06.051.

[17] Monika Chander, P.K. Sharma, S. Ram, Recent advances in triazole-benzenesulfonamide hybrids and their biological activities, Med. Chem. Res. 32 (2023) 777–801, https://doi.org/10.1007/s00044-023-03052-8.

[18] S. Bitla, S.R. Sagurthi, R. Dhanavath, M.R. Puchakayala, S. Birudaraju, A. A. Gayatri, V.K. Bhukya, K.R. Atcha, Design and synthesis of triazole conjugated novel 2,5-diaryl substituted 1,3,4-oxadiazoles as potential antimicrobial and anti-fungal agents, J. Mol. Struct. 1220 (2020) 128705, https://doi.org/10.1016/j.molstruc.2020.128705.

[19] X.L. Wang, K. Wan, C.H. Zhou, Synthesis of novel sulfanilamide-derived 1,2,3-triazoles and their evaluation for antibacterial and antifungal activities, Eur. J. Med. Chem. 45 (2010) 4631–4639, https://doi.org/10.1016/j.ejmech.2010.07.031.

[20] L. Deswal, V. Verma, D. Kumar, C.P. Kaushik, A. Kumar, Y. Deswal, S. Punia, Synthesis and antidiabetic evaluation of benzimidazole-tethered 1,2,3-triazoles, Arch. Pharm. 353 (2020) 2000090, https://doi.org/10.1002/ardp.202000090.

[21] S. Al-Taweel, Y. Al-Saraireh, S. Al-Trawneh, S. Alshahateet, R. Al-Tarawneh, N. Ayed, M. Alkhojah, A.K. Wisam, W. Zereini, O. Al-Qaralleh, Synthesis and biological evaluation of ciprofloxacin-1, 2, 3-triazole hybrids as antitumor, antibacterial, and antioxidant agents, Heliyon 9 (2023) e22592, https://doi.org/10.1016/j.heliyon.2023.e22592.

[22] K.R. Reddy, P.S. Rao, G.J. Dev, Y. Poornachandra, C.G. Kumar, P.S. Rao, B. Narsaiah, Synthesis of novel 1, 2, 3-triazole/isoxazole functionalized 2H-Chromene derivatives and their cytotoxic activity, Bioorg. Med. Chem. Lett. 24 (2014) 1661–1663, https://doi.org/10.1016/j.bmcl.2014.02.069.

[23] S. Chirra, R. Gondru, M. Manne, M. Azam, S.I. Resayes, R. Manchal, S. Narsimha, Synthesis of [1, 2, 4] triazolo [3, 4-b][1, 3, 4] thiadiazine-1, 2, 3-triazoles as potent EGFR targeting anti-breast cancer agents, J. Mol. Struct. 1306 (2024) 137803, https://doi.org/10.1016/j.molstruc.2024.137803.

[24] D.J. Boruah, D. Kathirvelan, K. Bora, R.A. Maurya, P. Yuvaraj, Efficient and environmentally friendly synthesis of 1,2,3-triazole derivatives via [3 + 2] cycloaddition and their potential as lung cancer inhibitors: an *in silico* study, Results Chem 5 (2023) 100903, https://doi.org/10.1016/j.rechem.2023.100903.

[25] F. Ghous, S. Shukla, S. Parveen, S. Kumar, M. Banerjee, A. Bishnoi, Synthesis, characterization, anti-lung cancer activity, and in-silico studies of some novel triazole-based analogues as Pellizzari products, J. Mol. Struct. 1304 (2024) 137578, https://doi.org/10.1016/j.molstruc.2024.137578.

[26] K. Gadali, M. Rafya, M. Maatallah, A. Mehdi, A. Ouahrouch, F. Benkhalti, H. B. Lazrek, Synthesis, structural characterization and antibacterial activity evaluation of novel quinolone-1, 2, 3-triazole-benzimidazole hybrids, J. Mol. Struct. 1282 (2023) 135179, https://doi.org/10.1016/j.molstruc.2023.135179.

[27] M. Aarjane, S. Slassi, A. Amine, Synthesis, antibacterial evaluation and computational studies of new acridone-1,2,3-triazole hybrids, J. Mol. Struct. 1241 (2021) 130636, https://doi.org/10.1016/j.molstruc.2021.130636.

[28] Y. Belay, A. Muller, P. Leballo, O.A. Kolawole, A.S. Adeyinka, T.Y. Fonkui, L. R. Motadi, Molecular hybrid of 1,2,3-triazole and schiff base as potential antibacterial agents: DFT, molecular docking and ADME studies, J. Mol. Struct. 1286 (2023) 135617, https://doi.org/10.1016/j.molstruc.2023.135617.

[29] S. Sutthivaiyakit, O. Thongnak, T. Lhinhatrakool, O. Yodchun, R. Srimark, P. Dowtaisong, M. Chuankamnerdkarn, Cytotoxic and antimycobacterial prenylated flavonoids from the roots of Eriosema chinense, J. Nat. Prod. 72 (2009) 1092–1096, https://doi.org/10.1021/np900021h.

[30] P.-C. Pan, M.-J. Cheng, C.-F. Peng, H.-Y. Huang, J.-J. Chen, I.-S. Chen, J. Secondary metabolites from the roots of Litsea hypophaea and their antitubercular activity, Nat. Prod. 73 (2010) 890–896, https://doi.org/10.1021/np100022s.

[31] Z.-Q. Xu, W.W. Barrow, W.J. Suling, L. Westbrook, E. Barrow, Y.-M. Lin, M. T. Flavin, Anti-HIV natural product (+)-calanolide A is active against both drug-susceptible and drug-resistant strains of Mycobacterium tuberculosis, Bioorg. Med. Chem. 12 (2004) 1199–1207, https://doi.org/10.1016/j.bmc.2003.11.012.

[32] A. Termentzi, I. Khouri, T. Gaslonde, S. Prado, B. Saint-Joanis, F. Bardou, E. P. Amanatiadou, I.S. Vizirianakis, J. Kordulakova, M. Jackson, R. Brosch, Y. L. Janin, M. Daffe, F. Tillequin, S. Michel, Synthesis, biological activity, and evaluation of the mode of action of novel antitubercular benzofurobenzopyrans substituted on A ring, Eur. J. Med. Chem. 45 (2010) 5833–5847, https://doi.org/10.1016/j.ejmech.2010.09.048.

[33] Y. Seo, J. Choi, J.H. Lee, T.G. Kim, S. Park, G. Han, W. Namkung, I. Kim, Diversity-oriented generation and biological evaluation of new chemical scaffolds bearing a 2,2-dimethyl-2*H*-chromene unit: Discovery of novel potent ANO1 inhibitors, Bioorg. Chem. 101 (2020) 104000, https://doi.org/10.1016/j.bioorg.2020.104000.

[34] P. Panda, S. Nayak, S. Bhakta, S. Mohapatra, T.R. Murthy, Design and synthesis of (Z/E)-2-phenyl/H-3-styryl-2H-chromene derivatives as antimicrotubule agents, J. Chem. Sci. 130 (2018) 127, https://doi.org/10.1007/s12039-018-1520-6.

[35] B.S. Panda, B. Samanta, S.S.S.S.S. Ambadipudi, S. Nayak, V.L. Nayak, S. Ramakrishna, S. Mohapatra, P.M. Behera, L. Samanta, New 2*H*-chromene-based hydrazone derivatives as promising anti-breast cancer agents: efficient synthesis, spectral characterization, molecular docking, and ADMET studies, Chem. Select 9 (2024) e202400115, https://doi.org/10.1002/slct.202400115.

[36] B. Samanta, B.S. Panda, S. Mohapatra, S. Nayak, D. Bhattacharya, C.R. Sahoo, Base catalyzed one-pot thia-Michael addition-oxidation reaction of hetero-aromatic thiols to 2-aryl-3-nitro-2*H*-chromenes and their antibacterial evaluation, New J. Chem. 48 (2024) 4953–4959, https://doi.org/10.1039/D3NJ05992H.

[37] V.T. Angelova, V. Valcheva, N.G. Vassilev, R. Buyukliev, G. Momekov, I. Dimitrov, L. Saso, M. Djukic, B. Shivachev, Antimycobacterial activity of novel hydrazide-hydrazone derivatives with 2*H*-chromene and coumarin scaffold, Bioorganic Med. Chem. Lett. 27 (2017) 223–227, https://doi.org/10.1016/j.bmcl.2016.11.071.

[38] D.R. Mishra, S. Nayak, B.P. Raiguru, S. Mohapatra, M.B. Podh, C.R. Sahoo, R. N. Padhy, Synthesis of (4S)-4-*C*-spiro-glycosyl-chromeno-[3,4-d] [1,2,3] triazoles: Biological evaluation and molecular docking investigation, J. Heterocycl. Chem. 58 (2021) 111–126, https://doi.org/10.1002/jhet.4151.

[39] D.R. Mishra, B.S. Panda, S. Nayak, N.K. Rauta, S. Mohapatra, C.R. Sahoo, R. N. Padhy, One-pot multi component synthesis of 4-((2*H*-chromen-3-yl)/(2-phenyl-2*H*-chromen-3-yl) methylene)-3-methylisoxazol-5 (4*H*)-ones and evaluation of their antibacterial activity, Tetrahedron 124 (2022) 133015, https://doi.org/10.1016/j.tet.2022.133015.

[40] S.Q. Yin, M. Shi, T.T. Kong, C.M. Zhang, K. Han, B. Cao, Z. Zhang, X. Du, L. Q. Tang, X. Mao, Z.P. Liu, Preparation of S14161 and its analogues and the discovery of 6-bromo-8-ethoxy-3-nitro-2H-chromene as a more potent antitumor agent in vitro, Bioorg. Med. Chem. Lett. 23 (2013) 3314–3319, https://doi.org/10.1016/j.bmcl.2013.03.097.

[41] A.K. Agrahari, P. Bose, M.K. Jaiswal, S. Rajkhowa, A.S. Singh, S. Hotha, N. Mishra, V.K. Tiwari, Cu(I) Catalyzed Click chemistry in glycoscience and their diverse application, Chem. Rev. 121 (2021) 7638–7795, https://doi.org/10.1021/acs.chemrev.0c00920.

[42] P. Bose, A.K. Agrahari, R. Singh, M. Singh, S. Kumar, R.K. Singh, V.K. Tiwari, Click inspired synthesis of piperazine-triazolyl sugar-conjugates as potent anti-Hela activity, Carbohydr. Res. 529 (2023) 108846, https://doi.org/10.1016/j.carres.2023.108846.

[43] M. Nieuwdorp, M.C. Meuwese, H.J. Mooji, C. Ince, L.N. Broekhuizen, J.J. P. Kastelein, E.S.G. Stroes, H.J. Vink, Measuring endothelial glycocalyx dimensions in humans:a potential novel tool to monitor vascular vulnerability, Appl. Physiol. 104 (2008) 845–852, https://doi.org/10.1152/japplphysiol.00440.2007.

[44] B. Anjaneyulu, G.B. Dharma Rao, T. Bajaj, Click chemistry: In vitro evaluation of glycosyl hybrid phosphorylated/thiophosphorylated 1, 2, 3-triazole derivatives as irreversible acetyl cholinesterase (AChE) inhibitors, Results Chem. 3 (2020) 100093, https://doi.org/10.1016/j.rechem.2020.100093.

[45] V.K. Tiwari, B.B. Mishra, K.B. Mishra, N. Mishra, A.S. Singh, X. Chen, Cu-catalyzed click reaction in carbohydrate chemistry, Chem. Rev. 116 (2016) 3086–3240, https://doi.org/10.1021/acs.chemrev.5b00408.

[46] V.V. Rostovtsev, L.G. Green, V.V. Fokin, K.B. Sharpless, A stepwise huisgen cycloaddition process: Copper(I)-catalyzed regioselective "ligation" of azides and terminal alkynes, Angew. Chem., Int. Ed. 41 (2002) 2596–2599.

[47] N.P. Mishra, S. Mohapatra, C.R. Sahoo, B.P. Raiguru, S. Nayak, S. Jena, R. N. Padhy, Design, one-pot synthesis, molecular docking study, and antibacterial evaluation of novel 2H-chromene based imidazo [1,2-a] pyridine derivatives as potent peptide deformylase inhibitors, J. Mol. Struct. 1246 (2021) 131183, https://doi.org/10.1016/j.molstruc.2021.131183.

[48] P. Panda, S. Nayak, S.K. Sahoo, S. Mohapatra, D. Nayak, R. Pradhan, C.N. Kundu, Diastereoselective synthesis of novel spiro indanone fused pyrano [3, 2-c] chromene derivatives following hetero-Diels-Alder reaction and in vitro anticancer studies, RSC Adv 8 (2018) 16802–16814, https://doi.org/10.1039/c8ra02729c.

[49] D. Ashok, P. Chiranjeevi, A.V. Kumar, M. Sarasija, V.S. Krishna, D. Sriram, S. Balasubramanian, 1,2,3-Triazole-fused spiro-chromenes as potential anti-tubercular agents: synthesis and biological evaluation, RSC Adv. 8 (2018) 16997–17007, https://doi.org/10.1039/c8ra03197e.

[50] R. Vroemans, Y. Verhaegen, M.T.T. Dieu, W. Dehaen, Assembly of fully substituted triazolochromenes via a novel multicomponent reaction or mechanochemical synthesis, Beilstein J. Org. Chem. 14 (2018) 2689–2697, https://doi.org/10.3762/bjoc.14.246.

[51] J.-M. Zhang, C.-L. Lou, Z.-P. Hu, M. Yan, Organocatalytic conjugate addition of nitroalkanes to 2*H*-chromene-3-carbaldehydes: synthesis of highly functionalized chroman derivatives, ARKIVOC 14 (2009) 362e375.

[52] I. Ibrahem, H. Sunden, R. Rios, G.L. Zhao, A. Cordova, One-pot pyrrolidine-catalyzed synthesis of benzopyrans, benzothiopyranes, and dihydroquinolidines, Chimia 61 (2007) 219–223, https://doi.org/10.2533/chimia.2007.219.

[53] C.B. Aakeroy, A.S. Sinha, K.N. Epa, C.L. Spartz, J. Desper, A versatile and green mechanochemical route for aldehyde-oxime conversions, Chem. Comm. 48 (2012) 11289–11291, https://doi.org/10.1039/C2CC36315A.

[54] A.R. Zala, H.N. Naik, I. Ahmad, H. Patel, S. Jauhari, P. Kumari, Design and synthesis of novel 1, 2, 3-triazole linked hybrids: Molecular docking, MD simulation, and their antidiabetic efficacy as α-Amylase inhibitors, J. Mol. Struct. 1285 (2023) 135493, https://doi.org/10.1016/j.molstruc.2023.135493.

[55] V. Kumar, S. Kumar, Ordering self-assembly structures via NH··· S and Br··· S interactions in (E)-2-(4-bromobenzylidene) hydrazinecarbothioamide: Insights from crystallographic and computational study, J. Mol. Struct. 1310 (2024) 138285, https://doi.org/10.1016/j.molstruc.2024.138285.

[56] G.M. Sheldrick, A short history of SHELX, Acta Cryst. A64 (2008) 112–122, https://doi.org/10.1107/S0108767307043930.

[57] O. Dolomanov, L.J. Bourhis, R.J. Gildea, J.A.K. Howard, H. Puschmann, OLEX2: a complete structure solution, refinement and analysis program, J. Appl. Cryst. 42 (2009) 339–341, https://doi.org/10.1107/S0021889808042726.

[58] S.S. Hamdani, B.A. Khan, M.N. Ahmed, S. Hameed, K. Akhter, K. Ayub, T. Mahmood, Synthesis, crystal structures, computational studies and α-amylase inhibition of three novel 1,3,4-oxadiazole derivatives, J. Mol. Struct. 1200 (2020) 127085, https://doi.org/10.1016/j.molstruc.2019.127085.

[59] G.M. Sheldrick, Crystal structure refinement with SHELXL, Acta Cryst. C71 (2015) 3–8, https://doi.org/10.1107/S2053229614024218.

[60] M. Ganesan, J. Sekar, S.P. Kandasamy, P. Srinivasan, Design, synthesis, spectral characterization, in silico ADMET studies, molecular docking, antimicrobial activity, and anti-breast cancer activity of 5, 6-dihydrobenzo [H] quinazolines, J. Mol. Struct. 1296 (2024) 136771, https://doi.org/10.1016/j.molstruc.2023.136771.

[61] V. Banoji, K.K. Angajala, S. Vianala, S. Manne, K.R. Ravulapelly, J. Vannada, Synthesis, characterization, cytotoxic evaluation, and molecular docking studies of novel 1, 2, 3-triazole-based chalcones for potential anticancer applications, Results Chem 7 (2024) 101294, https://doi.org/10.1016/j.rechem.2023.101294.

[62] P. Thomas, T.G. Smart, HEK293 cell line: a vehicle for the expression of recombinant proteins, J. Pharmacol. Toxicol. Met. 51 (2005) 187–200, https://doi.org/10.1016/j.vascn.2004.08.014.

[63] E.T. Warda, M.B. El-Ashmawy, E.S.E. Habib, M.S. Abdelbaky, S. Garcia-Granda, S. Thamotharan, A.A. El-Emam, Synthesis and in vitro antibacterial, antifungal, anti-proliferative activities of novel adamantane-containing thiazole compounds, Sci. Rep. 12 (2022) 21058, https://doi.org/10.1038/s41598-022-25390-0.

[64] A.S. de Souza, D.S. Dias, R.C. Ribeiro, D.C. Costa, M.G. de Moraes, D.R. Pinho, M. E. Masset, L.M. Marins, S.P. Valle, C.J. de Carvalho, G.S. de Carvalho, Novel Naphthoquinone-1H-1, 2, 3-triazole Hybrids: Design, Synthesis and Evaluation as Inductors of ROS-Mediated Apoptosis in the MCF-7 Cells, Bioorg. Med. Chem. 102 (2024) 117671, https://doi.org/10.1016/j.bmc.2024.117671.

[65] N. DeSouza, M. Zhou, Y. Shan, Cell cycle analysis of CML stem cells using hoechst 33342 and propidium iodide, CML Methods Protoc 1465 (2016) 47–57, https://doi.org/10.1007/978-1-4939-4011-0_5.

[66] J.A. Hardin, D.H. Sherr, M.A.D. Maria, P.A. Lopez, A simple fluorescence method for surface antigen phenotyping of lymphocytes undergoing DNA fragmentation, J. Immunol. Methods 154 (1992) 99–107, https://doi.org/10.1016/0022-1759(92)90217-H.

[67] A. Aamouche, G. Erik, FTIR-ATR biosensor based on self-assembled phospholipids surface: haemophilia factor VIII diagnosis, J. Spectrosc. 22 (2008) 2314–4920.

[68] E. Hamidov, A.A. Agar, K.E. El-Kelany, N. Dege, T.A. Yousef, H. Ferjani, A. Al-Janabi, Synthesis, crystallographic structure, Hirshfeld surface analysis and DFT calculations of Schiff base (Z)-4-methyl-2-(((3-nitrophenyl) imino) methyl) phenol, J. Mol. Struct. 1310 (2024) 138319, https://doi.org/10.1016/j.molstruc.2024.138319.

[69] D. Singh, R. Sharma, A. Nikam, J. Jadhav, S. Sankalp, S. Murugavel, R. Kant, Spectral, quantum chemical, X-ray crystallographic, Hirshfeld surface, energy framework, and molecular docking investigations of 4-acetylphenyl 4-methylbenzenesulfonate (APMBS), J. Mol. Struct. 1295 (2024) 136612, https://doi.org/10.1016/j.molstruc.2023.136612.

[70] R. Dennington, T.A. Keith, J.M. Millam, GaussView, version 6.0. 16, Semichem Inc., Shawnee Mission KS, 2016, pp. 143–150.

[71] T. Lu, F. Chen, Multiwfn: A multifunctional wavefunction analyzer, J. Comput. Chem. 33 (2012) 580–592, https://doi.org/10.1002/jcc.22885.

[72] N. Afza, P. Trivedi, A. Bishnoi, S. Parveen, S. Kumar, M. Banerjee, A convergent multicomponent synthesis, spectral analysis, molecular modelling and docking studies of novel 2*H*-pyrido [1, 2-a] pyrimidine-2, 4 (3*H*)-dione derivatives as potential anti-cervical cancer agents, J. Mol. Struct. 1279 (2023) 134982, https://doi.org/10.1016/j.molstruc.2023.134982.

[73] V. Mallikanti, V. Thumma, K.C. Veeranki, S. Gali, J. Pochampally, Synthesis, cytotoxicity, molecular docking and ADME assay of novel morpholine appended 1, 2, 3-triazole, Analogues 7 (2022) e202204020, https://doi.org/10.1002/slct.202204020.

[74] B.S. Hemanth, M.J. Deviprasad, M.B. Shivaswamy, S. Sumathi, R. Aswathy, M. A. Sangamesha, A.P. Ananda, H.S. Jayanth, T.N. Lohith, Synthesis of citral-tryptamine fused selenium nanospheres (CT@ SeNP's) and exploration of their anticancer, antibacterial, and electrochemical sensor applications, J. Mol. Struct. 1310 (2024) 138240, https://doi.org/10.1016/j.molstruc.2024.138240.

[75] S. Chirra, R. Gondru, M. Manne, M. Azam, S.I. Al-Resayes, R. Manchal, S. Narsimha, Synthesis of [1,2,4] triazolo [3,4-b][1, 3, 4] thiadiazine-1,2,3-triazoles as potent EGFR targeting anti-breast cancer agents, J. Mol. Struct. 1306 (2024) 137803, https://doi.org/10.1016/j.molstruc.2024.137803.

[76] F. Ghous, S. Shukla, S. Parveen, S. Kumar, M. Banerjee, A. Bishnoi, Synthesis, characterization, anti-lung cancer activity, and in-silico studies of some novel triazole-based analogues as Pellizzari products, J. Mol. Struct. 1304 (2024) 137578, https://doi.org/10.1016/j.molstruc.2024.137578.

[77] D.J. Boruah, D. Kathirvelan, K. Bora, R.A. Maurya, P. Yuvaraj, Efficient and environmentally friendly synthesis of 1,2,3-triazole derivatives via [3+ 2] cycloaddition and their potential as lung cancer inhibitors: an in silico study, Results Chem. 5 (2023) 100903, https://doi.org/10.1016/j.rechem.2023.100903.

[78] A.S. Rao, M.V. Vardhan, N.S. Reddy, T.S. Reddy, S.P. Shaik, C. Bagul, A. Kamal, Synthesis and biological evaluation of imidazopyridinyl-1,3,4-oxadiazole conjugates as apoptosis inducers and topoisomerase IIα inhibitors, Bioorg. Chem. 69 (2016) 7–19, https://doi.org/10.1016/j.bioorg.2016.09.002.

[79] R. Krishnamoorthy, M. Singh, P. Anaikutti, S. Dhanasekaran, T. Sathiah, Design and synthesis of novel N-terminal peptides of integrin and aminopeptidase are new finding for anticancer activity, Bioorg. Chem. 134 (2023) 106434, https://doi.org/10.1016/j.bioorg.2023.106434.

[80] V.K. Singh, I. Ahmad, H. Patel, J. Dwivedi, P. Singh, S. Rai, R.K. Singh, Design, docking, molecular dynamics, synthesis and antimicrobial studies on quinoline derivatives and some isosteres, J. Mol. Struct. 1294 (2023) 136387, https://doi.org/10.1016/j.molstruc.2023.136387.

[81] S. Rampogu, A. Zeb, A. Baek, C. Park, M. Son, K.W. Lee, Discovery of potential plant-derived peptide deformylase (PDF) inhibitors for multidrug-resistant bacteria using computational studies, J. Clin. Med. 7 (2018) 563, https://doi.org/10.3390/jcm7120563.

[82] W. Tian, C. Chen, X. Lei, J. Zhao, J. Liang, CASTp 3.0: computed atlas of surface topography of proteins, Nucleic Acids Res. 46 (2018) W363–W367, https://doi.org/10.1093/nar/gky473.

[83] M.N.D. Rocha, D.R. Alves, M.M. Marinho, S.M.D. Morais, E.S. Marinho, Virtual screening of citrus flavonoid tangeretin: a promising pharmacological tool for the treatment and prevention of Zika fever and COVID-19, J. Comput. Biophys. Chem. 20 (2021) 283–304, https://doi.org/10.1142/S2737416521500137.

[84] P. Banerjee, A.O. Eckert, A.K. Schrey, R. Preissner, ProTox-II: a webserver for the prediction of toxicity of chemicals, Nucleic Acids Res. 46 (2018) W257–W263, https://doi.org/10.1093/nar/gky318.

[85] B. Dey, P. Pahari, S.K. Sahoo, A.K. Atta, Triazole-based pyrene-sugar analogues for selective detection of picric acid in water medium and paper strips, J. Photochem. Photobiol. A 440 (2023) 114647, https://doi.org/10.1016/j.jphotochem.2023.114647.

[86] B.V.S. Reddy, K. Praneeth, J.S. Yadav, 1, 3-Dipolar cycloaddition of sugar azides with benzyne: a novel synthesis of 1, 2, 3-benzotriazolyl glycoconjugates, Carbohydr. Res. 346 (2011) 995–998, https://doi.org/10.1016/j.carres.2010.12.015.

[87] D. Kumar, K.B. Mishra, B.B. Mishra, S. Mondal, V.K. Tiwari, Click chemistry inspired highly facile synthesis of triazolyl ethisterone glycoconjugates, Steroids 80 (2014) 71–79, https://doi.org/10.1016/j.steroids.2013.11.022.

[88] B.S. Panda, CCDC 2314962: experimental crystal structure determination, (2024), 10.5517/ccdc.csd.cc2hpx6b.

[89] H. Prasad, A. Ananda, A. Mukarambi, N. Gaonkar, S. Sumathi, H. Spoorthy, P. Mallu, Design, synthesis, and anti-bacterial activities of piperazine based phthalimide derivatives against superbug-Methicillin-Resistant Staphylococcus aureus, Curr. Chem. Lett. 12 (2023) 65–78, https://doi.org/10.5267/j.ccl.2022.9.005.

[90] A.S. Lee, H. de Lencastre, J. Garau, J. Kluytmans, S. Malhotra-Kumar, A. Peschel, S. Harbarth, Methicillin-resistant Staphylococcus aureus, Nat. Rev. Dis. Primers 4 (2018) 1–23, https://doi.org/10.1038/nrdp.2018.33.

[91] J.B. Kaper, J.P. Nataro, H.L. Mobley, Pathogenic Escherichia coli, Nat. Rev. Microbiol. 2 (2004) 123–140.

[92] G.B. Raho, B. Abouni, Escherichia coli and Staphylococcus aureus most common source of infection, The battle against microbial pathogens: basic science, technological advances and educational programs (2015) 637–648.

[93] J.T. Poolman, A.S. Anderson, Escherichia coli and Staphylococcus aureus: leading bacterial pathogens of healthcare associated infections and bacteremia in older-age populations, Expert Rev. Vaccines 17 (2018) 607–618, https://doi.org/10.1080/14760584.2018.1488590.

[94] A.H. Shamina, V. Ganesan, V.B. Jothy, A. Manikandan, S. Muthu, S. Javed, Quantum chemical computations on molecular composition, spectroscopic properties, topology exploration, NLO, ligand protein interactions and pharmacokinetic evaluation of 8-hydroxyquinolium 3-nitrobenzoate, Chem. Phys. Impact 8 (2024) 100394, https://doi.org/10.1016/j.chphi.2023.100394.

[95] A. Irfan, A.G. Al-Sehemi, M.S. Al-Assiri, Modeling of multifunctional donor-bridge- acceptor 4,6-di(thiophen-2-yl)pyrimidine derivatives: a first principles study, J. Mol. Graph. Model. 44 (2013) 168–176, https://doi.org/10.1016/j.jmgm.2013.06.003.

[96] C. Yang, X. Li, N. Zhou, B. Chen, H. Dong, J. Jin, X. Hu, T. Huang, L. Shen, J. Yi, Q. Wang, J. Wang, D. Ouyang, The relationships between direct substituents, aromaticity and kinetic stability of pentazole ring, FirePhysChem 3 (2023) 350–355, https://doi.org/10.1016/j.fpc.2023.04.003.

[97] D.P.L. Renj, R.R.J. Geetha, A. Benifa, M. Amalanathan, M.S.M. Mary, Z. Ratkovi, J. Muskinja, J. Micheal, Density functional theory calculations, vibrational spectral analysis and topological analysis of 1-acethyl-2(4-isopropoxy-3-methoxyphenyl) cyclopropane with docking studies, Chem. Phys. Impact 8 (2024) 100524, https://doi.org/10.1016/j.chphi.2024.100524.

[98] P. Geerlings, F. De Proft, W. Langenaeker, Conceptual density functional theory, Chem. Rev. 103 (5) (2003) 1793–1874, https://doi.org/10.1021/cr990029p.

[99] S.W. Qader, A. Suvitha, M. Ozdemir, I. Benjamin, A.S.R. NSA, M.U. Akem, A. E. Frank, E.C. Eluwa, Investigating the physicochemical properties and pharmacokinetics of curcumin employing density functional theory and gastric protection, Chem. Phys. Impact 5 (2022) 100130, https://doi.org/10.1016/j.chphi.2022.100130.

[100] M. Khalid, M.A. Ullah, M. Adeel, M.U. Khan, M.N. Tahir, A.A.C. Braga, Synthesis, crystal structure analysis, spectral IR, UV-Vis, NMR assessments, electronic and nonlinear optical properties of potent quinoline based derivatives: Interplay of experimental and DFT study, J. Saudi Chem. Soc. 23 (2019) 546–560, https://doi.org/10.1016/j.jscs.2018.09.006.

[101] A.S. Kazachenko, N. Issaoui, A. Sagaama, Y.N. Malyar, O. Al-Dossary, L. G. Bousiakou, A.S. Kazachenko, A.V. Miroshnokova, Z. Xiang, Hydrogen bonds interactions in biuret-water clusters: FTIR, X-ray diffraction, AIM, DFT, RDG, ELF, NLO analysis, J. King Saud Univ. Sci. 34 (2022) 102350, https://doi.org/10.1016/j.jksus.2022.102350.

[102] M.J. Pramila, D.A. Dhas, I.H. Joe, S. Balachandran, G. Vinitha, Structural insights, spectral, flourescence, Z-scan, C-H…O/N-H…O hydrogen bonding and AIM, RDG, ELF, LOL, FUKUI analysis, NLO activity of N-2(Methoxy phenyl) acetamide, J. Mol. Struct. 1272 (2023) 134140, https://doi.org/10.1016/j.molstruc.2022.134140.

[103] S. Soumya, I.H. Joe, A combined experimental and quantum chemical study on molecular structure, spectroscopic properties and biological activity of anti-inflammatory glucocorticosteroid drug, dexamethasone, J. Mol. Struct. 1245 (2021) 130999, https://doi.org/10.1016/j.molstruc.2021.130999.

[104] R. Sukanya, D. Aruldhas, I.H. Joe, S. Balachandran, Spectroscopic and quantum chemical computation on molecular structure, AIM, ELF, RDG, NCI, and NLO activity of 4-VINYL benzoic acid: a DFT approach, J. Mol. Struct. 1253 (2022) 132273, https://doi.org/10.1016/j.molstruc.2021.132273.

[105] A. Bishnoi, N. Afza, P. Devi, A. Verma, S. Shukla, H. Parveen, R. Kumar, S. Rai, Synthesis, spectroscopic & DFT studies of novel N-((1H-benzo [d] imidazol-1-yl) methyl)-N-(2-(trifluoromethyl) phenyl)-4, 5-dihydrothiazol-2-amine, Indian J. Pure Appl. Phys. 59 (2021) 504–512, https://doi.org/10.56042/ijpap.v59i7.32324.

[106] B. Abdelaziz, Z. Mazouz, B. Gassoumi, N.E.I. Boukortt, S. Patane, S. Ayachi, Molecular engineering of D-π-A-type structures based on nitrobenzofurazan (NBD) derivatives for both organic solar cells and nonlinear optical response, J. Mol. Liq. 395 (2024) 123934, https://doi.org/10.1016/j.molliq.2023.123934.

[107] S. Rai, F. Ghous, S. Shukla, P. Sharma, P. Trivedi, A. Bishnoi, Experimental and In-Silico investigations on novel bioactive 4-phenyl-2-thioxo-3,4-dihydro-1*H*-pyrido [1,2-a]pyrimido[4,5-d] pyrimidin-5(2*H*)-one, J. Mol. Struct. 1292 (2023) 136116, https://doi.org/10.1016/j.molstruc.2023.136116.

[108] M.R. Xavier, M.M. Marinho, M.S.S. Juliao, E.S. Marinho, F.W.Q. Almeida-Neto, K. K.A. deCastro, J.P.D. Hora, M.N.D. Rocha, A.C.H. Barreto, G.D. Saraiva, P. N. Bandeira, H.S. Santos, H.D.M. Coutinho, A.M.R. Teixeira, Structural, topological, vibrational, and electronic analysis, and ADMET study of Methyl-2-(4-isobutylphenyl)propanoate, J. Mol. Struct. 1309 (2024) 138019, https://doi.org/10.1016/j.molstruc.2024.138019.

[109] C.A. Lipinski, F. Lombardo, B.W. Dominy, P.J. Feeney, Experimental and computational approaches to estimate solubility and permeability in drug discovery and development settings, Adv. Drug Deliv. Rev. 46 (2001) 3–26, https://doi.org/10.1016/j.addr.2012.09.019.

[110] Y. Belay, A. Muller, F.S. Mokoena, A.S. Adeyinka, L.R. Motadi, A.K. Oyebamiji, 1, 2, 3-triazole and chiral Schiff base hybrids as potential anticancer agents: DFT, molecular docking and ADME studies, Sci. Rep. 14 (2024) 6951, https://doi.org/10.1038/s41598-024-57689-5.

[111] H.N. Prasad, A.P. Ananda, S. Sumathi, K. Swathi, K.J. Rakesh, H.S. Jayanth, P. Mallu, Piperazine selenium nanoparticle (Pipe@ SeNP's): A futuristic anticancer contender against MDA-MB-231 cancer cell line, J. Mol. Struct. 1268 (2022) 133683, https://doi.org/10.1016/j.molstruc.2022.133683.

[112] A. Iqbal, M.T. Alam, A. Khan, T. Siddiqui, A. Ali, Inhibition of protein misfolding and aggregation by steroidal quinoxalin-2 (1H)-one and their molecular docking studies, Int. J. Biol. Macromol. 269 (2024) 132020, https://doi.org/10.1016/j.ijbiomac.2024.132020.

[113] P. Pragyandipta, R.K. Pedapati, P.K. Reddy, A. Nayak, R.K. Meher, S.K. Guru, S. Kantevari, P.K. Naik, Rational design of novel microtubule targeting anticancer drugs N-imidazopyridine noscapinoids: Chemical synthesis and experimental evaluation based on in vitro using breast cancer cells and in vivo using xenograft mice model, Chem. Biol. Interact. 382 (2023) 110606, https://doi.org/10.1016/j.cbi.2023.110606.